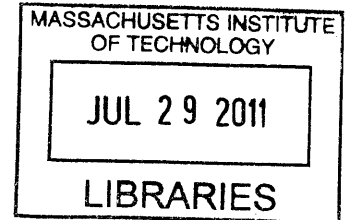# Feasibility of Novel Gait Training with Robotic Assistance: Dynamic Entrainment to Mechanical Perturbation to the Ankle

by

Jooeun Ahn

Master of Science in Mechanical Engineering
Massachusetts Institute of Technology, 2006

Submitted to the Department of Mechanical Engineering
in Partial Fulfillment of the Requirements for the Degree of

Doctor of Philosophy

at the

Massachusetts Institute of Technology

June 2011

Signature of Author . . . .
Department of Mechanical Engineering
May 20, 2011

Certified by. . . . .
Neville Hogan
Professor of Mechanical Engineering and Professor of Brain and Cognitive Sciences
Thesis Supervisor and Thesis Committee Chair

Accepted by. . . . .
David E. Hardt
Chairman, Department Committee on Graduate Students

Feasibility of Novel Gait Training with Robotic Assistance: Dynamic Entrainment to Mechanical Perturbation to the Ankle

by

Jooeun Ahn

Submitted to the Department of Mechanical Engineering
on May 20, 2011, in Partial Fulfillment of the Requirements for the Degree of
Doctor of Philosophy

Abstract

Rehabilitation of human motor function is an issue of the utmost significance, and the demand for the effective rehabilitation service is even growing with the graying of the population. Robotic technology has provided promising ways to assist recovery of the motor function of upper extremities. In contrast, current robotic therapy for lower extremities has shown inferior efficacy. In this thesis, the source of the limited efficacy of current robotic walking therapy is addressed. Essential mechanical components for robustly stable walking are identified as energy dissipation and proper compensation. Based on these essential components, design criteria of effective robotic walking therapy are suggested as foot-ground interaction and ankle actuation. A novel strategy of robot aided walking therapy reflecting the design criteria is proposed; dynamically entraining human gait with periodic ankle torque from a robot.

Experiments with normal subjects and neurologically impaired subjects support the feasibility of the proposed rehabilitation strategy. The gait period of subjects entrain to the periodic mechanical perturbation with a measurable basin of entrainment, and the entrainment always accompanies phase-locking so that the mechanical perturbation assists propulsion. These observations are affected neither by auditory feedback nor by a distractor task for normal subjects, and consistently observed in impaired subjects. A highly simplified one degree of freedom walking model without supra-spinal control or an intrinsic self-sustaining neural oscillator (a rhythmic pattern generator) encapsulated the essence of these observations. This suggests that several prominent limit-cycle features of human walking may stem from peripheral mechanics mediated by simple afferent feedback without significant involvement of supra-spinal control or central pattern generator. The competence of the highly simplified model supports that the proposed entrainment therapy may be effective for a wide range of neurological impairments.

Thesis Supervisor and Thesis Chair: Neville Hogan
Title: Professor of Mechanical Engineering and Professor of Brain and Cognitive Sciences

2

Acknowledgements

First and foremost, I express my deepest gratitude to my advisor, Professor Neville Hogan. Neville has been my advisor since 2005 spring when I started my Master program. He has advised my study with great leadership, outstanding insight and remarkably extensive knowledge throughout science and engineering. He has been a role-model of a great scholar and advisor with his great passion. I could find him excited whenever he encountered an interesting and challenging problem, and I could feel myself be energetic like him when I had conversation with him regarding engineering science. He has always encouraged me to think aloud alone and figure out the main plot of the study for myself; his advice has addressed the way of thinking instead of giving me an easy solution. He has also given me detailed advice on how to improve my way of presentation in English.

I would like to express my gratitude to Neville not only for his valuable academic advice, but also for his admirable mentorship. He has always been considerate of my personal situations. When I let him know that I should be absent from a meeting due to a hospital appointment, he showed his concern and asked regards. When my wife became pregnant, and my first son, Junghoo was born, I could feel his heart-warming congratulations. I am deeply thankful that I have an opportunity to have Neville as my advisor. After graduation, I am planning to go to academia rather than industry, and one of the reasons is that Neville has been my advisor; I would like to imagine myself as a good scholar and advisor as Neville in the future.

I am very much pleased to have this opportunity to express a lot of thanks to Doctor Hermano Igo Krebs for his advice and support. His great insight and expertise as a pioneer of robot-aided therapy have provided invaluable feedback to improve this study. He has pointed out important questions to be clarified and encouraged me to do my work with great pleasure. With his valuable support, I could easily perform much of the experimental work which is one of the core parts of this thesis. His support, academic advice, encouragement and sense of humor have been an important driving force for me to enjoy my "Newman lab life."

Great thanks also to Professor Russ Tedrake and Professor Triantaphyllos R. Akylas. With his great insight and expertise in robotics and control, Russ has brought up important points to be clarified and given me valuable advice to present this thesis more decently. When I encountered a significant confusion in nonlinear dynamics, an important tool of analysis in this thesis, I have

Contents

6

List of Figures

List of Tables

1. Introduction

Every year, numerous people lose their ability to move normally due to a stroke, a traumatic brain/spinal cord injury, or other neurological/orthopedic impairments; the necessity of effective rehabilitation service cannot be overestimated. The demand for rehabilitation service is increasing due to the growth of the elderly population and incidence of age-related disorders. With this enormous demand, robot-aided rehabilitation has been considered as a promising way to assist therapists and aid patients' recovery since robots are able to support human labor and provide more frequent therapy. In addition, direct interaction with a robotic device enables quantitative measurements of human performance, which enables more systematic training.

Though the idea of applying robotics to rehabilitation has appeared in literature since 1970's [1], therapeutic robotics which supplements the role of therapists and enhances the performance of patients beyond assistive technology does not have a long history. High standard of technology required for safe human-robot interaction had been one of the hindrances to development of effective therapeutic robots until Hogan et al. pioneered highly back-drivable robots that could deliver sensory-motor treatment safely [2]. By virtue of the progress in robotic technology, numerous therapeutic robots were developed for various human movements including reaching, grasping, wrist motion, and walking.

Apart from high level technology of robotic device, effective strategy is required for effective robot-aided rehabilitation; robotic therapy for motor function cannot show promise unless properly designed with consideration of human motor control. For upper extremities, accompanied by advances in the knowledge of motor control of upper limbs, robot-aided sensory-motor training has evolved to outperform conventional manual physical therapy. Numerous studies have shown the

11

effectiveness of human-interactive robots for upper-extremity therapy [3].

In contrast, efficacy of robotic therapy for lower extremities up to date is controversial. Even with advanced engineering technology close to the state of the art, robotic therapy for walking has not shown as much efficacy as upper limb therapy. Recent studies have reported that robotic walking therapy has not even outperformed conventional physical therapy [4, 5]. One plausible reason for this limitation is that an "effective strategy" is the missing part of current robot aided rehabilitation for walking; the high level technology may have been used improperly.

The main goal of this thesis is to propose a novel approach to robot aided walking therapy – dynamic entrainment with ankle mechanical perturbation, and address its feasibility. The new approach has been designed with consideration of bio-mechanical features of walking that are hitherto neglected in most current robot-aided walking therapy. This chapter mainly addresses the probable causes of limitation of current robotic therapy for walking, leading to the necessary components of a better strategy of walking therapy.

1.1. Why Robotic Therapy for Walking?

It is commonly accepted that a repetitive walking pattern is helpful for the injured central nervous system (CNS) to recover its function for locomotion. Conventionally, a repetitive walking pattern on the patient has been provided with the aid of physical therapists that manually move the patient's lower extremity. Robotic technologies can provide an advantageous alternative to this conventional physical therapy in several aspects. They can carry out the strenuous and labor-intensive process of moving patient's limbs, and provide cost effective therapy. Through direct interaction between robotic devices and patients, therapists can assess the patients' performance quantitatively and monitor important physiological variables related to recovery systematically. This

12

is also critical to provide therapy based on the patients' performance to enhance their participation, which is known as an essential component in neuro-restoration [6-8].

1.2. Limitations of Current Robotic Therapy for Walking

Since the pioneering study of MIT-Manus [9], various groups have developed robotic devices for rehabilitation. Many studies have shown the promise of robotic therapy for upper extremities [3, 10-12], whereas the efficacy of robotic therapy for lower extremities still remains debatable [4, 5, 13]. This section addresses plausible causes of these limitations.
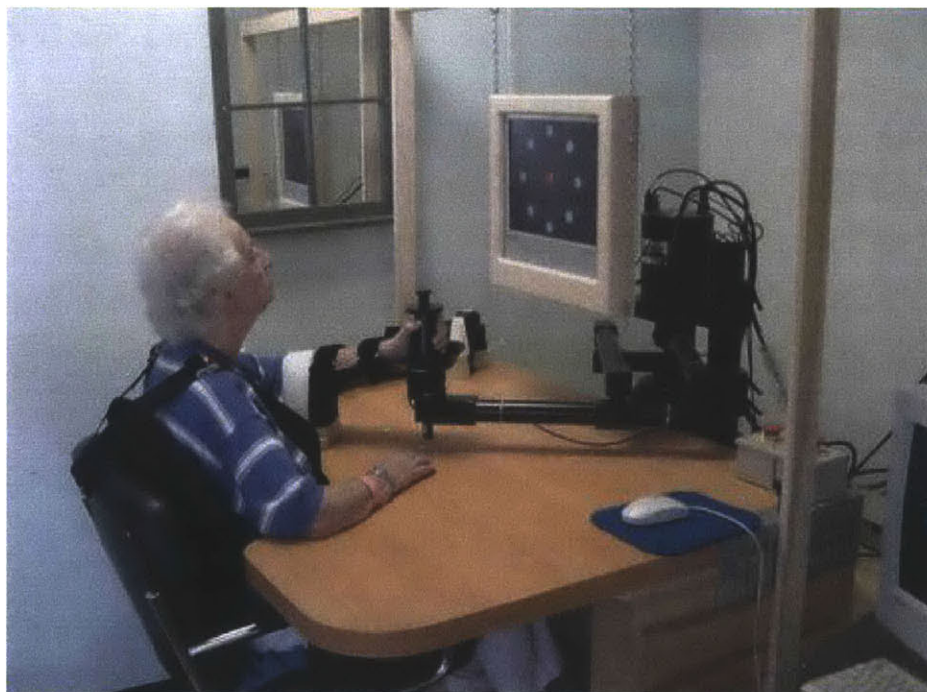
Figure 1-1:Stroke patient during robot-aided therapy with MIT Manus
MIT-Manus is specifically designed and built for rehabilitation of reaching movements of upper extremities. Post-stroke patients, both chronic and acute, who practiced reaching movements on this system improved their function.
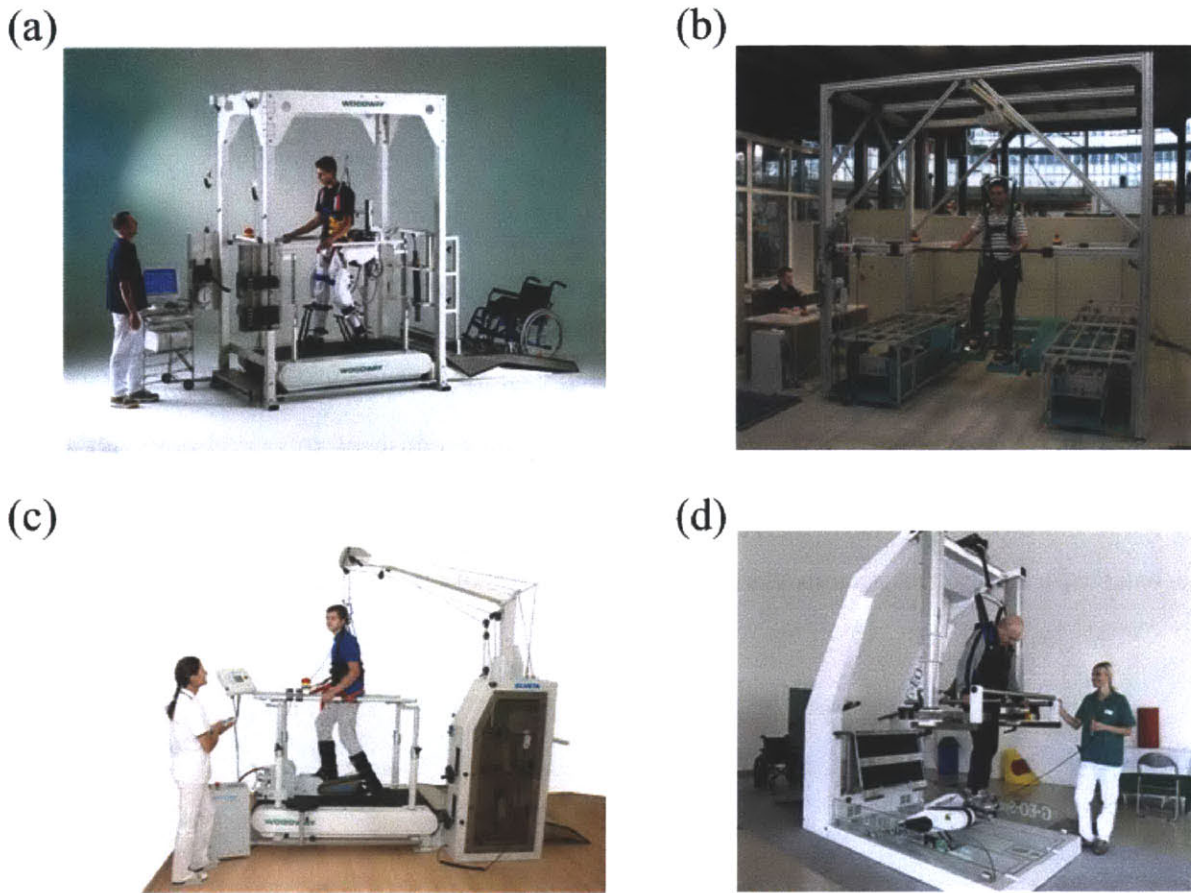
Figure 1-2: Therapeutic robots for walking
(a) Lokomat (Hocoma), (b) Haptic Walker (Hesse et al.), (c) Lokohelp Gait Trainer (Lokohelp group), and (d) GEO system (Reha Technologies). They all have two common components; one is body weight support system and the other is a set of actuators imposing kinematic patterns to the lower limbs of the participants. None of them allows natural dynamics of walking.

1.2.1. Assistance Level Is Difficult to Control

Most current therapeutic robots for walking impose the nominal kinematics of lower limbs [14-16]. This approach is faithful to the basic premise that exposure to a repetitive pattern results in recovery of motor function. However, by enforcing pre-recorded kinematic patterns of joints or feet regardless of patient's performance, this approach ignores the voluntary participation of the patients. This can be an important drawback; control of assistance level to promote the participation provides

14

a significant improvement in recovery of locomotion [8] as well as reaching [6, 7]. Furthermore, imposing a fixed trajectory may drive the CNS into the state of "learned helplessness" [8, 17].

A few robotic devices have evolved to have force-field controllers to resolve the drawback of fixed trajectory training [18, 19]. The force-field controller hinders undesired limb motion and assists the limbs towards a desired trajectory. With this force control strategy, voluntary active movements of the patients are allowed, which has been impossible with former position control of joints or feet. By controlling the strength of the force field, the level of assistance can also be controlled to promote the participation of the patients. This approach is analogous to that of robotic therapy for upper extremities which discourages lateral deviation from desired motion by finite mechanical impedance [20]. Considering the success of this approach in upper limb robotic therapy [7], the robotic therapy of walking with this similar strategy may be expected to show improved efficacy though systematic assessment is required.

1.2.2. Natural Oscillating Dynamics Is Not Allowed

As discussed in 1.2.1, absence of the control of voluntary participation may be a critical source of the limitations of the current robotic therapy for walking. However, it may not be the entire source. As an attempt to encourage the participation of the patients, guidance force of the robotic device, body weight support, and treadmill speed have been controlled in the training protocols. However, the robotic therapy of walking with this control to promote the engagement of the patients has shown less efficacy than conventional physical therapy [4], which suggests that the limitation of current robotic therapy for walking results from more elementary causes.

Fundamentally, walking is decidedly different from reaching; it is a rhythmic process, hybrid of continuous and discrete dynamics. To address the source of the limitation, it is necessary

to pay attention to the significant components of human locomotor control. Studies over decades have provided convincing evidences of dominant neural control of hand kinematics in reaching movement [21-24]. It is highly conceivable that the success of robotic therapy of upper extremities depends on the rehabilitation strategy focusing on the nominal trajectory or desired kinematic patterns. In contrast, the dominant component of human locomotor control remains considerably unclear. Though repeatable spatial trajectory of the foot of unimpaired adults [25] suggests supra-spinal control of foot kinematics, various studies in robotics and neuroscience have provided evidences supporting very different control schemes of human locomotion.

Robotic experiments and theoretical studies have shown that simple limit-cycle oscillators can exhibit stable walking. Passive dynamic walkers can remarkably mimic humanlike bipedal walking on a slight slope with no control and no actuation [26, 27]; inertia of periphery, gravity and intermittent foot-ground contact with energy dissipation generate a stable limit-cycle that mimics humanlike walking. This suggests that the mechanics involved with human periphery and gravity may play a non-negligible role in control of human walking.

Roles of different types of oscillators in human locomotion are suggested by various studies in animal locomotion. Unequivocal evidence of a rhythmic central pattern generator (CPG) in various vertebrates [28-32] has suggested plausible existence of a CPG in human spinal cord and its potential importance. Recently Gerasimenko et al. in fact reported that electromagnetic stimulation applied to unimpaired human vertebrae induced involuntary locomotor-like movement patterns [33]. Generally, a CPG, which can exhibit robustly sustained oscillation, can be modeled as a nonlinear oscillator with a limit-cycle [34-36] such as a van der Pol oscillator [37].

Taken together, various studies suggest the plausible role of limit-cycle oscillators in human locomotor control whether they originate from mechanical interaction or neural circuit. If any combination of these oscillators plays an important role in human locomotor control, the

current approach of most therapeutic robots may inadvertently interfere with the natural dynamics of walking by focusing only on the nominal kinematics. For example, Hidler and Wall reported significant differences in muscle activation patterns between walking on a treadmill and walking within a robotic orthosis that imposes a constrained kinematic pattern by limiting the degrees of freedom of leg and pelvis movement [13].

Replacing position control with force-field control in current robotic devices [18, 19] may not properly resolve the unnatural dynamics enforced by the robotic devices. In the current strategy of force-field control, the equilibrium trajectory yielding zero force is a pre-planned nominal trajectory; though the controller does not constrain the limb kinematics regardless of the force from the participants, it still impels the limb motion towards the nominal trajectory without proper consideration of natural dynamics. (Natural kinematic patterns resulting from natural oscillating dynamics may differ by patients depending on their severity of injury, muscle strength, inertia distribution, etc.) In addition, non negligible encumbrance or limited degree of freedom due to the robotic devices may affect the execution of natural dynamics.

The plausible interference from the pre-planned kinematic patterns cannot be cleared up as long as we are fixated on using a robotic device as a kinematic controller. It is worthwhile to abandon the idea of tracking the pre-planned trajectory and invent a novel approach that allows and even exploits the expression of natural oscillating dynamics without confining any important degree of freedom in walking.

From 1.2.1 to 1.2.2, plausible causes of the limitations of current robotic therapy for lower extremities have been discussed. First, the current approach of imposing kinematic patterns cannot allow the voluntary participation of the patients which is essential for neuro-restoration of motor function. Second, the current approach has not considered the plausible role of the natural

oscillating dynamics in locomotor control. A novel approach that allows 1) the control of participation and 2) the expression of natural oscillating dynamics may resolve the limitations of current robotic therapy for walking.

1.3. Thesis Road Map

This introductory chapter has attempted to point out the necessity of more effective robot-aided therapy for walking and expected causes of the current limitations. At this point, I hope the reader agrees that imposing nominal kinematics may not be the proper approach to walking therapy, and natural oscillating dynamics resulting from the interaction between the neuro-muscular periphery and gravito-inertial mechanics may have to be considered and exploited in robotic therapy for walking.

Chapter 2 provides design criteria of a new approach to robotic therapy for walking which can address the plausible causes of current limitations. The robotic therapy for walking should allow or even exploit the natural oscillating dynamics of walking. To specify this general goal, essential components of natural dynamics of walking are addressed. Design criteria of rehabilitation strategy are proposed based on mechanically essential components as well as on neurologically essential components. Modulation of ankle function is emphasized as the essential component, leading to the use of a robot module for ankle.

Chapter 3 proposes a strategy satisfying the design criteria discussed in Chapter 2. I pay attention to the fact that human locomotion exhibits behaviors of limit-cycles, and entrainment is observed in nonlinear oscillators with limit-cycles. Entraining the patients' walking to normal cadence with ankle mechanical perturbation is proposed as a way to rehabilitate walking by exploiting its natural oscillating dynamics.

Chapter 4 presents experimental works with unimpaired subjects to address the feasibility of the proposed strategy of dynamic entrainment with ankle mechanical perturbation. Experiment with unimpaired subjects shows clear evidences of entrainment and phase-locking.

Chapter 5 presents experimental works with neurologically impaired subjects. Impaired subjects also show consistent behaviors of entrainment and phase-locking. In addition, entrainment to gradually accelerating perturbation cadence is observed with clear after-effects, supporting the feasibility of the proposed strategy.

In Chapter 6, the minimal components of the observed entrainment are addressed by a simple mathematical model. A minimal model without supra-spinal control or self-sustained oscillating circuit such as a CPG can reproduce the entrainment and phase-locking observed in the experiment. This suggests that the proposed strategy may be applicable to various types of neurological impairment.

Finally, Chapter 7 provides a summary and suggests directions for future work.

2. Design Criteria of the Robotic Walking Therapy

In the previous chapter, the plausible causes of limitations of current robot aided therapy for walking were discussed. The natural oscillating dynamics of walking has to be considered and exploited if any form of a limit-cycle oscillator plays a prominent role in the neuro-motor execution of human locomotion. To propose specific and applicable criteria based on this general design goal, it is necessary to address the minimal components of the natural oscillating dynamics of walking. In this chapter, the minimal relevant physics required for stable walking and specific design criteria are addressed. The design criteria include neurologically crucial components as well as mechanically essential components for stable walking. Required properties of the robotic device are also discussed.

2.1. Essential Components of Stable Periodic Walking

Among various aspects of system performance, stability is the issue of the utmost significance in every system whether the system is biological, mechanical, electrical or any other. Walking is reasonably approximated as periodic motion. Stability of the periodic walking motion is a pre-eminent issue for design of walking robots; if the locomotion is not stable, evaluation of other aspects of performance such as energy efficiency, walking speed, versatility etc is meaningless and impossible in practice. For animal locomotion, stability of periodic walking is an essential and self-evident feature; without robust stability of locomotion, an animal cannot perform functional locomotion in an environment which contains various sources of disturbances. One obvious consequence is the inability to avoid predators or chase prey.

This section outlines the minimal components of periodic walking with robust stability. By clarifying that an energy-conservative walking model is not able to reproduce the robust stability seen in animal locomotion, I argue that an energy conservative walker is an overly simplified model of human locomotion, and energy dissipation and compensation through additional complexity are essential. Neurological importance of this mechanically essential mechanism is also reviewed.

2.1.1. Energy Conservative Walking Cannot Be Asymptotically Stable

It is a rather classic and commonly accepted assumption that animal locomotion, including bipedal walking, consumes minimal energy [38-43]. This widely believed assumption has been one of the important motivations of energy conservative walking models. They are faithful to this classic hypothesis and have nice mathematical properties.

However, any energy conservative walker cannot reproduce the robust stability of animal locomotion. Some studies have claimed stable limit-cycles of energy conservative models [44-46], but their stability cannot be concluded as *asymptotic* under an arbitrary perturbation. To clarify this obvious but not trivial point, I illustrate a flaw of stability analysis of a prior study which concluded stability of a conservative walking model. Examples of valid stability analysis of conservative systems further elucidate the weakness of the prior study and inability of conservative walkers to have an asymptotically stable behavior.

Invalid Stability Analysis of a Conservative Walking Model

As a representative example of invalid stability analysis of a conservative walking model, I take H. Geyer's work on a springy legged model with double stance [46]. Figure 2-1 shows the schematic of the model. In a sagittal plane, a point mass, m is supported by two identical massless

springs with stiffness, k, and unloaded length, l_0, under gravity, g. The model has both single and double stance phases. The model controls the leading leg to maintain a fixed angle as α_0 at every touch down. By virtue of the zero mass of legs, this control consumes zero energy, and the springy legs preclude energy dissipation due to foot-ground collision; the model is energy conservative.

In [46], to investigate stability of a periodic gait, linearized stability analysis is performed around periodic gaits, fixed points of a Poincaré map which is defined from one apex to the next apex. Because the dynamics of the point mass is described as a set of 2nd order ordinary differential equations (ODE) in 2 degrees of freedom (DOF), a 4-dimensional vector (e.g., $\mathbf{x} = (x, \dot{x}, y, \dot{y})$) is required to describe the model dynamics. To define the Poincaré map from one apex to the next apex, one variable, $\dot{y}$, is set to zero at the Poincaré section; the Poincaré map should be defined in 3-dimensional vector space, saying $R : (x_{rel}, \dot{x}, y)_i \rightarrow (x_{rel}, \dot{x}, y)_{i+1}$, where x_{rel} is the x position of the point mass relative to the foot point of the stance leg.
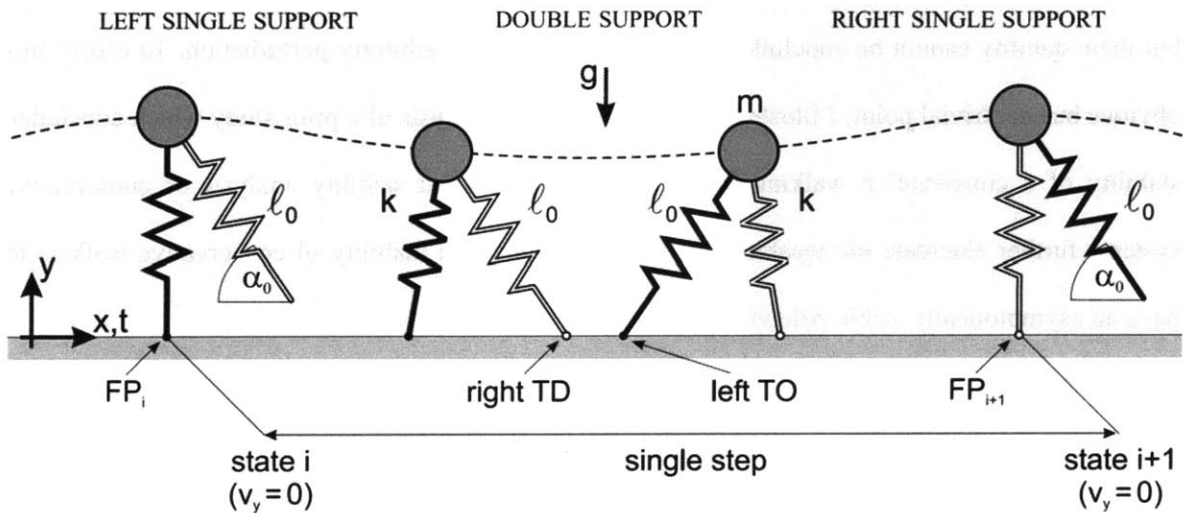
Figure 2-1: H. Geyer's model – Springy legged walker with double stance (from [46])

However, in [46], the dimension of the state vector on the Poincaré section is reduced further to be 2-dimensional as $R : (x_{rel}, y)_i \rightarrow (x_{rel}, y)_{i+1}$ based on that the model is energy conservative ($\dot{x}$ is substituted for $\dot{x} = \sqrt{\dfrac{2E_s}{m} - \dfrac{k(l_0 - l)^2}{m} - 2gy}$, where E_s means the energy level of the system). This cannot provide a valid way to analyze stability of a fixed point. In this analysis, the energy level of the system is treated as a parameter value that does not change under any arbitrary perturbation. In other words, any perturbation that changes the energy level from the periodic motion is not allowed in this analysis.

An example of a simple pendulum immediately demonstrates the flaw of this analysis. A simple pendulum is a classic example of an energy conservative system. It has two distinct fixed points (one at the bottom and the other at the top); the fixed point at the bottom is marginally stable whereas the other at the top is unstable. Focusing on the local behavior, the unstable fixed point yields an exponentially growing error under any small perturbation though the energy of the system is globally fixed due to energy conservation. In contrast, a small perturbation to the stable fixed point keeps the evolution around the fixed point, yielding marginal stability. Please note that any perturbation, including those that change the energy level must be allowed when analyzing the stability of these fixed points. For example, for the fixed point at the bottom, if the energy level is regarded as a parameter value that is independent of the evolution of the state variables and remains constant under any perturbation, then no perturbation is allowed in the state space; any non-zero perturbation in state space increases the energy level of the fixed point at the bottom.

Energy Conservation Does Not Conclude Neutral Stability

As in the example of a simple pendulum, the property that a system is energy conservative does not necessarily mean that the system is neutrally stable as it evolves in the state space. For the

unstable fixed point of a simple pendulum, any small perturbation changing the energy level induces a locally but exponentially growing error in state space though the energy level stays exactly at the perturbed level. Review of the definition of stability (in the Lyapunov sense) and the linearized stability analysis may clarify this point further.

Stability of a Continuous System Let X_{fixed} be a fixed point of a dynamical system $\dot{X} = f(x)$.

In other words, $f(X_{fixed}) = 0$. The fixed point is *stable* when for $\forall \varepsilon > 0$ and $\forall t$,

which is the time, $\exists \delta = \delta(\varepsilon) > 0$, such that for $\forall X_0$, $\left| X_0 - X_{fixed} \right| < \delta$, we have

$$\left| X - X_{fixed} \right| < \varepsilon.$$

Asymptotic Stability of a Continuous System The fixed point $X = X_{fixed}$ is *asymptotically stable* when $X = X_{fixed}$ is stable and $\exists \delta = \delta(\varepsilon) > 0$ such that for $\forall X_0$,

$\left| X_0 - X_{fixed} \right| < \delta$, we have $\left| X - X_{fixed} \right|$ go to zero as time, t, goes to ∞.

Stability of a Discrete System Let X_{fixed} be a fixed point of a discrete map $X_{k+1} = f(X_k)$.

In other words, $X_{fixed} = f(X_{fixed})$. The fixed point is *stable* when for $\forall \varepsilon > 0$ and

$\forall n \in \mathbf{N}$, which is the set of positive integers, $\exists \delta = \delta(\varepsilon) > 0$, such that for $\forall X_0$,

$\left| X_0 - X_{fixed} \right| < \delta$, we have $\left| f^n(X_0) - X_{fixed} \right| < \varepsilon$.

Asymptotic Stability of a Discrete System The fixed point $X = X_{fixed}$ is *asymptotically stable* when $X = X_{fixed}$ is stable and $\exists \delta = \delta(\varepsilon) > 0$ such that for $\forall X_0$, $\left| X_0 - X_{fixed} \right| < \delta$,

we have $\left| f^n(X_0) - X_{fixed} \right|$ go to zero as n goes to ∞.

24

Linearized Stability Analysis   Eigenvalues of $\dfrac{\partial \mathbf{f}}{\partial \mathbf{x}}$ may conclude stability of the fixed point.

$$\mathbf{f}(\mathbf{x}) = \mathbf{f}(\mathbf{x}_{\text{fixed}} + \boldsymbol{\varepsilon}) = \mathbf{f}(\mathbf{x}_{\text{fixed}}) + \left.\frac{\partial \mathbf{f}}{\partial \mathbf{x}}\right|_{\text{fixed}} \boldsymbol{\varepsilon} + O(\varepsilon^2)$$. Assuming a small

enough perturbation, and ignoring 2$^{\text{nd}}$ and higher order terms of initial perturbation,

$$\mathbf{f}(\mathbf{x}) - \mathbf{f}(\mathbf{x}_{\text{fixed}}) \cong \left.\frac{\partial \mathbf{f}}{\partial \mathbf{x}}\right|_{\text{fixed}} \boldsymbol{\varepsilon} = \boldsymbol{\xi}$$. Let $\left.\dfrac{\partial \mathbf{f}}{\partial \mathbf{x}}\right|_{\text{fixed}} = \mathbf{D}$. If $\mathbf{D}$ is full rank and all

eigenvectors are independent, then $\boldsymbol{\varepsilon} = \displaystyle\sum_{j=1}^{m} v_j \mathbf{e}_j$, where $\mathbf{e}_j$'s are the eigenvectors of

$\mathbf{D}$ and v_j's are the corresponding scalar factors. The error due to the perturbation

can be written $\boldsymbol{\xi} = \mathbf{D}\boldsymbol{\varepsilon} = \mathbf{D}\displaystyle\sum_{j=1}^{m} v_j \mathbf{e}_j = \sum_{j=1}^{m} \mathbf{D} v_j \mathbf{e}_j = \sum_{j=1}^{m} v_j \lambda_j \mathbf{e}_j$, where λ_j's are the

eigenvalues. For a continuous dynamical system, $\boldsymbol{\xi} \cong \dot{\boldsymbol{\varepsilon}}$. If every λ_j has a negative

real part, the initial error converges to zero, which concludes *asymptotic stability*,

and if there is any λ_j with a positive real part, the fixed point is *unstable*. If the

maximal real part of the eigenvalues is zero (neither of the above), the fixed point

is *non-hyperbolic*, and this linearized analysis is *not conclusive* for stability. For a

discrete dynamical system, if every λ_j is inside the unit circle, the initial error

converges to zero, which concludes *asymptotic stability*, and if there is any λ_j

outside the unit circle, the fixed point is *unstable*. If the maximal magnitude of the

eigenvalues is unity (neither of the above), the fixed point is *non-hyperbolic*, and

this linearized analysis is *not conclusive* for stability.

As defined, the stability in the Lyapunov sense, which is widely used in stability analysis of walking models, generally depends on whether an error in the state space diverges, converges or stays constant. As illustrated in the example of a simple pendulum, whether the energy level stays at a constant level, increases, or decrease is not a direct measure of convergence or local divergence of an error in the state space. Therefore, assuming neutral stability of an energy conservative system cannot be justified.

It is also necessary to pay attention to the fact that neutral stability cannot be concluded by linearized analysis. For non-hyperbolic fixed points, the linearized stability is no longer conclusive, and alternative methods such as Lyapunov's 2nd method or center manifold reduction should be considered to conclude the stability.

Re-analysis of the Springy Legged Model in [46]

One probable defense of the stability analysis in [46] is that neutral stability is assumed for the perturbation that changes the energy level. However, as discussed above, marginal stability of an energy conservative system cannot be assumed blindly without proper analysis. Though parameter regimes with stable gaits are diagnosed at various energy levels in [46], a system response in state space to any energy changing perturbation cannot be addressed in the incorrect stability analysis.

To perform valid linearized stability analysis, I found the equations of motions and reconstructed the model without parameterizing the energy level. The return map from apex to apex was re-defined in 3-dimensional space; $R : (x_{rel}, \dot{x}, y)_i \rightarrow (x_{rel}, \dot{x}, y)_{i+1}$. Parameter values like mass, spring stiffness, unloaded leg length and the angle of touch down were selected to be same as the original model in [46]. A normalized error between the initial state vector and the state vector after one stride was defined as $\xi = (\dfrac{\Delta x_{rel}}{l_0}, \dfrac{2\pi\Delta\dot{x}}{l_0\sqrt{k/m}}, \dfrac{\Delta y}{l_0})$, and a periodic gait

minimizing the norm of the error was searched by numerical optimization. The optimization and numerical integration of the equations of motion were implemented in MATLAB R2006a (Mathworks Inc.). The periodic gait should yield zero difference between the neighboring strides; the criterion for termination of the optimization was that the norm of ξ should be smaller than 10^{-8}. Absolute error tolerance and relative error tolerance for the numerical integration were 10^{-8}.

The reconstructed model successfully found periodic gaits of the original model. With parameter values of $\alpha_0 = 69°$ (angle of the leading leg), and $kl_0 / mg = 17.8$, the optimization found a fixed point at $(x_{rel}, \dot{x}, y) = (0.00000, 1.11333, 0.97657)$, whose (x_{rel}, y) corresponds to the fixed point of the original model with same parameter values (Figure 2-2). The stability was analyzed in 3-dimensional Poincaré section so that any perturbation was allowed without parameterizing the energy level. In the linearized stability analysis, the eigenvalues of the derivative matrix of the Poincaré map (**D**) were found as $\lambda_{1,2} = 0.77487 \pm 0.48804\,i$, and $\lambda_3 = 1.00000$; the fixed point is non-hyperbolic though the first and second eigenvalues are inside the unit circle. The eigenvector corresponding to the non-hyperbolic eigenvalue was $(0.00000, 0.76142, 0.64826)$ in $(\delta x_{rel}, \delta\dot{x}, \delta y)$ direction. This newly found non-hyperbolic mode should be related with change of the energy level. The zero component in δx_{rel} direction is consistent with this physical intuition. At the configuration of this fixed point, x_{rel} is zero at the apex, and infinitesimal displacement in δx_{rel} does not alter the length of the spring; none of the kinetic energy, gravitational potential energy, and spring potential energy changes due to δx_{rel}, whereas the other components are directly related with changes of either kinetic energy or potential energy.
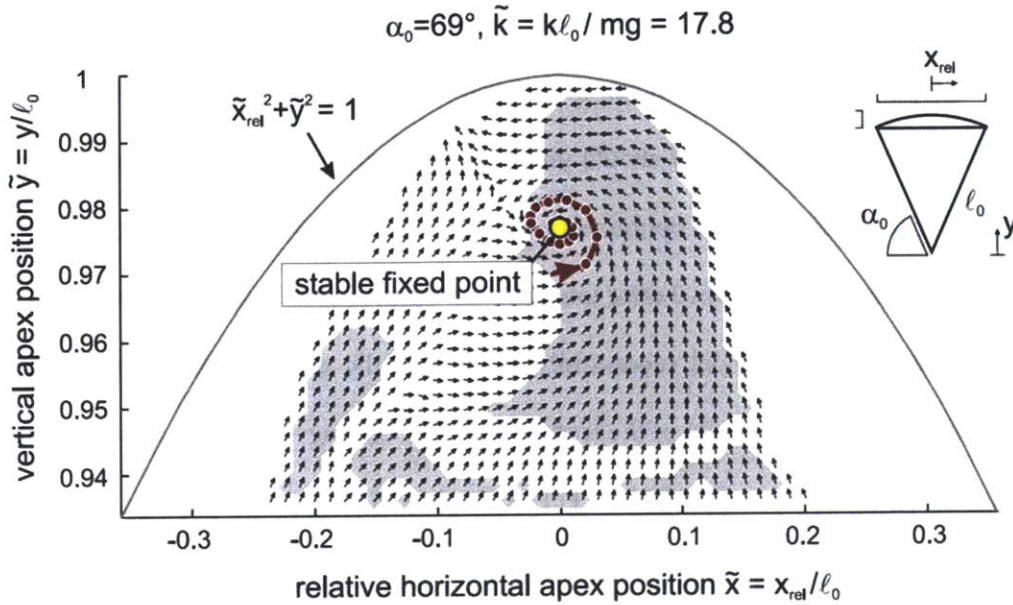
Figure 2-2: A fixed point of the return map of the model in [46] (from [46])
The fixed point approximately corresponds to $(x_{rel}, y) = (0, 0.977)$ in the 2-dimensional Poincaré section; the component of $\dot{x}$ vanished by parameterizing the energy level.

The non-hyperbolic mode of the fixed point invalidates the formal stability which was concluded from the incorrect linearized analysis. Physically, this model is neutrally stable at best. Considering that this model is energy conservative, the model cannot return to its original periodic trajectory when an energy-changing perturbation is added to the model. The original limit-cycle evolves in a sub-space with a constant energy level, and an energy-changing perturbation will shift the evolution to a different sub-space with a different energy level from which the model cannot go back to its original limit-cycle. However, as illustrated in the example of a simple pendulum, staying in a sub-space of constant energy level does not guarantee neutral stability in the state space. The fixed point may also be unstable. Whether the fixed point is unstable or neutrally stable cannot be concluded by linearized analysis because it is non-hyperbolic.

Instability of an Energy Conservative Walking Model

The unstable fixed point of a simple pendulum provides an example of continuous and holonomic dynamical system which is energy conservative but strictly unstable. Generally, walking involves discrete dynamics and non-holonomic constraints unlike a pendulum dynamics; it might require caution to generalize the behavior of a simple pendulum to a walking model.

To address this, I constructed a counterpart in a walking model which shows strict instability with a constant energy level. A point mass m moves on level ground in a sagittal plane under the influence of gravity g, restrained by a springy massless leg whose stiffness and unloaded length are k and l_0 respectively. Neither double stance nor flight phase is allowed. Each leg is allowed only to be compressed and cannot be stretched. Figure 2-3 shows the schematic of the model and definitions of state variables.

I derived equations of motion using the Lagrangian approach. The only constraint force is the ground reaction force that does no work due to the assumption of no slip of each foot. Therefore, all non potential generalized forces are zero. Let the generalized coordinates be (l, θ), and the Lagrangian be L.

$$L = T - V \text{, where}$$

$$T = \frac{1}{2}m\{\dot{l}^2 + (l\dot{\theta})^2\} \text{, and } V = \frac{1}{2}k(l - l_0)^2 + mgl\cos\theta.$$

$$\Rightarrow L = \frac{1}{2}m\{\dot{l}^2 + (l\dot{\theta})^2\} - \frac{1}{2}k(l - l_0)^2 - mgl\cos\theta.$$

Because non potential generalized forces are zero, $\dfrac{d}{dt}\dfrac{\partial L}{\partial \dot{q}} - \dfrac{\partial L}{\partial q} = Q = 0$,

$$\frac{d}{dt}\frac{\partial L}{\partial \dot{l}} - \frac{\partial L}{\partial l} = 0 \Rightarrow \ddot{l} - \dot{\theta}^2 l + \frac{k}{m}(l - l_0) + g\cos\theta = 0 \text{, and}$$

$$\frac{d}{dt}\frac{\partial L}{\partial \dot{\theta}} - \frac{\partial L}{\partial \theta} = 0 \Rightarrow l\ddot{\theta} + 2\dot{l}\dot{\theta} - g\sin\theta = 0.$$

29

Figure 2-3: A springy legged model without double stance

The state of the model can be described by leg length l and the leg angle θ. The end of one step is defined as the moment when the stance leg reaches its unloaded length; the mass is carried by the other leg as soon as the previous stance leg recovers its unloaded length. The foot of the new leg is positioned so that the leg can begin to support the point mass at its unloaded length.

To define a Poincaré map whose input and output are the state vectors at the end of one step and the next step respectively, I defined the Poincaré section as the moment when a springy leg recovers its unloaded length with positive velocity. As the equations of motion are 2nd order ODEs in 2 DOFs, a 4-dimensional vector ($\mathbf{x} = (l, \dot{l}, \theta, \dot{\theta})$) is required to describe the model dynamics, and the Poincaré section is defined in 3-dimensional state space Σ, which is

$$\Sigma = \{(l, \dot{l}, \theta, \dot{\theta}) \,|\, l = l_0 \wedge \dot{l} > 0 \wedge -\pi < \theta < \pi \wedge \dot{\theta} \in \mathbf{R}\}, \text{ where "}\wedge\text{" means "AND."}$$

After the Poincaré section determines the state vector at the end of a step, the state vector at the onset of the next step is determined by continuity of the velocity of the point mass. This is valid because the only force acting on the point mass at the end or beginning of one step is gravity which is not impulsive and therefore cannot change the velocity with infinitesimal time duration.

To find a periodic gait, a normalized error between initial state vector and state vector after one stride was defined, and a periodic gait minimizing the norm of the error was searched by numerical optimization. The optimization and numerical integration of the equations of motion were implemented in MATLAB R2006a (Mathworks Inc.). The periodic gait should yield zero difference

between the neighboring strides; the criterion for termination of the optimization was that the norm of the normalized error should be smaller than 10^{-8}. Absolute error tolerance and relative error tolerance for the numerical integration were 10^{-8}. Parameter values such as m (80 kg) and l_0 (1 m) were chosen to be comparable with a human adult, and k (10 kN/m) was chosen to make the periodic gait of the model have similar speed to normal human walking with the chosen m and l_0.

Numerical optimization found periodic gaits. Figure 2-4 shows the path of the point mass and the state variables of a periodic gait. The leg is not stretched, and therefore the ground reaction force always pushes the point mass, which means that the gait found does not violate the physics of locomotion. In the periodic gait, the velocity of the point mass at the end of each step is purely horizontal, pushing the next leg at the beginning of the next step. The average speed of the periodic gait is 1.9939 m/s, which is comparable to that of normal human walking.
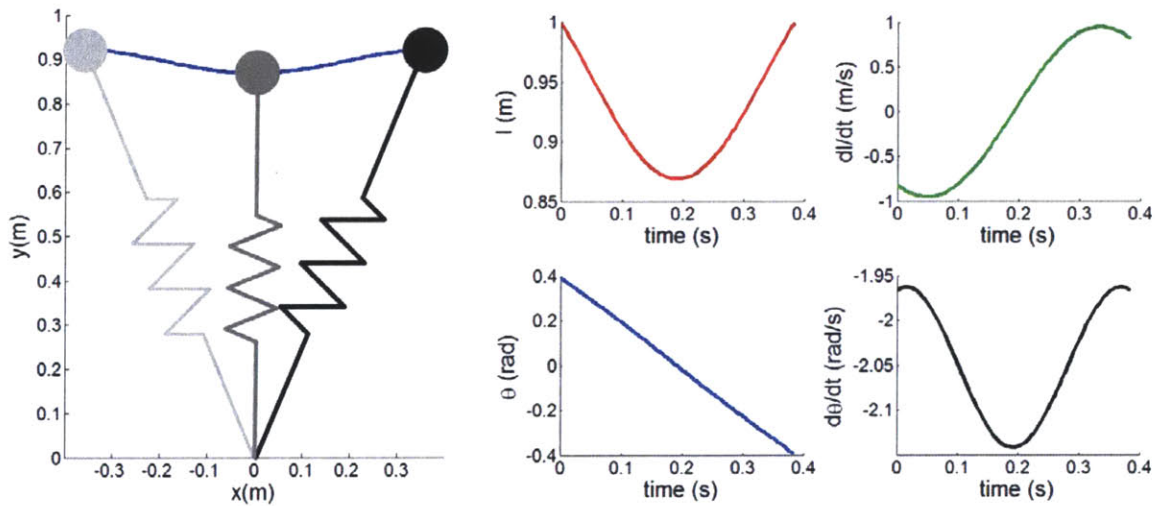
Figure 2-4: A periodic gait of the springy legged model without double stance
The path of the point mass (left) and state variables (right) of a periodic gait are shown. The leg is not stretched, and the ground reaction force pushes the point mass during each step. At the end of a step, the point mass has velocity only in the x direction. As the velocity of the point mass is continuous at a transition, the point mass compresses the new leg at the beginning of the next step. Step duration and length are 0.384 (s) and 0.765 (m) respectively, yielding an average speed of 1.994 m/s.

31

Stability of this periodic gait was analyzed in the 3-dimensional Poincaré section. In the linearized stability analysis, the eigenvalues of the derivative matrix of the Poincaré map (**D**) were found as $\lambda_1 = -2.50820$, $\lambda_2 = -0.39869$, and $\lambda_3 = 1.00000$; the linearized analysis concludes that the fixed point is unstable and a small error in state space may grow exponentially due to the unstable mode corresponding to the eigenvalue of λ_1 which is outside the unit circle. The local instability with exponential growth of the initial error is shown in Figure 2-5. Inconsistent with physics, the energy level also fluctuates due to numerical artifacts, but it stays almost constant compared to the growing errors in the state space.

It may be argued that the model cannot avoid flight phase or negative ground reaction force when a perturbation increases l at the beginning of a step because l is already l_0 at the onset of one step. However, as the periodic gait yields horizontal velocity at the beginning of one step, the point mass compresses the springy leg at the beginning of each step. For a perturbation to make a flight phase or stretch the leg it must have a stretching component which is large enough to overcome the compressing component of the unperturbed periodic gait. Such a large perturbation beyond the threshold is out of concern as the local stability is investigated by linearized analysis.

To summarize, though this walking model with piecewise-holonomic constraint is energy conservative, its periodic motion is not neutrally stable but unstable. Small deviation from the limit-cycle can result in local instability with exponentially growing error.
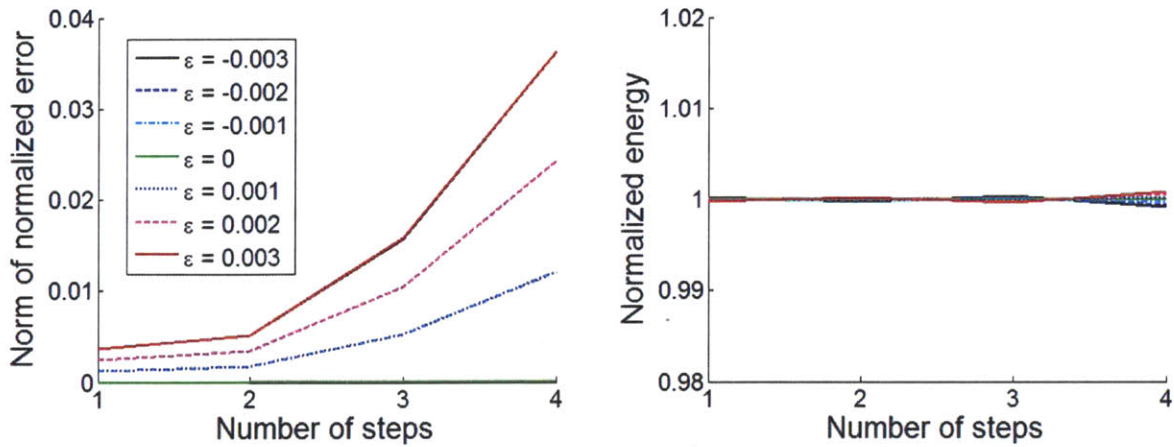
Figure 2-5: Instability of the periodic gait of the energy conservative walker
The periodic gait is unstable; a small error in the initial condition (ε) grows exponentially as step number increases. Though the energy also slightly changes due to numerical artifacts, it remains almost constant compared to the growing errors in the state space.

Non-holonomic Constraints Cannot Make Energy Conservative System Have Asymptotic Stability under Arbitrary Perturbations

Legged locomotion is not holonomic in the sense that the dimension of the accessible configuration space is larger than the dimension of the instantaneously accessible velocity space; in legged locomotion, feet do not slide though arbitrary foot position is achievable by adjusting the position of foot if anatomically possible. It has been known that non-holonomic systems may possess asymptotically stable fixed points since the late nineteenth century [47]. Extensive studies have systematically analyzed and reviewed the stability of various non-holonomic systems [48-50]. The global non-holonomic features of piecewise holonomic systems and their asymptotic behavior were studied by Ruina [51], and extended by Coleman and Holmes [52].

Theses prior studies showed that energy conservative non-holonomic systems (including piecewise holonomic systems) may exhibit asymptotic stability in some modes. However, this interesting feature of non-holonomy should not be misinterpreted as capability to impose

33

asymptotic stability on energy conservative systems. A classic example of non-holonomic systems is the Chaplygin sleigh. Depending on the position of the center of mass of a sleigh, the sleigh motion may become either asymptotically stable or unstable under angular velocity perturbations. However, even if the angular velocity is stabilized and the sleigh recovers its zero angular velocity asymptotically, this energy conservative system cannot return to its original motion from any energy changing perturbation. If a perturbation increases the kinetic energy, the final speed of the sleigh will remain as increased even if its rotational movement is stabilized asymptotically. In addition, any perturbation with a nonzero component that increases the translational speed accelerates the sleigh, and the sleigh has no means to return to its original speed.

Generally, an energy conservative system cannot have asymptotic stability under arbitrary perturbation whether it is holonomic or non-holonomic. Suppose that an energy conservative system has a limit-cycle. The limit-cycle must stay in a sub-space with a constant energy level. Any perturbation with a nonzero energy-changing component will displace the evolution to a different sub-space with a different energy level, and the energy conservative system cannot recover the difference. If we confine our interest to some selected modes or state variables ignoring the energy change, asymptotic stability may be claimed in those modes or variables depending on the dynamical system. (An example is the rotational movement of the Chaplygin sleigh.) This is equivalent with that a dynamical system evolves around a fixed point, and we investigate the behavior of only the projection of the evolution onto a sub-space with reduced dimensions. (The missing dimension should be parallel to the energy-changing mode.) The projected evolution may be identical with the actual evolution only when the initial perturbation has a zero energy-changing component. However, the probability that any physical perturbation does not change the energy level is "volume of $n - 1$ dimensional space over volume of n dimensional space" which is mathematically zero.

34

To summarize, an energy conservative walking model cannot yield asymptotically stable gait. Legged animal locomotion, including human walking, is reasonably robust against external perturbation; the periodic motion is well recovered after a few strides. This behavior requires asymptotic stability which a conservative walking model cannot reproduce. Though non holonomic constraints may allow some modes that are asymptotically stable in a "projected" sub-space, and legged locomotion may be regarded as non-holonomic, an energy conservative walker cannot have asymptotically stable gait under an arbitrary perturbation with non-zero energy changing component.

2.1.2. Energy Dissipation and Compensation Are Essential

In the previous section, I clarified that energy conservative walking cannot yield asymptotic stability which is a common and essential characteristic of legged animal locomotion. This justifies that an energy conservative walking model is overly simplified; additional complexity due to energy dissipation and compensation is essential to reproduce the robust stability of animal locomotion.

Asymptotic Stability of Passive Walkers with Energy Dissipating Foot Collision

There already exist various examples of passive walkers that walk stably; the existence and asymptotic stability of periodic gaits have been studied theoretically and experimentally [26, 27, 53, 54]. Though extensive review of the detailed analyses of each walker is out of the scope of this thesis, the essential mechanism of asymptotic stability is illustrated and encapsulated by the simplest example of a rimless spoked wheel model in this section.

The rimless spoked wheel model is simple but captures some key features of bipedal

walking. This model imitates foot-ground collision due to foot placement and the inverted pendulum motion of the single stance phase. Three dimensional motion of a rimless wheel spoked wheel was studied in [53]. To gain insight into the essential components of asymptotic stability, this section only reviews the simpler case of rolling in a vertical plane. Figure 2-6 shows the schematic of the model and state variable θ. A point mass moves in a vertical plane under the influence of gravity, constrained by a rigid massless leg.
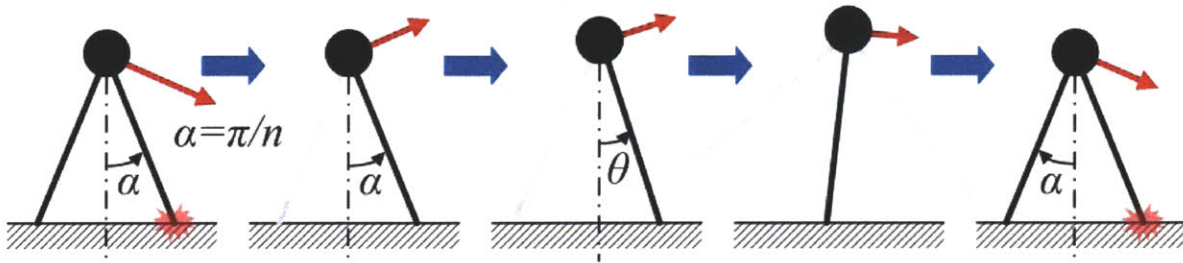
Figure 2-6: A rimless spoked wheel model on a horizontal surface
A point mass vaults over a foot restrained by a massless leg. The parameter α is π/n, where n is the number of spokes. The leg angle θ is a generalized coordinate of this model.

The foot-ground collision dissipates energy, and there is no way to compensate for the lost energy; this model cannot make a periodic gait on a level ground. However, on a slope, gravity can do work to compensate for the lost energy, and the model can exhibit an asymptotically stable periodic gait. The asymptotic stability of the periodic gait on a slope originates from (1) gravity does constant amount of work on each step and (2) each foot-ground collision reduces the kinetic energy by a constant ratio of $\cos^2 2\alpha$. Derivation of this constant ratio of $\cos^2 2\alpha$ will be presented in 2.1.4. If a perturbation increases the kinetic energy, the model suffers greater energy loss than the case of the periodic gait because the reduction ratio is fixed as $\cos^2 2\alpha$. Therefore, kinetic energy becomes closer to the kinetic energy of the periodic gait after one step. By repeating such progress for several steps, the gait of the model asymptotically approaches the unperturbed periodic gait. A

36

similar argument applies to the case in which a perturbation decreases the kinetic energy.

Quantitative return map analysis further clarifies the asymptotic stability. A Poincaré map can be analytically constructed by defining a Poincaré section as the moment of foot-ground collision. Using the work energy principle, the Poincaré map whose input and output are $\dot{\theta}$ at the beginning of one step and the next step respectively can be written

$$\dot{\theta}_{i+1} = -\cos 2\alpha \sqrt{\dot{\theta}_i^2 + \frac{4g\sin\alpha\sin\gamma}{l}} = \mathbf{f}(\dot{\theta}_i),$$

where l is the leg length and γ is the angle of the slope on which the model is rolling. The analytical expression of $\dot{\theta}$ of the periodic gait can also be found using the work energy principle as

$$\dot{\theta}_{\text{fixed}} = -\cos 2\alpha \sqrt{\frac{4g\sin\alpha\sin\gamma}{l(1-\cos^2 2\alpha)}}.$$

Taken together, the eigenvalue of the derivative matrix of the Poincaré map (**D**), evaluated at the fixed point, is $\dfrac{\partial \mathbf{f}(\dot{\theta}_i)}{\partial \dot{\theta}_i}\bigg|_{\dot{\theta}_i = \dot{\theta}_{\text{fixed}}} = \cos^2 2\alpha$, which stays inside the unit circle as long as α is neither zero nor π. (Neither of them is feasible for reasonable bipedal walking). The linearized analysis concludes asymptotic stability of the periodic gait.

It is worth noting that the eigenvalue of the derivative matrix of the Poincaré map, which determines the stability, is same as the reduction ratio of the kinetic energy per step due to foot-ground collision. This is neither a coincidence nor a specific feature of this specific model. Any model with one dimensional Poincaré section, constant energy supply and constant reduction ratio of kinetic energy shows asymptotic stability, and the eigenvalue of the derivative matrix of the Poincaré map (Floquet multiplier) is the reduction ratio of the kinetic energy per step. Proof is presented in Appendix B.

Trade-off between Minimal Energy Consumption and Stability

Minimal energy consumption of animal locomotion has been commonly assumed or hypothesized in many studies [38-43]. However, an energy conservative walker, which models the ideal case of walking with minimum energy cost, cannot reproduce robust stability of animal locomotion. In addition, for the rimless spoked wheel model, the determinant of stability, the eigenvalue of the derivative matrix of the Poincaré map, is the reduction ratio of the kinetic energy per step. Assuming that the parameter values such as the angle of foot placement, the angle of slope and initial velocity are proper so that the walker has a periodic gait, the greater (smaller) energy dissipation yields the stronger (weaker) stability.

Considering that the rimless spoked wheel model encapsulates key features of bipedal walking, including foot-ground collision and the inverted pendulum motion, this trade-off between energy efficiency and stability may be an inevitable result of peripheral mechanics of general legged locomotion. This suggests that energy consumption cannot be the complete objective function that legged animal locomotion minimizes; strictly minimal energy consumption may jeopardize stability. Assuming evolution as optimizing the probability of reproduction [55], reliable performance based on robust locomotor stability, which has a negative correlation with minimal energy consumption, should be included in the objective function. Indeed, the impulsive and energy dissipating interaction between a foot and ground is a common characteristic of almost all legged animal locomotion.

Energy Dissipation Is Necessary but Not Sufficient

The stability of the rimless spoked wheel model is based not only on the energy dissipating foot-ground collision but also on the constant amount of work done by gravity in each step. Generally, energy dissipation by itself does not guarantee asymptotic stability of periodic gaits; a

counter example is presented in [56]. The lost energy should be properly compensated for by actuation and proper control.

2.1.3. Comments on Lyapunov Stability

Lyapunov stability is well-defined and widely used in various fields of dynamics and control. Stability analysis in this thesis is also based on the definition of stability in the Lyapunov sense. However, it is necessary to clarify the limitation of Lyapunov stability. A dynamical system which is stable in the Lyapunov sense may be vulnerable to a small perturbation in practice. In this section, an example illustrates the limitation of Lyapunov stability.

I constructed a spring pendulum model under gravity. A point mass m is restrained by a spring whose stiffness and unloaded length are k and l_0 respectively. Figure 2-7 shows the schematic of the model and definitions of state variables. I derived equations of motion using Lagrangian approach. The constraint is holonomic, and all the active forces are conservative. Therefore, all non potential generalized forces are zero. Let the generalized coordinates be (l, θ), and Lagrangian be L.

$$L = T - V \text{ , where}$$

$$T = \frac{1}{2}m\{\dot{l}^2 + (l\dot{\theta})^2\} \text{ , and } V = \frac{1}{2}k(l - l_0)^2 - mgl\cos\theta .$$

$$\Rightarrow L = \frac{1}{2}m\{\dot{l}^2 + (l\dot{\theta})^2\} - \frac{1}{2}k(l - l_0)^2 + mgl\cos\theta .$$

Because non potential generalized forces are zero, $\dfrac{d}{dt}\dfrac{\partial L}{\partial \dot{q}} - \dfrac{\partial L}{\partial q} = Q = 0$,

$$\frac{d}{dt}\frac{\partial L}{\partial \dot{l}} - \frac{\partial L}{\partial l} = 0 \Rightarrow \ddot{l} - \dot{\theta}^2 l + \frac{k}{m}(l - l_0) - g\cos\theta = 0 \text{ , and}$$

$$\frac{d}{dt}\frac{\partial L}{\partial \dot{\theta}} - \frac{\partial L}{\partial \theta} = 0 \Rightarrow l\ddot{\theta} + 2\dot{l}\dot{\theta} + g\sin\theta = 0 .$$

39

Figure 2-7: A spring pendulum model

The state of the model can be described by length l and angle θ. To assess the stability of a periodic motion, a discrete return map is defined. One cycle ends when the angle becomes $2n\pi$, where n is a positive integer.

To analyze existence and stability of a periodic motion using the same method I used for walking models, I defined a Poincaré map whose input and output are the state vectors at the end of one cycle and the next cycle respectively. I defined the end of one cycle as the moment when the spring crosses the section of $\theta = 2n\pi$, where n is a positive integer. As the equations of motion are 2nd order ODEs in 2 DOFs, a 4-dimensional vector ($\mathbf{x} = (l, \dot{l}, \theta, \dot{\theta})$) is required to describe the model dynamics, and the Poincaré section is defined in 3-dimensional state space Σ, which is

$$\Sigma = \{(l, \dot{l}, \dot{\theta}) \,\big|\, \theta = 2n\pi, \text{where } n \in \mathbf{N}\}.$$

To find a periodic motion, a normalized error between initial state vector and state vector after one cycle was defined, and a periodic motion minimizing the norm of the error was searched for by numerical optimization. The optimization and numerical integration of the equations of motion were implemented in MATLAB R2006a (Mathworks Inc.). The periodic motion should yield zero difference between the neighboring cycles; the criterion for termination of the optimization was that the norm of the normalized error should be smaller than 10^{-8}. Absolute error tolerance and relative error tolerance for the numerical integration were 10^{-8}. Parameter values were chosen as $m = 1$ kg, $l_0 = 0.9$ m, and $k = 500$ N/m. Numerical optimization found periodic motions.

40

Figure 2-8 shows the state variables of a periodic motion.
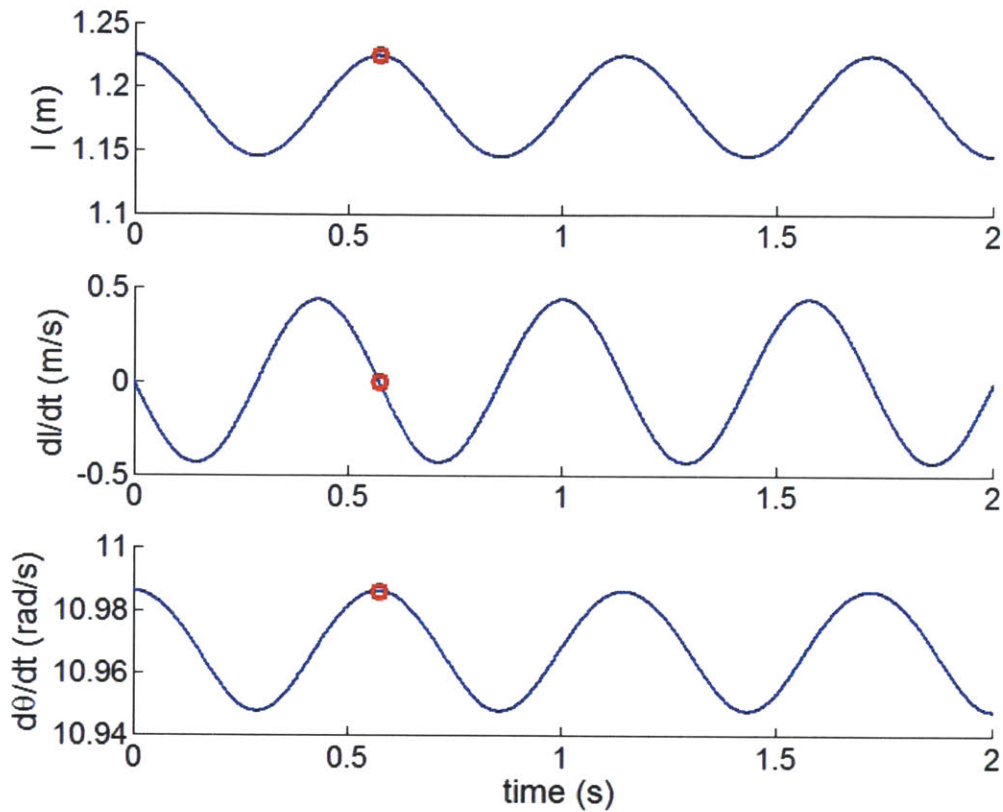
Figure 2-8: A periodic motion of the spring pendulum model
The state variables of a periodic motion are plotted. The red circle mark indicates the end of the first cycle.

Stability of this periodic motion was numerically analyzed in 3-dimensional Poincaré section. In the linearized stability analysis, the eigenvalues of the derivative matrix of the Poincaré map (**D**) were found as $\lambda_1 = 1.0000$ and $\lambda_{2,3} = -0.4538 \pm 0.8910\,i$; all eigenvalues have magnitude of 1.0000 or 0.9999, showing negligible numerical difference from unity. In fact, this spring pendulum model is Hamiltonian which has only conservative forces and is only constrained by workless holonomic constraint. By virtue of the nature of Hamiltonian, this system cannot have exponential stability in any of the configuration variables. (The physics validates the

41

numerical scheme.)

  The error dynamics around the periodic motion is shown in Figure 2-9. Even with all the

eigenvalues on the unit circle, initial errors grow up to over 20 times after the first cycle. This is not

obvious considering the linearized dynamics; the relation between an initial error (ε) and the

resulting error at the next step (ξ) is approximated $\xi \cong \mathbf{D}\varepsilon = \mathbf{D}\sum_{j=1}^{m} v_j \mathbf{e}_j = \sum_{j=1}^{m} \mathbf{D}v_j \mathbf{e}_j = \sum_{j=1}^{m} v_j \lambda_j \mathbf{e}_j$, where

λ_j's are the eigenvalues of $\mathbf{D}$, the derivative of the return map, and $\mathbf{e}_j$'s and v_j's are the eigenvectors

of $\mathbf{D}$ and the corresponding scalar factors respectively. The magnitude of λ_j's directly determines the

error dynamics; with small λ_j, the error is not expected to grow much. However, Figure 2-9 clearly

shows the counter example. With all eigenvalues on the unit circle, the error grows by a factor of 20

in one cycle.
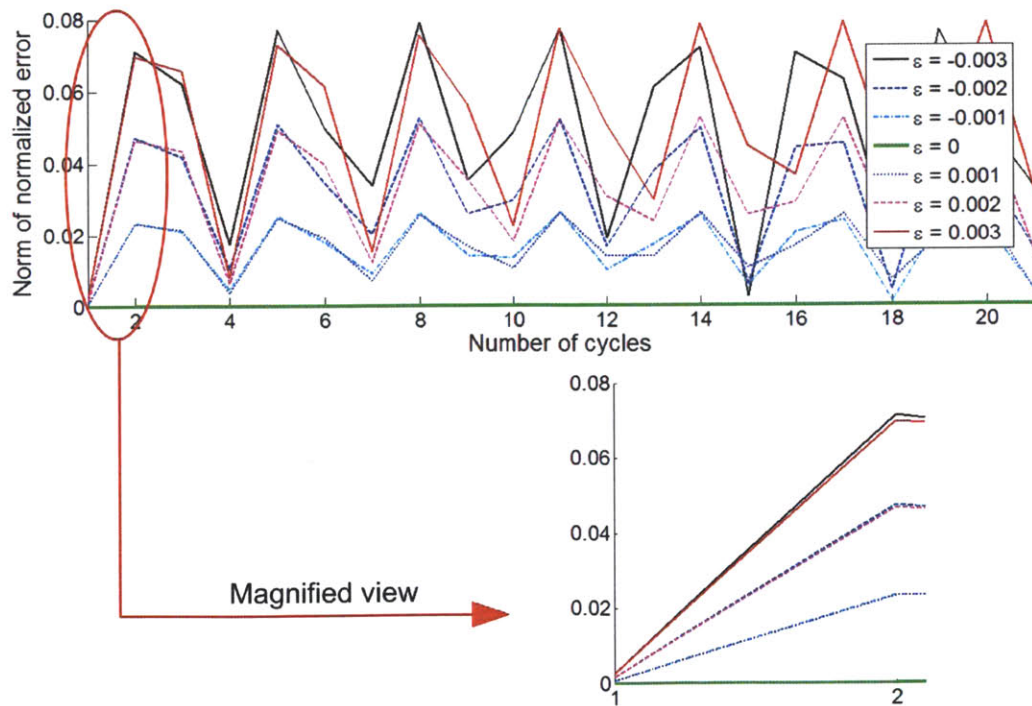
Figure 2-9: The error dynamics around a periodic motion of the spring pendulum
The initial error (ε) grows by a factor of 20 in the first cycle though the error is globally bounded
due to the nature of the system.

The derivative matrix of the return map, evaluated at the periodic motion is

$$\mathbf{D} = \begin{pmatrix} 0.37 & -0.015 & 1.13 \\ 23.46 & -0.45 & -42.21 \\ 0.46 & 0.011 & 0.17 \end{pmatrix}.$$

At the very next cycle, an initial error vector $\varepsilon = (\varepsilon, 0, 0)$ results in the error vector ξ as

$$\xi = \mathbf{D} \begin{pmatrix} \varepsilon \\ 0 \\ 0 \end{pmatrix} = \begin{pmatrix} 0.37 & -0.015 & 1.13 \\ 23.46 & -0.45 & -42.21 \\ 0.46 & 0.011 & 0.17 \end{pmatrix} \begin{pmatrix} \varepsilon \\ 0 \\ 0 \end{pmatrix} = \begin{pmatrix} 0.37\varepsilon \\ 23.46\varepsilon \\ 0.46\varepsilon \end{pmatrix}.$$

Comparing the norm, $\|\xi\| = \|\mathbf{D}\varepsilon\| = 23.47\|\varepsilon\|$. It is clear that the error growth by a factor of 23 with eigenvalues on the unit circle is not due to the ignored higher order terms in the linearized dynamics. This behavior remains same even for a perfect linear system of $\xi = \mathbf{D}\varepsilon$; it is solely due to the specific matrix $\mathbf{D}$.

To address the mode responsible for the magnified error, I decomposed the initial perturbation in the eigenvector space. The eigenvectors of the matrix $\mathbf{D}$ are

$$\mathbf{e}_{1,2,3} = \begin{pmatrix} -0.874 \\ -0.0002 \\ -0.4858 \end{pmatrix}, \begin{pmatrix} 0.0164\,i \\ 0.9998 \\ -0.0120\,i \end{pmatrix}, \begin{pmatrix} -0.0164\,i \\ 0.9998 \\ 0.0120\,i \end{pmatrix}.$$

Expressing $\varepsilon = (\varepsilon, 0, 0)$ using the set of eigenvectors as a basis,

$$\varepsilon \begin{pmatrix} 1 \\ 0 \\ 0 \end{pmatrix} = (-0.651)\varepsilon\mathbf{e}_1 + (-0.0001 - 13.17\,i)\varepsilon\mathbf{e}_2 + (-0.0001 + 13.17\,i)\varepsilon\mathbf{e}_3 ,$$

showing that the second and the third components are large enough to increase the initial error. This example illustrates that a small perturbation in the physical state space can be represented as a large

perturbation in the eigenvector space. Considering the linearized system of $\xi \cong \mathbf{D}\varepsilon = \sum_{j=1}^{m} v_j \lambda_j \mathbf{e}_j$, even

though the magnitudes of λ_j's are unity, large v_j's may induce a large error as in this system.

The initial growth of the error from the periodic motion of this spring pendulum is only due to the large scalar component of v_j's, and has nothing to do with the eigenvalues; the error growth cannot be exponential. As a result, the periodic motion (a fixed point of the Poincaré map) is stable in the Lyapunov sense because we can always define a δ-ball which confines the error in an ε-ball for an arbitrarily small ε. (E.g., under any given ε, the δ-ball may be defined to be 30 or 50 times smaller than the ε ball to satisfy Lyapunov stability.)

Consequently, this example of a spring pendulum reveals the weakness of Lyapunov stability. Error growth by a factor of 23 may not be acceptable in many practical situations. For example, for a walking robot, error growing that quickly may cause falling down, and for walking models, such error growth may cause either falling down or flying off by pushing the state of the model to the region that makes the ground reaction force negative.

This vulnerability can be especially critical for a marginally stable system. If a system is neutrally stable, the error is bounded but does not necessarily decrease as the system evolves. As in Figure 2-9, the initially imposed error resides in the system rather than vanishing, and the error can bounce back beyond some critical value while the system evolves. As applied to walking, this re-emphasizes the fragility of energy conservative walking models. In principle, the energy conservative walkers are marginally stable at best (with or without non-holonomic constraints). A rigorous stability analysis may conclude the bounded error dynamics and marginal stability in the Lyapunov sense, but the conservative walker may easily go outside a region in state space of reasonable walking due to the error magnified by a large scalar factor of an eigenvector.

Though a similar argument may apply to an asymptotically stable system including

walkers with energy dissipation and compensation, the impact of the possibly large scalar factor (v_j) should be significantly weak for an asymptotically stable system. For a system with asymptotic stability, by definition, the error should converge to zero as the system evolves. Particularly for a system with a hyperbolic fixed point (and asymptotic stability), the effect of the large scalar factor fades due to the exponential decay. Furthermore, for the walking models with one dimensional Poincaré sections and exponentially stable periodic gaits (including the previously illustrated rimless wheel model and the model in Chapter 6) the initially imposed perturbation can never grow as long as the linearized dynamics is dominant. (Limitation of the linearized analysis is a separate issue, which will not be covered in this section.) If the Poincaré section is one dimensional and the fixed point in the Poincaré section (the periodic motion) is hyperbolic and stable, the derivative matrix $\mathbf{D}$ is a real value scalar inside the unit circle. As a result, the error vector can not rotate but only converge to zero as the system evolves; the magnitude of the initial error only decreases.

To summarize, Lyapunov stability is a standard that is generally used in various dynamical systems including walking models, but has limitations. It may not be a sufficient condition for functional walking though it is a reasonable choice as a necessary condition; a system that satisfies Lyapunov stability may fail under a small perturbation in practice. This frailty may be especially crucial for conservative walkers which have marginal stability at best.

2.1.4. Importance of Foot-Ground Interaction

The preceding sessions demonstrated that robust stability of legged animal locomotion cannot be reproduced by energy conservative walkers, and therefore energy dissipation and compensation are mechanically essential to encapsulate the robust stability. In this session, the role of foot-ground interaction as an important mechanism stabilizing walking is illuminated. The

neurological significance of foot-ground interaction as a key mechanism regulating gait pattern is also reviewed along with its mechanical importance.

Non-Elastic Foot-Ground Collision Dissipates Kinetic Energy

As briefly mentioned in the review of the rimless wheel model in 2.1.1, the non-elastic foot-ground collision dissipates energy. The angular momentum principle with respect to the landing foot immediately explains this for the rimless wheel model. Let $\vec{H}$, $\vec{M}$, $\vec{r}$, $\vec{v}$ and $\vec{P}$ indicate angular momentum, applied torque about a specific point, a position vector from one point to another, a velocity vector and linear momentum respectively. Figure 2-10 shows the free body diagram of the rimless wheel model at the moment of collision; the impulsive ground reaction force is the only contact force. By the angular momentum principle about the foot-ground contact point B,

$$\frac{d}{dt}\overrightarrow{H_B} + \overrightarrow{v_B} \times \overrightarrow{P} = \overrightarrow{M_B} = \overrightarrow{r_{BC}} \times m\overrightarrow{g} \ .$$

Because the velocity of point B is zero, the second term on the left hand side vanishes, and

$$\overrightarrow{H_B}(t_{0+}) - \overrightarrow{H_B}(t_{0-}) = \int_{t_{0-}}^{t_{0+}} (\overrightarrow{r_{BC}} \times m\overrightarrow{g}) dt \ .$$

The right hand side equals zero because the time gap between t_{0-} and t_{0+} goes to zero, and the integrated term is not impulsive. Therefore, the angular momentum about point B is conserved during the collision;

$$\overrightarrow{H_B}(t_{0+}) = \overrightarrow{H_B}(t_{0-}) \ .$$

Assuming that the model finishes its inverted pendulum motion at t_{0-} and starts a new inverted pendulum motion about B at t_{0+}, the velocity of the point mass C can be written

$$\overrightarrow{v_c}(t_{0-}) = \overrightarrow{v_0} = (v_o \cos \alpha)\vec{i} - (v_o \sin \alpha)\vec{j} \ , \text{ and}$$

$$\overrightarrow{v_c}(t_{0+}) = \overrightarrow{v_1} = (v_1 \cos \alpha)\vec{i} + (v_1 \sin \alpha)\vec{j} \ ,$$

46

where $\vec{i}$ and $\vec{j}$ are the unit vectors directing right and upward respectively. From the conservation of angular momentum,

$$\vec{r_{BC}} \times m\vec{v_1} = \vec{H_B}(t_{0+}) = \vec{H_B}(t_{0-}) = \vec{r_{BC}} \times m\vec{v_0} \text{, or}$$

$$-(mlv_1)\vec{k} = mlv_0(\sin^2\alpha - \cos^2\alpha)\vec{k} = -(mlv_0\cos 2\alpha)\vec{k} \text{, resulting in}$$

$$v_1 = v_0\cos 2\alpha .$$

Therefore, the kinetic energy is reduced by a factor of $\cos^2 2\alpha$ due to the foot-ground collision.

Though this analysis is performed for a highly simplified model rather than actual bipedal walking of humans, the modeled mechanism of non-elastic collision and the resulting change of the velocity of the center of mass can be regarded as general features of foot-ground interaction of legged locomotion; the energy dissipating foot collision of the model may serve as a template of foot-ground interaction. Indeed, a recent experimental study reported that in human walking, muscles do more positive mechanical work than negative work even when walking at constant average speed on level ground, which uses counterbalancing phases of positive and negative work to maintain a constant average energy [57]. Considering that the effect of friction in muscles, tendons and joints are negligible especially for low frequency movement like stance or swing in walking [58-60], more positive muscle work than negative [57] suggests that the interaction with the environment is mainly responsible for the energy dissipation. For level ground walking, neglecting the ignorable drag force from the air, the energy dissipating foot-ground interaction is the only possible component that explains more positive work done by muscles. Indeed, work by Kuo et al. concluded that step-to-step transition due to foot-ground interaction is the most significant source of energy dissipation that is responsible for 60 to 70 % of the net metabolic cost of human walking at comfortable speed [61].
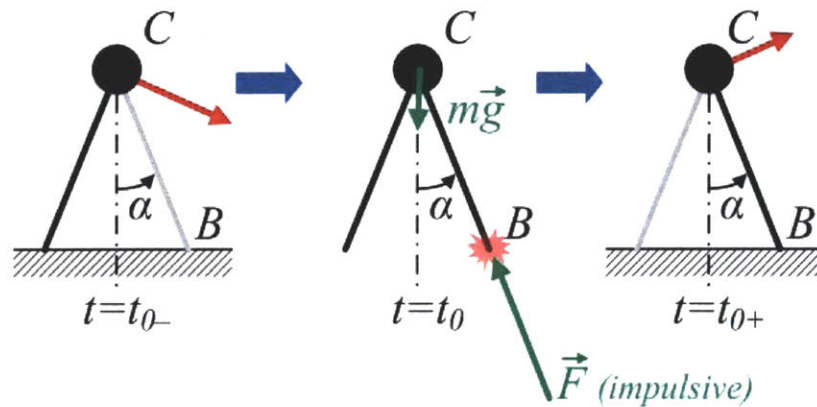
Figure 2-10: The free body diagram of the rimless wheel model at the moment of collision

To summarize, in normal human walking, foot-ground interaction dissipates kinetic energy, requiring more positive mechanical work than negative work to be done by muscles. This energy dissipating foot-ground interaction mechanically facilitates the robust stability of walking as in the rimless spoked wheel model.

Foot-Ground Interaction Provides Key Components of Gait Regulation

In addition to its mechanical importance in stable walking, foot-ground interaction provides a neurologically essential component in regulating gait pattern. Loading and unloading due to foot-ground interaction has been known as critical in the rhythmic pattern of walking of humans [62, 63] as well as cats [64, 65]. The load-related afferent information includes proprioceptive inputs from muscles and mechanoreceptors in ankle-foot complex. These afferent signals due to foot-ground interaction are plausibly integrated into the spinal reflex pathway and adapt the automated gait to the actual ground conditions [63]. In addition, cutaneous reflexes due to foot-ground contact may participate in the regulation of locomotion [66, 67]. All these afferent signals modulate the rhythmic pattern and reinforce muscle activity [63].

48

2.1.5. Minimal and Essential Energy Compensation via Ankle Actuation

As mentioned in 2.1.2, energy dissipation alone does not guarantee asymptotic stability of periodic gaits. Energy compensation is also essential; the lost energy should be compensated for by actuation and proper control. However, to exploit the natural oscillating dynamics of walking in the process of rehabilitation, the encumbrance should be minimized. Assistance in ankle actuation is the logical choice in this sense because ankle actuation is the most significant source of propulsive torque [68] and carries out the most portion of energy input (53 %) [69] during human walking.

Furthermore, the ankle is a distal joint, directly responsible for the control of foot-ground interaction whose importance in stable walking has been emphasized in the preceding sessions. Mechanically, the ankle-foot complex is the most distal actuator that is responsible for the direct interaction between the body and the ground. Neurologically, the ankle-foot complex contains receptors for afferent signals that are critical in regulation of locomotor pattern.

From 2.1.1 to 2.1.5, the essential components of stable walking have been discussed. Particularly, it has been demonstrated that energy dissipation and compensation are mechanically essential for stable walking. Please note that my analysis is confined to a mechanical model. It may be argued that energy dissipation and compensation may not be essential in normal human walking. For example, one may argue that normal human may achieve stable walking with negligible energy dissipation by use of neural control. However, an energy conservative system cannot be asymptotically stable under a perturbation that changes the energy level regardless of the control scheme unless the controller changes the energy level. The controller must be able to change the energy level to make the system asymptotically stable under an arbitrary perturbation. For example,

as a specific instance of *physical equivalence postulate* [70], when a proportional-derivative controller stabilizes a system under increased energy, the derivative component acts as a damper which dissipates the energy. Energy dissipation and compensation are required for robust stability of a system whether the system has a controller or not. In practice, the foot-ground interaction is not only the most significant source of energy dissipation [61], but also the only mechanism for energy dissipation that we can control in the physical therapy through mechanical interaction. In addition, the foot-ground interaction also provides a key neurological cue to regulate locomotor patterns. The neural control and mechanical process for stability are coupled in real animal locomotion.

Separate from neural control, addressing mechanically essential components of stable walking has its own value. Neurologically impaired population may not have intact neural control; it is critical to understand the minimal "mechanical components" of robustly stable walking to provide an effective rehabilitation strategy for neurologically impaired people. In a similar context, energy dissipation and compensation through mechanics facilitate the robust stability of walking, which may reduce the burden of neural control. The experimental study showing more positive mechanical work than negative work during normal walking [57] is consistent with the hypothesis that the central nervous system is taking advantage of the peripheral mechanics that stabilizes walking.

2.2. Hardware Criteria

As discussed in Chapter 1, the important limitation of current therapeutic robots for walking is that they do not allow 1) participation of the patients and 2) natural oscillating dynamics of walking by imposing pre-planned kinematics to the lower limbs of the patients. To allow the participation of the patients, which is known as essential for neuro-motor rehabilitation [6-8], the

actuators of the robot module must be back-drivable. One way to implement back-drivability is to design the actuators to have low end-point intrinsic impedance with low inertia and friction.

To allow the natural oscillating dynamics of walking, important degrees of freedom must not be confined by the robotic system. All current therapeutic robots do not satisfy this criterion. Lokomat, Haptic Walker, GEO system and Lokohelp Gait Trainer (Figure 1-2) all confine their assistance to the sagittal plane motion. However, joint torque and motion in frontal plane are significant in normal walking [68] and therefore cannot be ignored; mechanically frontal motion is critical to maintain balancing during locomotion. At a minimum, natural or voluntary motion in frontal plane must be considered.

Finally, as discussed in 2.1, the foot-ground interaction must be considered; the robot should be designed to allow the patients to learn how to interact with the ground and exploit the natural oscillating dynamics resulting from the interaction. Most current therapeutic robots do not satisfy this criterion. Haptic Walker, GEO system and Lokohelp Gait Trainer (Figure 1-2) impose the entire foot trajectory and do not allow the patients to learn proper interaction between the foot and the ground.

3. A Strategy: Entrainment to Ankle Mechanical Perturbation

In the preceding chapters, plausible sources of limitations of current robot aided therapy for walking were discussed and specific design criteria to resolve them were proposed based on the minimal relevant physics of stable walking. The natural oscillating dynamics of walking has to be considered and exploited in rehabilitation of walking, and energy dissipation and compensation through foot-ground interaction and ankle actuation have to be included in the rehabilitation strategy. In this chapter, a specific strategy of a novel gait training strategy is proposed based on those criteria. Motivated by the plausible role of nonlinear oscillators in human locomotor control, *entrainment with ankle mechanical perturbation* is proposed as a way by which robotic therapy exploits the natural oscillating dynamics of walking through the essential components, dissipating energy by foot-ground interaction and supplying energy by ankle actuation.

3.1. Motivation

Human walking shares some fundamental behaviors with nonlinear oscillators. In the aspect of dynamical systems, the rhythmic pattern of normal walking is well modeled as a limit-cycle of a nonlinear oscillator. Biologically, it is plausible that a rhythmic pattern generator or a CPG, the nervous system networks that are capable of generating a patterned muscular activity in the absence of supra-spinal control, participates in the human locomotor control, and a nonlinear oscillator is a competent model of the CPG.

Robotic experiments and theoretical studies have provided evidence showing the competence of simple nonlinear oscillators to exhibit stable bipedal walking. Passive dynamic walkers can startlingly mimic humanlike bipedal walking on a gentle slope with no control and no actuation [27, 52, 71]; the interaction between the inertial and the gravitational mechanics of legs and their intermittent impacts with the ground produces a nonlinear limit-cycle oscillation sufficient to yield remarkably coordinated walking. On the other hand, algebraic analysis proves that robustly sustained autonomous oscillation can only emerge from a nonlinear dynamical system; a linear system would be an overly simplified model of locomotion, which cannot have a robustly stable limit-cycle. While a linear spring interacting with a mass without friction exhibits oscillatory behavior, it is neither asymptotically stable nor robust. Robustly sustained autonomous oscillation emerges as a *limit-cycle attractor* from a nonlinear dynamical system such as a van der Pol oscillator [37].

Nonlinear limit-cycle oscillators not only encapsulate the robust and stable rhythmic motion of periphery in human walking but also serve as competent models of neural rhythmic pattern generators [34-36], which may play roles in human locomotion. Clear evidence of a rhythmic pattern generator (CPG) in various vertebrates [28-32] suggests plausible importance of a similar nonlinear oscillator in human locomotion. Theoretical studies supported the plausible role of a CPG in human locomotion by demonstrating stability of CPG driven bipedal walking [72, 73]. Additionally, Gerasimenko et al. reported that electromagnetic stimulation applied to unimpaired human vertebrae induced involuntary locomotor-like movements in a gravity neutral position [33], suggesting the existence of a CPG in human spinal cord. If a pattern generator plays a role in human locomotion as these observations suggest, it is logical to expect that we can manipulate human walking with a similar way that we influence nonlinear limit-cycle oscillators.

One of the distinctive characteristics of limit-cycle oscillators is that they may exhibit

dynamic entrainment (an observation credited to Christiaan Huygens in 1665 [74]) (Figure 3-1).
Under certain conditions they synchronize their period of oscillation to that of an imposed
perturbation, *phase-locking* to establish a particular phase relation with it. Usually entrainment
occurs only for a limited range of perturbation frequencies; it exhibits a *finite basin of entrainment*.
As a consistent observation, entrainment to mechanical perturbation has been reported in various
non-human vertebrates which show clear evidence of spinal pattern generators [29, 75-77].

Assuming that any form of a nonlinear limit-cycle oscillator plays a role in human
locomotion, I propose a new strategy of robot aided therapy for walking that exploits the essential
components of a stable walking and the resulting natural dynamics – *entrainment with ankle
mechanical perturbation*. The plausible choice of the robotic device and a scenario are described in
the following sessions.
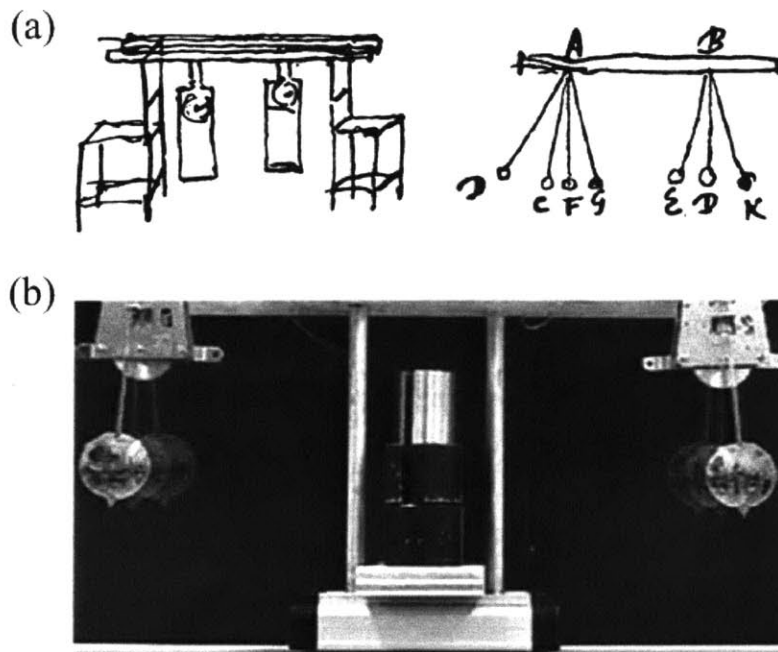
Figure 3-1: Entrainment of Huygens' clock
Entrainment was coined by Christiaan Huygens; (a) is the original drawing of Christiaan Huygens
illustrating his observation of pendulum clocks' synchronization. He observed that the two
pendulums stabilized in the same frequency, but in anti-phase as in (b). This phenomenon of
convergence of period is called entrainment.

54

3.2. A Plausible Therapeutic Robot

Anklebot [78] (Figure 3-2), a therapeutic robot module that assists ankle motion satisfies the design criteria discussed in Chapter 2. The actuators of Anklebot have low intrinsic static friction (less than 1 N·m) opposing ankle motion and are highly back-drivable. Anklebot interacts with the leg via a shoe and a knee-brace, and weighs 3.6 kg, but most of that mass is concentrated near the knee, minimizing the end-effect inertia during locomotion. In a recent study of 9 chronic stroke survivors who walked overground and on a treadmill with and without Anklebot mounted on the paretic leg, Anklebot had no significant effect on the spatio-temporal patterns of gait, even though that study was sufficiently sensitive to detect greater interlimb symmetry during treadmill walking [79]. This suggests that intrinsic impedance of Anklebot does not significantly affect human locomotion.

Figure 3-2: An unimpaired human subject wearing Anklebot while walking on a treadmill.

The assistive torque and impedance are controllable not only in sagittal plane but also in frontal plane motion. The motion in transverse plane is also allowed passively so that the robot allows the natural dynamics of walking, and does not confine any important degree of freedom as most current therapeutic robots do.

Use of Anklebot allows the patients to execute and (re-)learn foot-placement, and we can adjust the assistance to the ankle actuation to control the foot-ground interaction. Control of impedance and torque in multi-degree of freedoms also allows us to adjust the robotic assistance to promote the participation of the patients; Anklebot can provide assistance based on patients' performance.

3.3. Scenario

The specific scenario is as follows: Anklebot initially assists the patient at a preferred walking cadence, which is usually slower than normal cadence of an unimpaired person. Then periodic interaction is applied via the ankle to *entrain* the patient's cadence using Anklebot. With proper control, the robot can progressively increase the perturbation frequency to speed up the patient's cadence. In other words, the robot can drag the patient's gait toward normal cadence.

How this proposed strategy is distinct from the common approach of current robot aided therapy for walking may be highlighted by an analogy between walking and swinging. In fact, walking and swinging share some common features: both are periodic; interaction between inertia and gravity is important; and the intermittent actuation from external force drives the body to maintain the motion overcoming the energy dissipation. The typical and effective way we teach our children to play swing is to apply periodic perturbation. We add periodic mechanical work and let

the children take advantage of inertia and gravity. They gradually learn how to interact with the periodic dynamics and how to generate the proper periodic excitation to maintain or even amplify the periodic motion. The proposed approach of entraining gait to mechanical perturbation is similar to this and clearly distinct from "imposed kinematics" of current therapeutic robots, which is analogous to grabbing the body of the children and imposing the swinging motion.

4. Feasibility of Entrainment to Ankle Mechanical Perturbation of Unimpaired Subjects

In the previous chapter, a novel rehabilitation strategy of entrainment to ankle mechanical perturbation was proposed. This chapter demonstrates the experimental works to address the feasibility of the proposed strategy. It is also discussed that the experiments address the structure of human locomotor control which has been a primary problem in motor neuroscience.

4.1. Introduction

Understanding the global structure of human locomotor control has remained a primary problem in neuroscience, and the main challenge of this problem lies in the coexistence of diverse evidences supporting different control schemes. Though entrainment to mechanical perturbation as a rehabilitation strategy is motivated by limit-cycle behaviors of human walking, the importance of limit-cycle oscillators in human locomotor control is considerably less clear than the case of non-human vertebrates. Contrary to the unequivocal evidence of CPG in various animals [28-32], a primitive rhythmic stepping reflex of human infants [80] typically disappears at about 6 weeks after birth. When toddlers begin walking at about a year old, their initial gaits do not exhibit the rhythmic pattern of mature walking, and this cannot be ascribed to immature postural control [81].

In addition, there are evidences supporting the central control of limb kinematics rather than pattern generation through a semi autonomous limit-cycle oscillator. Walking in unimpaired adults is characterized by a remarkably repeatable spatial trajectory of the foot [25]. Patients with

spinal cord injury (SCI) who recovered following body-weight supported treadmill training also generated a foot trajectory that closely matched the normal pattern, although they used very different joint coordination patterns [82]. These observations support neural control of kinematics of the foot, plausibly maneuvered by supra-spinal structure. Combined with convincing evidences of neural control of hand kinematics in reaching movement [21-24], the conjecture of supra-spinal control of foot trajectory in human locomotion is consistent with the theory of motor coordination based on stochastic optimal feedback control [83].

Alternatively, execution of human locomotion through an autonomous system of periphery and spinal pattern generator is also plausible as discussed in 3.1. Gurfinkel et al. found locomotor-like stepping induced by continuous leg muscle vibration in unimpaired humans when they were suspended in a gravity-neutral position [84]. Gerasimenko et al. also reported that spinal electromagnetic stimulation applied to unimpaired human vertebrae induced involuntary locomotor-like movements in gravity-neutral position [33], suggesting the existence of a CPG in human spinal cord. In addition, the important role of load-related input and hip afferent input in generating human locomotor pattern [63], and the presence of the location specific information from the skin of the foot in cutaneous reflexes during human walking [85] suggest the contribution of semi-autonomous periphery with afferent feedback to control of human locomotion.

However, behavioral evidence of a semi-autonomous oscillator which is not necessarily mediated by supra-spinal structure but contributes to human locomotor control is still weak. For example, though spinally induced locomotor-like movements were observed in human [33, 84], the movements were observed in a gravity-neutral position, rendering it difficult to generalize the result to upright walking. In contrast, here I report behavioral experiments with walking human subjects.

In this study, subjects were asked to walk on a treadmill, and Anklebot applied periodic plantar flexion torque to the ankle. Entrainment and phase-locking were evaluated quantitatively to

address the feasibility of the proposed rehabilitation strategy. In the following sections, the experiments with unimpaired and neurologically impaired subjects are described in detail.

The experimental works in this chapter do not only test the feasibility of the proposed strategy of entrainment therapy but also address the primary problem of human locomotor control. Whether and to what extent human gaits can be entrained to mechanical perturbations may provide an assessment of the role of limit-cycle oscillators in human walking. For example, entrainment to mechanical perturbation may not be observed if locomotion is dominantly controlled by a central kinematic specification rather than semi autonomous periphery; entrainment would imply a steadily growing error between actual and specified kinematics which a stable kinematic controller would act to minimize. Conversely, if entrainment to mechanical perturbation is observed, it would support the feasibility of the proposed strategy and also suggest direct behavioral evidence of a non-negligible role of limit-cycle oscillators in human locomotor control.

4.2. Materials and Methods

Nineteen young adult subjects (ages 23 to 35) participated in the study. They reported no neurological or biomechanical impairment and gave informed consent to participate as approved by MIT's institutional review board. They walked on a treadmill at a self-selected comfortable speed while Anklebot applied a program of mechanical perturbations in plantar extension direction.

The time profile of ankle torque actuation was programmed at a sampling rate of 200 Hz with a precision ≤ 2.82 N·m. Onboard sensors measured ankle angles in both dorsi/plantar-flexion and inversion/eversion with a precision ≤ 1.5 degrees. A treadmill (Sole Fitness F80 with a 0.84 m × 1.90 m deck and 0.1 mph (0.045 m/s) belt speed resolution) was used. In some experiments, subjects wore acoustic noise-cancelling headphones (Bose QuietComfort 3).

4.2.1. Experimental Protocols

Experimental 1: Entrainment

To compensate for its possible effect on walking dynamics, throughout all trials Anklebot was programmed to act like a torsional spring and damper with constant equilibrium position, stiffness and damping. The equilibrium position was determined as the ankle angle when the subject stood upright. The stiffness was set as 5 N·m/rad, selected to approximate the stiffness necessary to compensate for the effect of Anklebot's inertia on the natural frequency of the body about the ankle. (Almost all of Anklebot's mass, approximately 3.6 kg, is concentrated around the knee at an average height of roughly 0.5 m above the ankle. Its inertia about the ankle is approximately 3.6×0.5^2 kg m^2. The average center of mass height of human adults is approximately 0.997 m [86], and the ratio of ankle stiffness to body mass during walking was estimated to be 5.73 N·m/rad-kg [87]. To keep the ratio of stiffness to inertia of walking with Anklebot comparable to walking without Anklebot, I approximated the Anklebot stiffness as 5 N·m/rad.) The damping was chosen empirically to be 1 N·m·sec/rad; minimal to avoid impeding walking yet sufficient to stabilize Anklebot.

Before applying periodic mechanical perturbations, each subject's preferred stride duration was measured. Subjects were instructed to walk on the treadmill at their preferred gait cadence while wearing Anklebot on one leg. Each subject adjusted the speed of the treadmill to be comfortable for walking, and this treadmill speed was maintained throughout the subsequent experimental session. Each subject's preferred stride duration (τ_0) was measured as the average duration of 15 successive strides.

After measuring τ_0, periodic square torque pulses of magnitude 10 N·m and duration 0.1 second were added to the torque due to the programmed spring-damper behavior. A magnitude of 10 N·m is comparable to 10% of maximum ankle torque during normal walking in adults [68], and 0.1 second is comparable to 10% of one stride duration in normal walking [88, 89]. Subjects were

instructed to continue walking until asked to stop. A trial began with a subject walking at preferred speed for at least 20 strides without perturbation. Then the experimenter initiated the periodic perturbation approximately coincident with the push-off portion of stance phase of the leg wearing Anklebot. Under computer control, Anklebot subsequently generated 30, 40 or 50 torque pulses at intervals of τ_P. Thereafter the torque pulses were discontinued (but the spring-damper behavior was maintained). Subjects continued walking for at least 20 strides before being instructed to stop.

On different trials the period of perturbation (τ_P) varied from lower to higher than τ_0, discretized with a resolution of 50 ms. The subject's preferred stride duration was rounded to the nearest 50 ms and adjusted by adding and subtracting 50 ms and 100 ms respectively to determine four initial perturbation periods. An additional 20 ms was added by the Anklebot controller. Thus for a subject with a preferred stride duration of 1416 ms, I determined initial perturbations with periods of 1320 ms, 1370 ms, 1470 ms and 1520 ms. These were applied in random order. If the first three perturbations showed clear evidence of a finite basin of entrainment (defined in Data Analysis) the fourth was omitted and the session ended. If four perturbations did not show clear evidence of a finite basin of entrainment, further perturbation periods were added. If subjects exhibited entrainment to the shortest (longest) perturbation period, on subsequent trials I further reduced (increased) the period in steps of 50 ms until entrainment was no longer observed. All 19 subjects participated in this experiment. For 2 subjects, τ_P was discretized with 100 ms intervals; for 5 subjects, τ_P was discretized with 25 ms intervals.

Experiment 2: Transient Phase Dynamics

To investigate the transient process by which entrainment and phase-locking were achieved, the protocol was revised as follows. A perturbation period was selected which had evoked entrainment in experiment 1. As before, subjects walked at preferred speed for at least 20 strides

62

without perturbation. Then the experimenter initiated the periodic perturbation, taking care that initiation occurred at one of a wide range of gait phases significantly different from the push-off portion of stance phase of the leg wearing Anklebot. Under computer control, Anklebot subsequently generated 80 or 100 torque pulses at intervals of τ_P. Thereafter the torque pulses were discontinued (but the spring-damper behavior was maintained). Subjects continued walking for at least 20 strides before being instructed to stop. Seven of the 19 subjects participated in this experiment.

Role of Auditory Feedback

When producing the square torque pulse, Anklebot made a small but perceptible noise. To assess and minimize the possible effect of auditory input on entrainment, 6 of the above 7 subjects were instructed to wear noise-cancelling headphones through which white noise was played during experiments 1 and 2. The volume of white noise was increased until subjects were unable to detect the noise made by Anklebot.

Role of Voluntary Intervention

To assess and minimize the likelihood of voluntary adjustment to the perturbation, 4 of the above 6 subjects (who wore noise-cancelling headphones) were asked to perform a distracting task, counting aloud backwards from 100 to 1 in their second language during experiments 1 and 2.

4.2.2. Data Analysis

The torque profile exerted by Anklebot and the kinematics of the ankle and knee wearing the device were recorded at a sampling rate of 200 Hz using the onboard sensors. A gait cycle was

defined from the knee angle data. Stride duration was compared before, during and after the perturbation in each trial. All statistical analysis was performed at a significance level of 5%

Gait Cycle

The knee angle profile was low-pass filtered with 7 Hz cutoff frequency. Landmarks in the gait cycle were estimated from extrema of the filtered profile: (1) maximum stance phase knee flexion, (2) maximum knee extension in terminal stance phase, (3) maximum swing phase knee flexion and (4) maximum knee extension adjacent to heel strike (Figure 4-1). For each stride, the knee angle profile was normalized to define a gait phase from 0 to 100 % with 0% as the moment of local maximum knee extension (4) following maximum swing phase knee flexion (3), based on the observation that (4) is adjacent to the initial loading or heel strike in normal walking [68, 89].

It is conventional to define initial loading or heel strike as 0% of gait cycle [68, 88, 89], and pressure sensors like foot switches directly measure the moment. Though knee angle data do not provide a direct measure of the heel strike, defining gait cycle using the knee angle may be advantageous in some aspects. First, considering that the perturbation torque is applied to the ankle foot complex, the force-related information at foot may not provide a reliable measure of the gait phase; kinematics of the other joints (e.g., a knee or a hip) may be relatively unaffected and therefore provide a better measure of the gait phase. Second, defining gait cycle based on knee angle reduces the number of necessary sensors, and accordingly reduces complexity and the set up time of the experiment; knee angle is directly measured from a potentiometer embedded in the knee brace for Anklebot.

Reliability of measuring initial loading phase based on knee angle data was tested. In Figure 4-2, the knee angle is superimposed on the pressure at toe and heel for unperturbed treadmill walking of one healthy subject. The local maximum knee extension after swing almost coincides

with the initial loading, indicating that knee angle provides a reliable measure of initial loading. Quantitative assessment with more healthy subjects was performed, and reliability of knee angle in defining heel strike was concluded; the details are described in Appendix C.

Defining initial loading based on knee angle heavily depends on the assumption that the gaits of subjects are stereotyped, which is valid for unimpaired subjects [89]. For impaired subjects, this method may not be valid due to their irregular movements. A footswitch is required to detect the initial loading phase and the gait phase might be further specified by onset of muscle activation if necessary. The detailed method to define gait cycle for impaired subjects is described in 5.1.
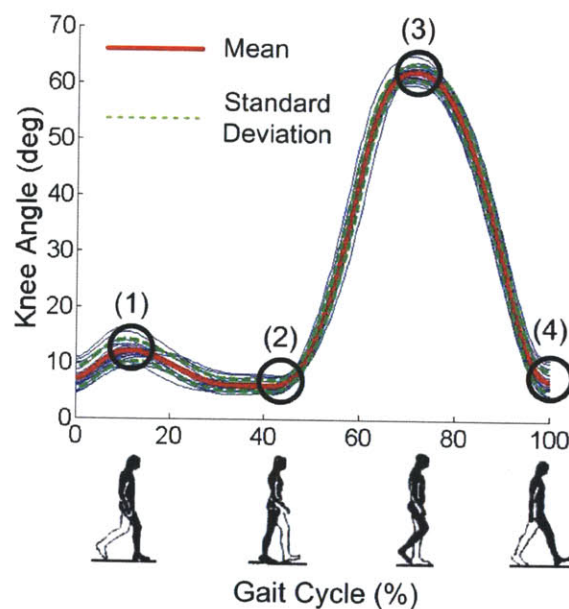
Figure 4-1: Typical knee angle as measured by Anklebot vs. phase (% of gait cycle). The miniature icons of a walker illustrate the corresponding phases of a gait cycle. Four extrema were identified from zero crossings of the knee angular velocity: (1) maximum knee flexion during stance phase, (2) maximum knee extension during terminal stance phase, (3) maximum knee flexion during swing phase and (4) maximum knee extension adjacent to heel strike.
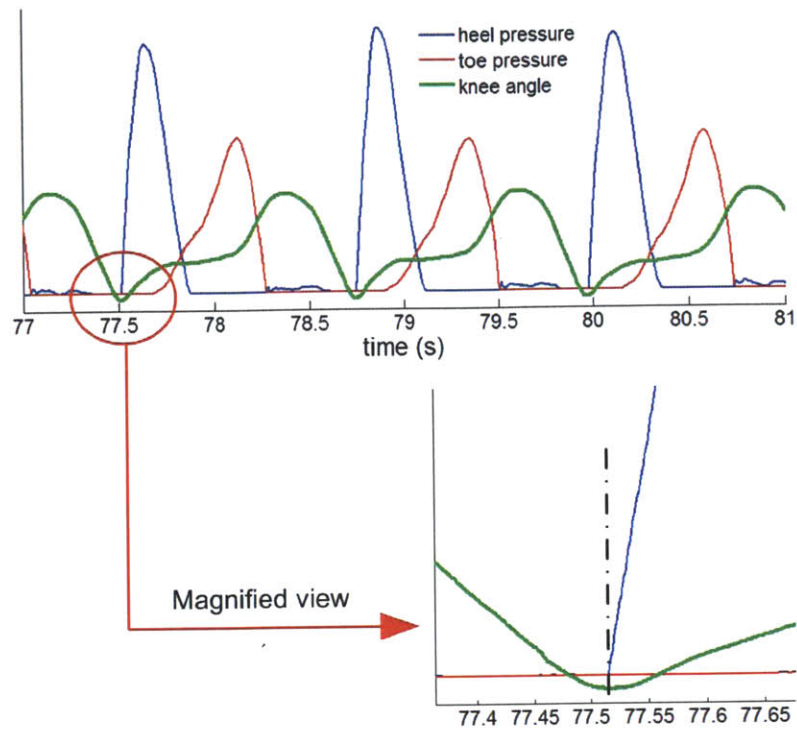
Figure 4-2: Knee angle, toe pressure and heel pressure of a normal gait of one subject
The local maximum knee extension (minimal knee flexion) after swing almost coincides with the rapid increase of heel pressure, which indicates the initial loading phase

Assessment of Entrainment

The torque perturbation was delivered at constant period throughout any one trial but the gait phase at which it occurred could vary (Figure 4-3). Entrainment requires gait to have the same period as the perturbation, which requires the perturbation phase to be independent of stride number. A linear regression of gait phase (Y) with respect to stride number (x) (i.e., $\mu_{Y|x} = \alpha + \beta x$) was performed on the last 15 strides when perturbation was present. Entrainment was assessed by testing whether slope (β) was different from zero. The null hypothesis, $H_0: \beta = 0$ was tested with 95% confidence and if accepted, entrainment was concluded. If H_0 was rejected, $\beta > 0$ was classified as "slow" perturbation; conversely, $\beta < 0$ was classified as "fast" perturbation.

66
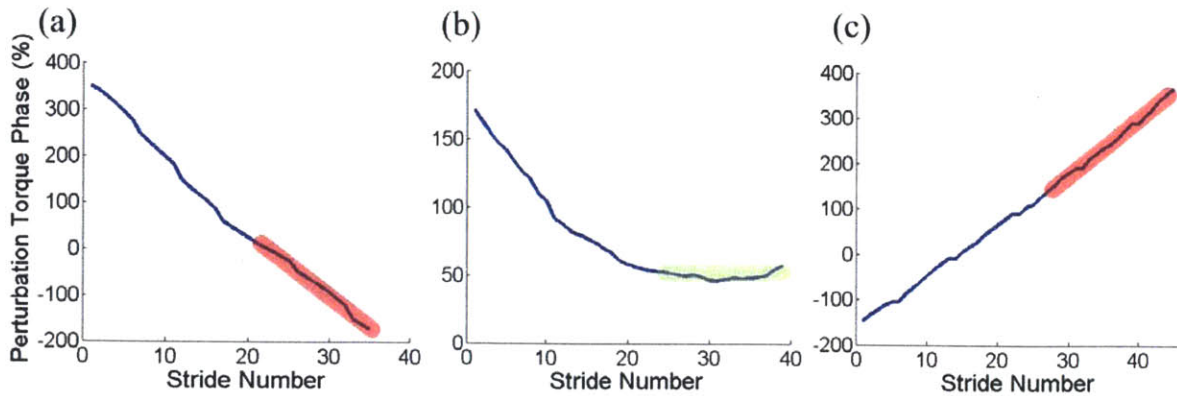
Figure 4-3: Phase of perturbation torque pulse vs. stride number plotted for three different trials Entrainment was determined by testing the null hypothesis H_0: $\beta = 0$ with 95% confidence level assuming $\mu_{Y|x} = \alpha + \beta x$ (x = stride number, Y = phase of perturbation pulse) for the last 15 strides during perturbation: (a) the 95% confidence interval of β is [-14.44 -12.76], hence $\beta < 0$: a fast perturbation; (b) the 95% confidence interval of β is [-0.186 0.456], hence H_0 is accepted: an entrained gait; (c) the 95% confidence interval of β is [12.15 13.37], hence $\beta > 0$: a slow perturbation.

After-Effect

If entrainment occurred, possible after-effects of the perturbation were assessed by comparing the durations of 15 successive strides immediately before the beginning of perturbation with 15 successive strides immediately after the end of perturbation. An after-effect was defined as a statistically significant difference between stride duration before and after perturbation with 95% confidence level.

Basin of Entrainment

The basin of entrainment was estimated from the highest and lowest perturbation periods that entrained gait. The upper (lower) boundary was assigned to the mid-point between the largest (smallest) perturbation period that entrained gait and the smallest (largest) perturbation period identified as slow (fast) perturbation.

67

Analysis of Phase Convergence

From the data of experiment 1 for each subject, the standard deviation, σ, of the gait phases at which the torque pulse occurred in the last 15 strides during perturbation of all entrained trials was determined. The distribution of these phases appeared Gaussian (Figure 4-9) hence about 95% of them were expected to lie within an interval $\pm 2\sigma$ wide. In experiment 2, the onset of phase-locking was determined by plotting the gait phase at which the torque pulse occurred as a function of stride number. A converged phase value, $\varphi_{converged}$, was found which made an interval $\varphi_{converged} \pm 2\sigma$ contain the greatest number of strides. In finding $\varphi_{converged}$, some strides were allowed to exceed this range provided that no more than 5% of the total number of perturbed strides did so in succession (Figure 4-10). The onset of phase-locking was determined as the first stride within the interval $\varphi_{converged} \pm 2\sigma$.

4.3.   Results

4.3.1.   Entrainment

Entrainment was observed in 18 of 19 subjects when the perturbation period, τ_P, was sufficiently close to the preferred stride period, τ_0. Typical results are presented in Figure 4-4, Figure 4-6, and Figure 4-5.

Before Perturbation

Table 4-1 shows preferred treadmill walking speed, stride duration (mean, standard deviation and coefficient of variation) and stride length (normalized by subject height) of 15

successive strides immediately before the beginning of perturbation individually for each subject and averaged over all subjects. The values observed were comparable to those typically reported for slow overground walking [90].

During Perturbation

If the period of perturbation was sufficiently short (Figure 4-4) or long (Figure 4-5) entrainment was not observed. Maximum knee flexion, which should occupy an almost constant phase of gait cycle, varied continuously with respect to the perturbation. In all, statistical analysis identified 46 trials out of 80 as not entrained. In 27 of those 46 trials, no significant difference ($p > 0.05$) between stride duration before and during perturbation was observed, indicating that the perturbation had little influence on gait in these cases.

Conversely, if the perturbation period, τ_P, was sufficiently close to the preferred stride period, τ_0, entrainment was observed (Figure 4-6). Subjects' gait adapted so that the phase at which the imposed torque pulse occurred converged to a constant. Statistical analysis identified entrainment in 18 of 19 subjects in one or more trials, and in 34 out of 80 trials overall. Entrainment also implied that the stride period converged to the perturbation period. Although the perturbation period always differed from preferred stride period, due to the variability of normal walking, the pre-perturbation stride period often deviated from the preferred period, so that entrainment did not always accompany a significant difference between stride duration before and during perturbation. However, a significant difference ($p < 0.05$) was observed for 20 of the 34 entrained trials.

After Perturbation

An after-effect, which was defined as a statistically significant difference ($p < 0.05$) between stride duration before and after perturbation, was detected in 11 out of 18 subjects who

showed entrainment. Nine of those 11 continued walking at the perturbation period, with no significant difference between stride duration during and after perturbation (as in Figure 4-6). Of the 20 entrained trials with a significant difference between stride duration before and during perturbation, 16 exhibited an after-effect. In 12 of those 16 trials, walking continued at the perturbation period with no significant difference between stride duration during and after perturbation (as in Figure 4-6). In the 4 remaining trials (from 2 subjects) the mean stride duration after perturbation was significantly different from its value during perturbation but lay between its values during and before perturbation. Representative data for each case are shown in Figure 4-7.
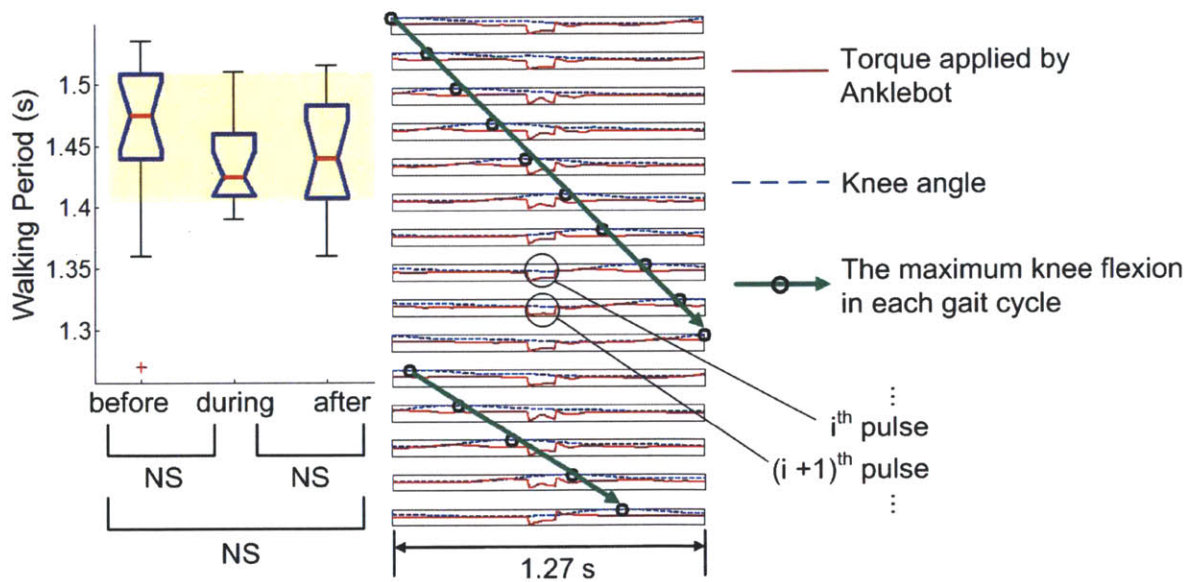
Figure 4-4: Typical results of a gait that did not entrain to "fast" perturbation ($\tau_P < \tau_0$)
The box plot shows the distribution of walking periods of the last 15 strides before perturbation, the last 15 strides during perturbation and the first 15 strides after the end of perturbation. The knee angle and the torque pulse imposed by Anklebot during the last 15 perturbation periods are plotted next to the box plot; each row indicates knee angle (the dotted blue curve) and Anklebot torque profile (the solid red curve) during one perturbation cycle. For each cycle, the phase of maximum knee flexion is identified (the black circle) and the trend of the maximum knee flexion phase is visualized with green arrow. Stride duration (shown in the box plot) did not change significantly due to the mechanical perturbations, and the phase of maximum knee flexion drifted continuously relative to the perturbation.
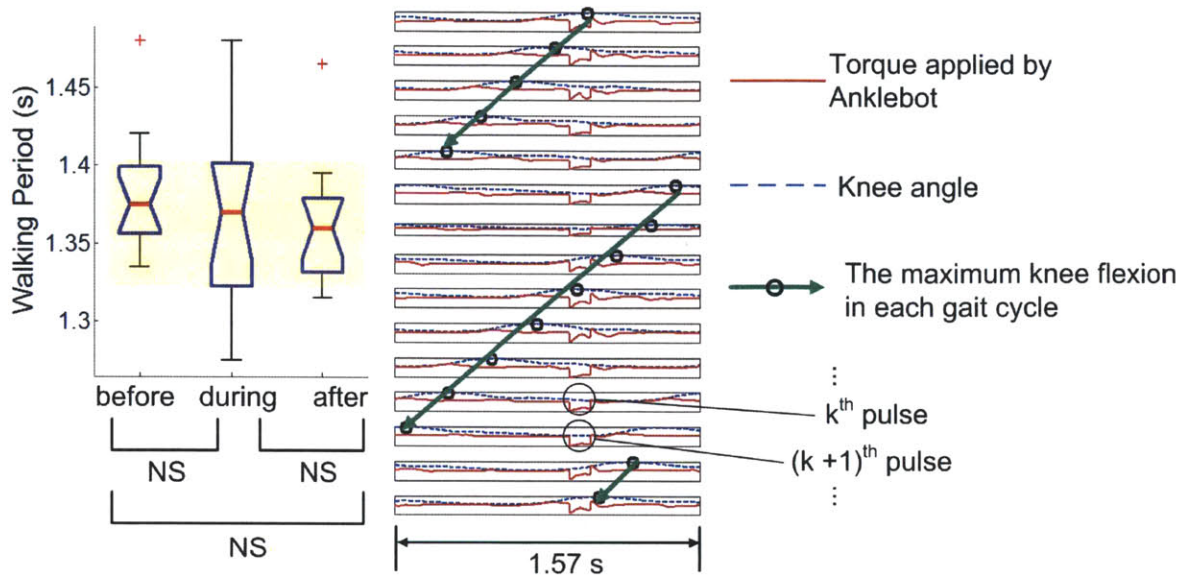
Figure 4-5: Typical results of a gait that did not entrain to "slow" perturbation ($\tau_P > \tau_0$)
Stride duration (shown in the box plot) did not change significantly due to the mechanical perturbations, and the phase of maximum knee flexion drifted continuously relative to the perturbation. The direction of the drifting is opposite to Figure 4-4.
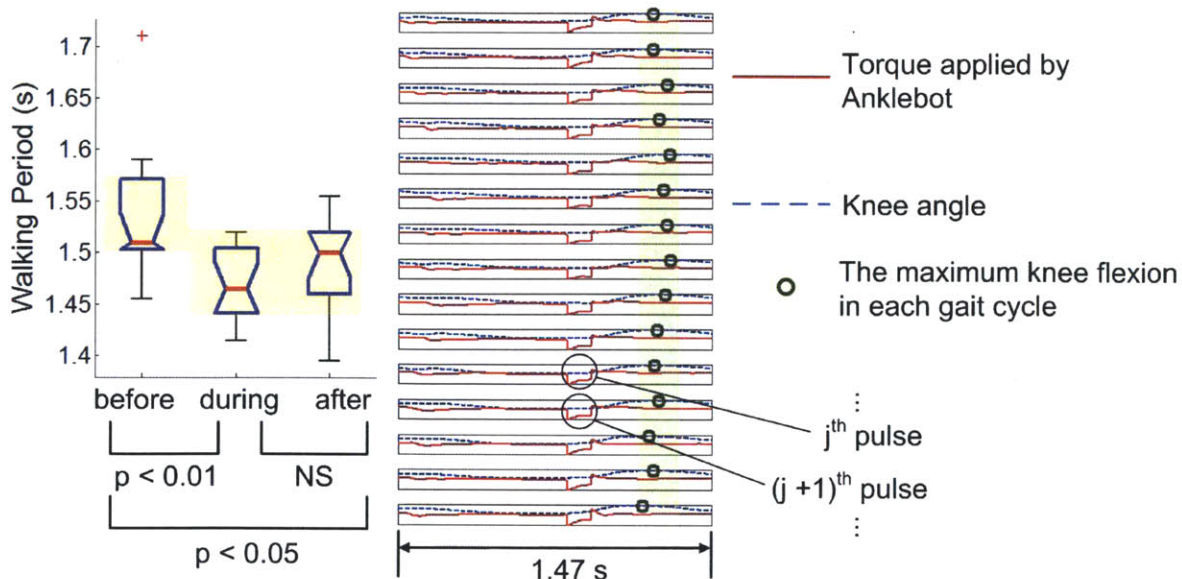
Figure 4-6: Typical results of a gait that entrained to perturbation
Stride duration (shown in the box plot) approximated τ_P with a statistically significant difference from the walking period before perturbation. The subject's cadence changed from the originally preferred value to synchronize with the periodic perturbation. The maximum knee flexion phase, which represents the gait phase, maintained a constant phase difference from the perturbation pulse instead of drifting relative to the perturbation pulse.

71

Table 4-1: Subjects' preferred speeds, walking periods and normalized stride lengths
Abbreviations – SD: standard deviation; CV: coefficient of variation (standard deviation / mean)

Subject ID (Gender)	Preferred treadmill speed (m/s)	Stride period before perturbation (s)			Anklebot on dominant leg	Stride length % Height
		Mean	SD	CV%		
1 (M)	0.99	1.44	0.074	5.1	No	80
2 (M)	0.81	1.40	0.025	1.8	No	65
3 (M)	0.81	1.20	0.038	3.2	No	53
4 (M)	0.86	1.31	0.063	4.8	No	62
5 (M)	0.99	1.20	0.020	1.7	No	65
6 (M)	0.81	1.54	0.059	3.8	No	69
7 (M)	0.99	1.28	0.031	2.4	No	71
8 (M)	0.95	1.21	0.033	2.7	No	63
9 (M)	0.90	1.24	0.031	2.5	No	63
10 (F)	0.90	1.22	0.030	2.5	No	66
11 (M)	0.99	1.33	0.033	2.5	No	74
12 (M)	0.86	1.45	0.043	2.9	Yes	68
13 (M)	0.99	1.23	0.026	2.1	No	67
14 (M)	0.95	1.32	0.048	3.6	Yes	70
15 (M)	0.77	1.64	0.037	2.3	Yes	72
16 (M)	0.77	1.67	0.049	2.9	Yes	73
17 (M)	0.9	1.47	0.078	5.3	Yes	73
18 (M)	0.77	1.50	0.071	4.7	Yes	62
19 (M)	0.99	1.19	0.028	2.3	No	71
All subjects	Mean = 0.89 SD = 0.086	1.38	0.16	Mean = 3.12 SD = 1.14	N/A	Mean = 68 SD = 5.9

(a)

(b)
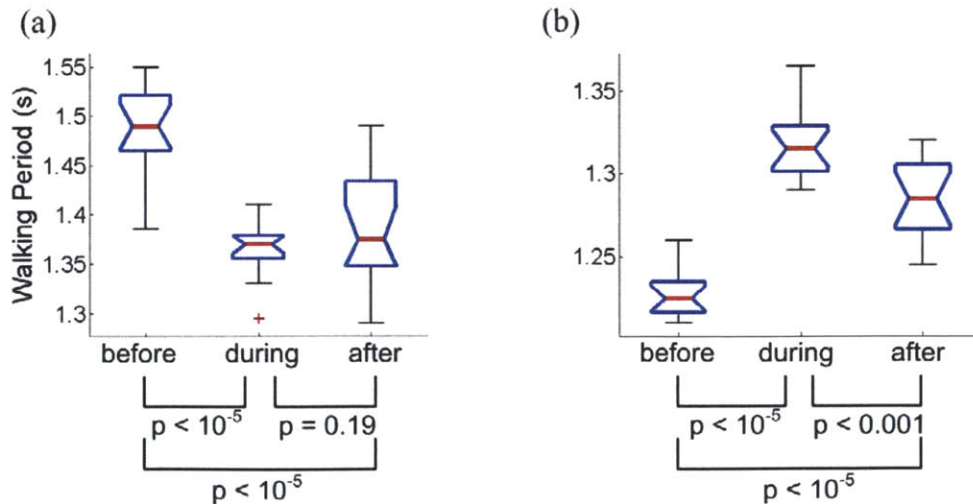
Figure 4-7: Two types of aftereffect
(a) significant difference between stride duration before and during perturbation, but no significant difference between during and after perturbation; (b) significant difference between stride duration before, during and after perturbation. For all trials classified into (b), the mean stride duration after perturbation lay between its during-perturbation and pre-perturbation values.

Finite Basin of Entrainment

The observation that entrainment only occurred if the perturbation period was sufficiently similar to the preferred stride duration indicates a *finite basin of entrainment*. Table 4-2 shows the basin of entrainment of each subject expressed as a percentage of the subject's average walking period before perturbation, τ_{before}. To compare it with the normal variability of walking, Table 4-2 also shows the basin of entrainment expressed as a percentage of a range containing 95% of the observed stride durations, four times the standard deviation of the subject's walking period before perturbation, σ_{before}. The mean basin of entrainment was 6.7% of the pre-perturbation walking period and 56% of its four-sigma range. Only one subject (#11) out of 18 exhibited a basin of entrainment wider than the variability of pre-perturbation walking, and then only by 10 %.

Table 4-2: Basin of entrainment normalized by walking cadence and its variability
The basin of entrainment was compared with the average walking period and four times the standard deviation of walking periods before perturbation. Nomenclature – τ_{before}: average walking period of last 15 strides before perturbation; σ_{before}: standard deviation of walking period of last 15 strides before perturbation. Abbreviation – SD: standard deviation.

Subject ID	Number of trials	$\dfrac{\text{Basin of entrainment}}{\tau_{before}}$ (%)	$\dfrac{\text{Basin of entrainment}}{4 \times \sigma_{before}}$ (%)
1	4	7.0	34
2	4	7.1	100
3	4	4.2	33
4	5	3.8	20
5	5	4.2	62
6	5	3.1	20
7	3	3.9	40
8	3	4.1	38
9	5	8.1	79
10	3	2.1	21
11	5	11	110
12	4	6.9	59
13	3	2.0	24
14	3	7.6	52
15	5	9.2	100
16	5	9.0	77
17	4	14	64
18	6	13	71
19	4	N/A	N/A
All subjects	80	Mean = 6.7 SD = 3.6	Mean = 56 SD = 30

Phase-locking

In principle, entrainment only requires a subject's stride duration to converge to the period of the perturbation. That is, the relative phase difference between gait and perturbation must converge to a constant, but it may be any constant. Remarkably, when gait was entrained, synchrony occurred at a specific phase was observed. This is termed *phase-locking*. Figure 4-8 shows the transient behavior of one subject. The phase on which the perturbation torque pulse converged is close to 50 % of the gait cycle. This is near the boundary between the terminal stance and pre-swing phases, and coincides with maximum ankle actuation in normal human walking [68].

Figure 4-9 (d) shows a histogram of the phase in gait cycle, φ_P at which the perturbation torque pulses occurred in the last 15 strides during perturbation of all entrained gaits. The average and standard deviation of φ_P were 50.2 and 3.80 (%) respectively. This narrow distribution justified the use of standard statistical tests based on a Gaussian distribution.

(a)

(b)

n^{th} pulse

$(n+1)^{th}$ pulse

1.17 s

0   50   100

Gait cycle (%)

——— Torque applied by Anklebot

– – – – Knee angle

—o→ The maximum knee flexion in each gait cycle

····► Phase of onset of torque pulse
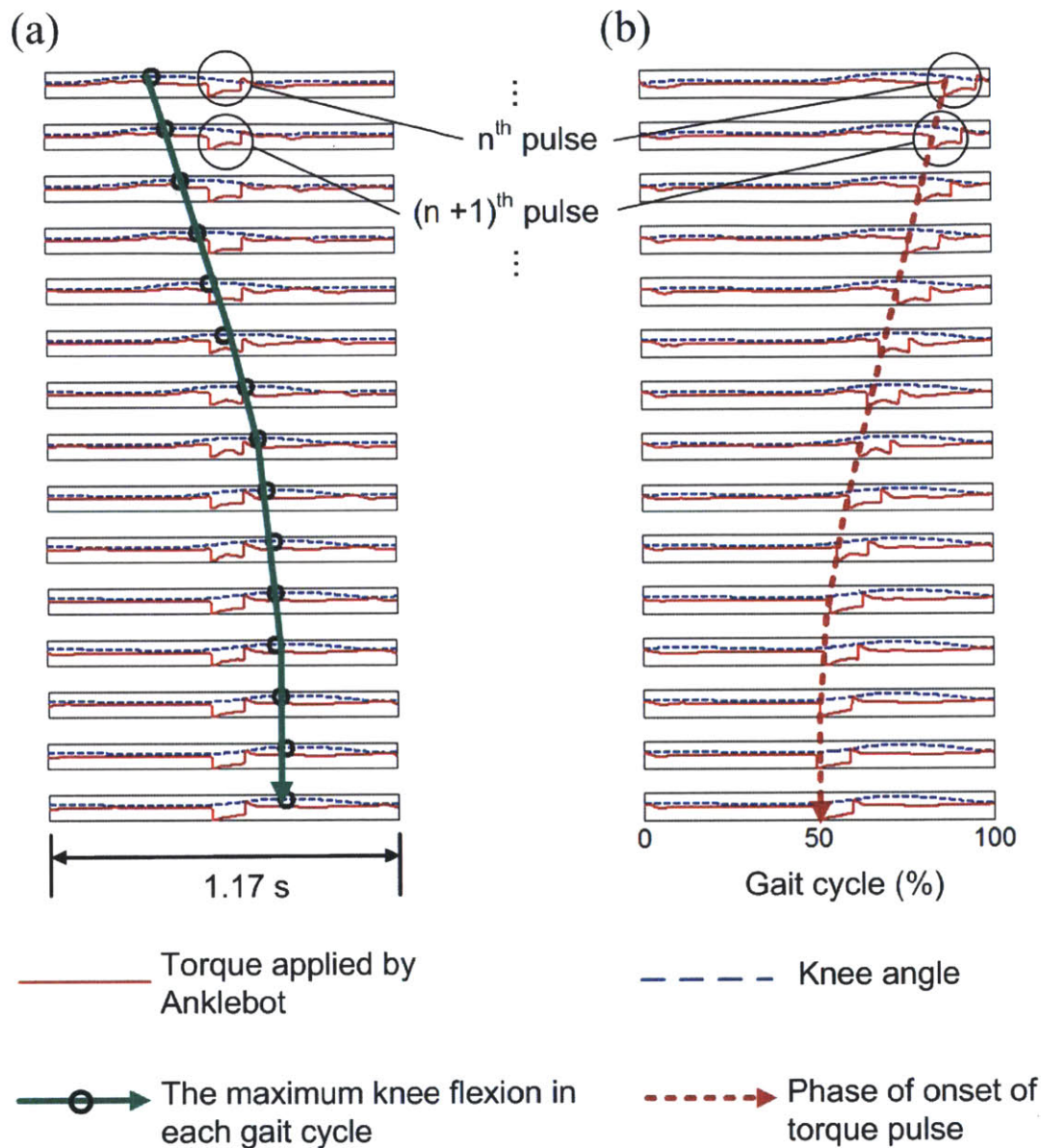
Figure 4-8: Transient behavior under perturbation

(a) shows the knee angle (the dotted blue curve), Anklebot torque profile (the solid red curve), and maximum knee flexion phase (the black circle and the green arrow) during the last 15 *perturbation cycles*, and (b) shows knee angle and Anklebot torque profile with the onset of torque pulse marked (the dotted brown arrow) during the last 15 *gait cycles* under perturbation. In (a), the maximum knee flexion which should occupy an almost constant phase of gait cycle drifted initially but converged on a specific phase of the perturbation cycle. The convergence is also shown in (b); the onset of torque pulse drifted initially, but converged on a specific phase of the gait cycle around 50 %.

75
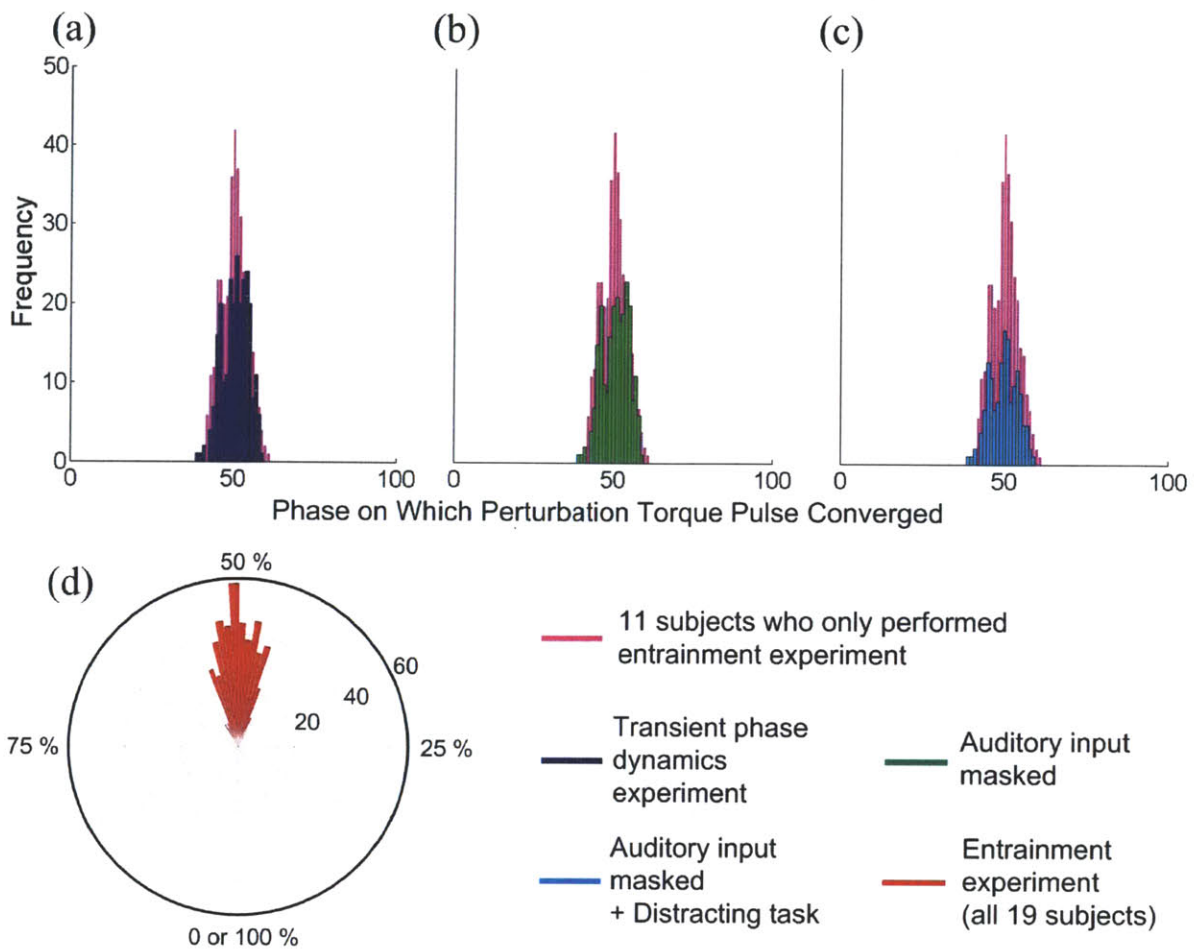
Figure 4-9: Histograms of the phase, φ_P at which perturbation pulses occurred in entrained strides. Purple bars in (a), (b) and (c) show the distribution of φ_P in the last 15 strides of all entrained trials of 11 subjects who only performed experiment 1. Superimposed on this histogram in (a) is the distribution of φ_P of phase-locked strides in experiment 2 (dark blue bars), in (b) with auditory input masked (green bars), and in (c) with auditory input masked and a distracting task (light blue bars). A polar ("rose") plot of the histogram of all entrained trails of all 19 subjects in experiment 1 is shown in (d) showing that the distribution occupied a narrow region of the gait cycle. Statistical analysis indicated no significant difference between these distributions in mean or standard deviation.

4.3.2. Transient Phase Dynamics

To test whether phase-locking was an artifact of initiating the periodic perturbation at the same approximate phase of gait, I performed experiment 2, initiating the periodic mechanical perturbation at phases far from ankle push-off. All seven subjects who participated in this experiment exhibited entrainment, and all seven showed phase-locking to the same narrow range of phase. A typical result is shown in Figure 4-10. The mean number of strides before phase-locking was 53 (106 steps) occupying more than one minute.
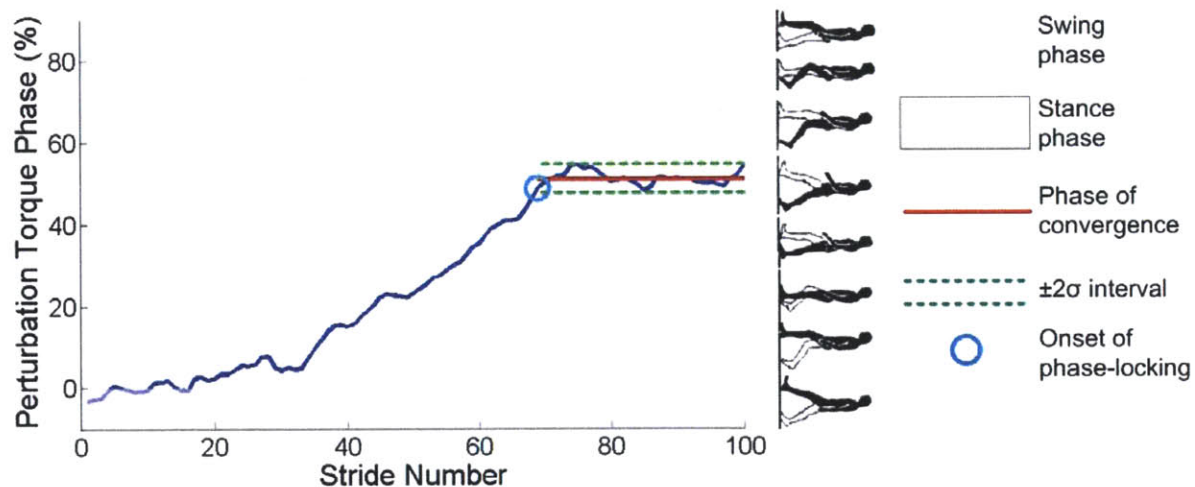
Figure 4-10: Phase of perturbation torque pulse vs. stride number in experiment 2
Nomenclature – σ: the standard deviation of the gait phases at which the torque pulse occurred in the last 15 strides during perturbation of all entrained trials of each subject in experiment 1. The phase of convergence and the onset of phase-locking were determined as explained in Data Analysis. The miniature icons of a walker illustrate the corresponding phases of a gait cycle. The initial perturbation pulse was applied just before the beginning of a double stance phase (-5 % gait cycle). Over 70 subsequent strides (140 steps) taking approximately 100 seconds, the subject gradually changed cadence to phase lock with the perturbation at 50 % gait cycle, approximately the maximum ankle-actuation phase of normal human walking.

The phase φ_P at which the perturbation torque pulses occurred was assessed for all strides after the onset of phase-locking. The mean was 50.7 %, the standard deviation 4.00 %; a histogram is shown in Figure 4-9 (a). The distribution of φ_P for experiment 2 was compared with the

distribution for the 11 subjects who performed experiment 1 only. An F-test assessed whether φ_P of these populations came from normal distributions with the same variance; a T-test assessed whether φ_P of the two populations had the same mean when the standard deviations were assumed equal. Both hypotheses were accepted with 95% confidence level.

4.3.3. Role of Auditory Feedback

To test whether entrainment and phase-locking were due to auditory feedback, 6 of the 7 subjects who participated in experiment 2 wore noise-cancelling headphones to mask auditory inputs during both experiments 1 and 2. Entrainment was identified in one or more trials for all 6 subjects, and the mean and standard deviation of φ_P in experiment 2 were 50.7 % and 4.14 % respectively (Figure 4-9 (b)), statistically indistinguishable from experiment 1.

4.3.4. Role of Voluntary Intervention

To test whether entrainment and phase-locking were due to voluntary intervention, four of the 6 subjects were instructed to perform a distracting task, counting backward from 100 to 1 in their second language during both experiments 1 and 2. Entrainment was identified in one or more trials for all four subjects, and the mean and standard deviation of the distribution of φ_P in experiment 2 were 49.8 % and 4.13 % respectively (Figure 4-9 (c)), statistically indistinguishable from experiment 1.

4.4. Discussion

4.4.1. Semi-Autonomous Oscillator in Normal Human Walking

In this study, direct evidence of semi-autonomous oscillators in normal human walking was observed. First, robustly sustained oscillation (what von Holst referred to as *Beharrungstendenz* [91]) requires nonlinear dynamics; nonlinear oscillators serve as competent models of semi-autonomous biological systems exhibiting rhythmic motion including CPGs [34-36]. Second, entrainment (what von Holst referred to as *Magneteffekt* [91]) is a distinctive characteristic of nonlinear oscillators. Entrainment was first reported by Huygens in 1665 [74] as an interaction between the periods of two clocks, but a closely related phenomenon can be observed as the response to a strictly periodic perturbation, and that was the approach of this study. Periodic pulses of plantar-flexion torque were applied while subjects walked at constant speed on a treadmill. This entrained the gait of 18 of 19 subjects. Furthermore, phase-locking was observed; the perturbation assisted plantar-flexion near the ankle push-off phase. To my knowledge, these observations provide the first direct behavioral evidence that some form of nonlinear neuro-mechanical oscillator participates in upright human locomotion.

The results suggest the hypothesis that motor control of locomotion in humans is hierarchically organized to implement *central supervisory control of a semi-autonomous periphery*. The essence of supervisory control [92, 93] is that the "operator" (the supra-spinal nervous system) has the *option* to intervene directly in the detailed control of "low-level" system behavior (the spinal neuro-mechanical periphery) but—importantly—need not do so continuously. Instead, it only intervenes when need arises (e.g. to react to a stumble or place a foot on a target). In this hypothesis, the neuro-mechanical periphery is conceived to be *semi-autonomous*: it is capable of robustly stable rhythmic walking with minimal central intervention. That requires a nonlinear oscillator because

robustly sustained autonomous oscillation can only result from a nonlinear dynamical system. In consequence, the neuro-mechanical periphery would exhibit behavior characteristic of limit-cycle oscillations, including a tendency to entrain to periodic perturbations and converge to a constant phase-locked relation with them, just as observed in this study.

Supervisory control of a semi-autonomous physical system is proven engineering technology, introduced to minimize the computational burden of control and mitigate detrimental effects of delays due to remote (tele-) operation, especially in space exploration [93, 94]. Applied to human motor control, the key idea is that, because of the limited response speed of muscles and the substantial delays due to neural conduction, *the supra-spinal nervous system tele-operates the neuro-mechanical periphery*. Supervisory control is a plausible compromise that allows the neuro-mechanical periphery to operate semi-autonomously to unburden the supra-spinal nervous system, yet reserves the option of central intervention as needed to offset the limitations of a semi-autonomous periphery.

Effects of Experiment Apparatus and Protocols on Results Are Not Significant

Although differences between treadmill and overground walking have been reported [95], they are subtle, and many studies have employed treadmills as in this study. Anklebot was used to deliver mechanical perturbation. However, as mentioned in 3.2, Anklebot is highly back-drivable with a low intrinsic impedance, and wearing Anklebot itself has shown no significant effect on the spatio-temporal patterns of gait even for chronic stroke survivors [79].

For practical reasons, perturbations were applied at periods 50 ms apart. This necessarily limited the resolution with which I could detect a basin of entrainment and may account for the single exceptional subject for whom entrainment was never observed. To minimize uncontrolled variables, all measurements in a single experimental session were made at a constant treadmill

speed selected by the subject. Entrainment typically required stride duration to change to synchronize with the periodic perturbation. As treadmill speed did not change, this required a compensatory change of stride length. Consequently, anatomical considerations (e.g. leg length) determined an upper limit on the perturbation period to which entrainment might be observed. However, no anatomical factor would determine a lower limit. The observed narrow basin of entrainment (Table 4-2) does not seem to reflect these anatomical constraints.

Voluntary Adaptation or Entrainment to Auditory Stimuli Cannot Account for the Results

When generating torque pulses, Anklebot made a perceptible periodic sound. Unimpaired humans may synchronize their motions with periodic sounds. However, synchronization to sounds can occur over a wide range of periods—consider the various cadences of fast and slow dancing—while I observed entrainment only over a very narrow range, 6.7 % of preferred gait cadence (Table 4-2). Furthermore, I observed no change when auditory stimuli were masked by white noise played through noise-cancelling headphones. Entrainment to periodic auditory stimuli cannot account for these observations.

If entrainment was voluntary, most normal walking frequencies should have been entrained. In contrast, it was observed that the basin of entrainment was narrower than the typical variability of preferred cadence (Table 4-2). Furthermore, voluntary adaptation of gait would be expected to occur within a small number of steps. In contrast, I observed a long, slow convergence to achieve phase-locking, occupying as many as 70 strides (140 steps) over a minute and a half or more (Figure 4-10). Finally, when subjects performed a distractor task, no change in entrainment behavior was observed. Voluntary adaptation is not a plausible explanation for the results.

Though involuntary adaptation mediated supra-spinally by afferent feedback may not be

81

ruled out, the weight of evidence is consistent with some combination of peripheral neuro-mechanical factors—oscillatory neural networks (e.g. in the spinal cord); afferent sensory feedback; musculo-skeletal dynamics; and the physical environment.

4.4.2. Potential Feasibility of a Novel Entrainment Therapy

Though observed in unimpaired subjects, entrainment to the periodic mechanical perturbation supports the promise of the novel strategy for gait rehabilitation; based on a patient's performance, a robot may be programmed to entrain the patient's walking cadence and gradually "drag" it towards the normal walking cadence. In such a way, rehabilitation by entraining the embedded oscillator might provide an essential but hitherto neglected element of walking therapy by exploiting the natural dynamics of walking; instead of mimicking the kinematic patterns of leg motion and interfering with normal execution of locomotor function, the role of interaction between the neuro-muscular periphery and gravito-inertial mechanics may be considered and capitalized on.

The entrainment to mechanical perturbation is distinct from entrainment to auditory input in that mechanical interaction may supply the additional power that may be needed to enable more normal gait especially when the patients cannot produce enough propulsion. By controlling not only the frequency but also the amplitude of the supplementary torque, we can also continuously adjust the robotic assistance to promote patient participation, which has proven to be an essential component of neuro-restoration [6-8]. In addition, if an embedded neural oscillator interacting with peripheral musculo-skeletal mechanics plays a prominent role in the entrainment to mechanical perturbation, this approach may be able to promote recovery without a significant involvement of supra-spinal control including auditory feedback. In particular, rehabilitation after spinal cord injury may also be feasible. Even in the case that entrainment of supra-spinal central nervous system to the

periodic afferent stimuli is mainly responsible for the entrainment to mechanical perturbation, the proposed strategy holds potential to provide effective therapy for patients with neurological impairments other than spinal cord injury. To test further the feasibility of the proposed approach of entrainment to mechanical perturbation as a rehabilitation strategy of robotic walking therapy, I performed similar experiments with neurologically impaired subjects the experimental procedures and the results are presented in the next chapter.

5. Feasibility of Entrainment to Ankle Mechanical Perturbation of Neurologically Impaired Subjects

In the previous chapter, the feasibility of a novel rehabilitation strategy of entrainment to ankle mechanical perturbation was assessed by the experiments with unimpaired subjects. This chapter demonstrates the experimental works with neurologically impaired subjects to further assess the feasibility of the proposed approach as a rehabilitation strategy.

5.1. Materials and Methods

Three stroke patients (ages 51 to 71) and one Multiple Sclerosis (MS) patient (age 48) participated in the study. They gave informed consent to participate as approved by the institutional review board of MIT's Committee on the Use of Humans as Experimental Subjects and the Providence Veterans Affairs Medical Center (PVAMC) where the experiments were conducted. They walked on a treadmill at a self-selected comfortable speed while Anklebot applied a program of mechanical perturbations in plantar extension direction on the sagittal plane.

The time profile of ankle torque actuation was programmed at a sampling rate of 200 Hz with a precision ≤ 2.82 N·m. Onboard sensors measured ankle angles in both dorsi/plantar-flexion and inversion/eversion with a precision ≤ 1.5 degrees. A treadmill (Woodway Loko S55 with a 0.55 m $\times$ 1.57 m walking surface and 0.02 m/s belt speed resolution) was used.

Figure 5-1: Experiment with a neurologically impaired subject
The experiment was conducted in the research facilities of Providence Veterans Affairs Medical Center (PVAMC)

5.1.1. Experimental Protocols

As in the experiment with healthy subjects (4.2.1), to compensate for its possible effect on walking dynamics, throughout the entire session, Anklebot was programmed to act like a torsional spring and damper with constant equilibrium position, stiffness and damping. The equilibrium position was determined as the ankle angle when the subject stood upright. The stiffness was set as 5 N·m/rad, selected to approximate the stiffness necessary to compensate for the effect of Anklebot's inertia on the natural frequency of the body about the ankle. (Almost all of Anklebot's mass, approximately 3.6 kg, is concentrated around the knee at an average height of roughly 0.5 m above the ankle. Its inertia about the ankle is approximately 3.6×0.5^2 kg m^2. The average center of mass height of human adults is approximately 0.997 m [86], and the ratio of ankle stiffness to body mass during walking was estimated to be 5.73 N·m/rad-kg [87]. To keep the ratio of stiffness to inertia of walking with Anklebot comparable to walking without Anklebot, I approximated the Anklebot stiffness as 5 N·m/rad.) The damping was chosen empirically to be 1 N·m·sec/rad; minimal to avoid impeding walking yet sufficient to stabilize Anklebot.

Before applying periodic mechanical perturbations, each subject's preferred stride duration was measured. Subjects were instructed to walk on the treadmill at their preferred gait cadence while wearing Anklebot on the more affected side. Each subject adjusted or asked one of the experimenters to adjust the speed of the treadmill to be comfortable for walking, and this treadmill speed was maintained throughout the subsequent experimental session. Approximate value of each subject's preferred stride duration (τ_0) was measured using a stopwatch; an experimenter visually detected the moment of heel strike of the leg wearing Anklebot, and then took the average interval of 10 successive heel strikes.

After measuring τ_0, periodic square torque pulses of magnitude 10 N·m and duration 0.1 second were added to the torque due to the programmed spring-damper behavior. The period of

perturbation (τ_P) was initiated at the estimated value of preferred stride duration, τ_0. After 20

perturbation cycles, the perturbation period gradually decreased by 50 ms over 10 cycles and then

held at that period ($\tau_P = \tau_0 - 50$ ms) over 20 perturbation cycles. This procedure of gradual decrease

and hold of τ_P was repeated until τ_P became noticeably faster than the cadence of the subject's gait.

Subjects were instructed to continue walking until asked to stop. This procedure is depicted in

Figure 5-2.
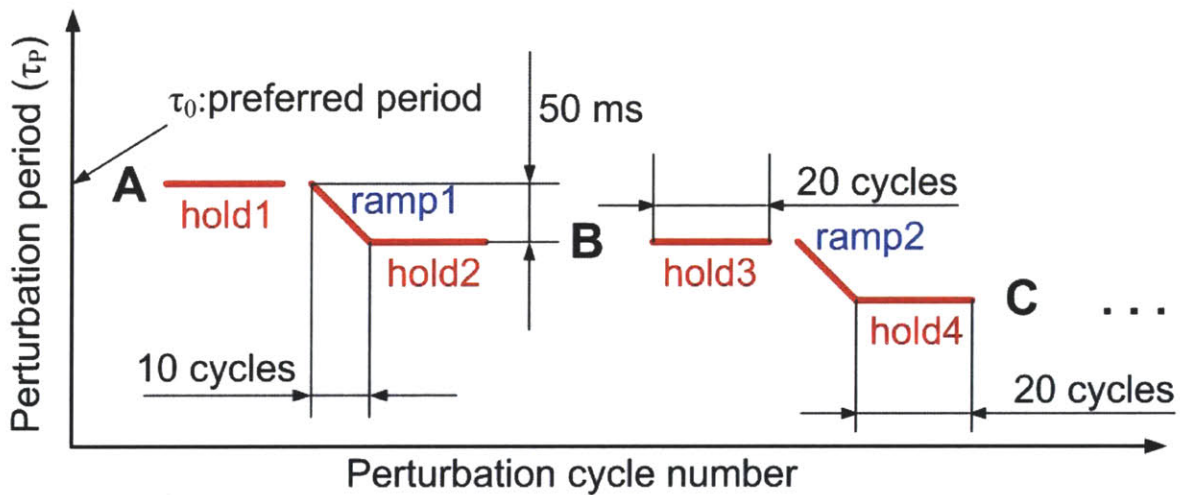
Figure 5-2: Scheme of perturbation applied in the experiment with impaired subjects
The subject walked without periodic perturbation (A). Then, Anklebot applied square torque pulses
with period τ_0, the subject's preferred walking cadence. After 20 perturbation pulses, another
sequence of perturbation pulses whose interval decreased linearly with cycle number was applied
over 10 cycles until the interval became $\tau_0 - 50$ms. This sequence was immediately followed by
another set of perturbations whose period was constant over 20 cycles. No perturbation was applied
for the following 20 strides (B). After that, the same program of perturbation was initiated with the
last value of τ_P of the previous sequence. (For the cycles just before C, the period of the perturbation,
τ_P was $\tau_0 - 100$ms.) This program was continued until the experimenter visually observed that the
subject could not keep up with the perturbation cadence. Segments of constant perturbation period
were labeled as hold1, hold2 etc, and segments of gradual change in perturbation cadence were
labeled as ramp1, ramp2 etc.

5.1.2. Data Analysis

The torque profile exerted by Anklebot and the kinematics of the ankle and knee wearing the device were recorded at a sampling rate of 200 Hz using sensors onboard Anklebot. In addition, foot contact, knee angle of the less impaired side, and activation of 8 muscles (Tibialis anterior, Peroneus longus, Gastrocnemius and Soleus of both legs) were respectively measured by pressure sensors at the toes and heels of both feet, a goniometer, and electromyography (EMG) sensors at a sampling rate of 1000 Hz using a wireless Myomonitor IV system by Delsys Inc. Heel strike of the paretic leg was defined as 0 (or 100) % of each gait cycle. All statistical analysis was performed at a significance level of 5%

Gait Cycle

It is conventional to define initial loading or heel strike as 0% of gait cycle [68, 88, 89]. In the experiment with healthy subjects, knee angle profile successfully estimated the moment of heel strike. However, the success of measuring initial loading using knee angle heavily depended on that the gaits of the subjects were stereotyped, which might not be valid for neurologically impaired walking. In this study, instead of relying on the knee kinematics, pressure sensors at heel of the paretic side directly measured the heel strike of the leg wearing Anklebot.

The typical data acquired by the pressure sensor at a heel of the paretic side of a neurologically impaired gait are shown in Figure 5-3. The onset of the rapid increase of the foot switch signal indicates the initial loading phase. To detect these moments systematically, the onset of the increase was estimated as an intersection between the baseline signal and a linear approximation of the rapid increase (Figure 5-4). The baseline was measured as a mean value of the signal for a relatively flat region, (1) of Figure 5-3. Though the signal from foot switch varies even

in those regions, the fluctuation is considerably small compared with the range of the signal. The linear approximation of the rapid increase was evaluated using 5 successive points centered at a point closest to a threshold. The threshold was determined high enough to avoid any improper measure due to the small hills during swing phase ((3) of Figure 5-3) but low enough to locate the center point close to the actual onset of the rapid increase.

It might be argued that different threshold may cause different estimation of the initial loading phase. However, the effect of threshold on the estimation of the initial loading phase is negligible by virtue of two reasons. First, the rapid change of the foot switch signal around the heel strike is almost linear. Therefore, the intersection point is not sensitive to the location of the center of the linearization. Second, the slope of the rapid increase of the pressure is steep; the difference in the center point of the linearization can change the estimation of a phase only to a negligible extent.
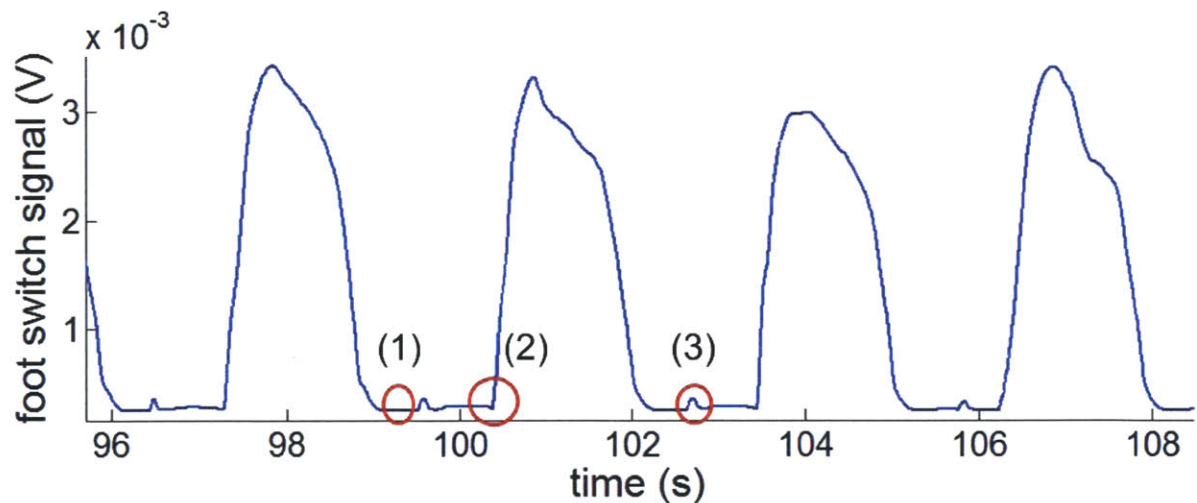
Figure 5-3: Typical data from the pressure sensor at a heel of the paretic side
The signal is relatively flat when the heel is detached from the ground and the center of pressure moves to the frontal foot: (1). When the initial loading occurs after swing phase, the pressure increases rapidly: (2). There are some small hills during swing phase: (3), which may be due to the interaction between the shoe and the heel.
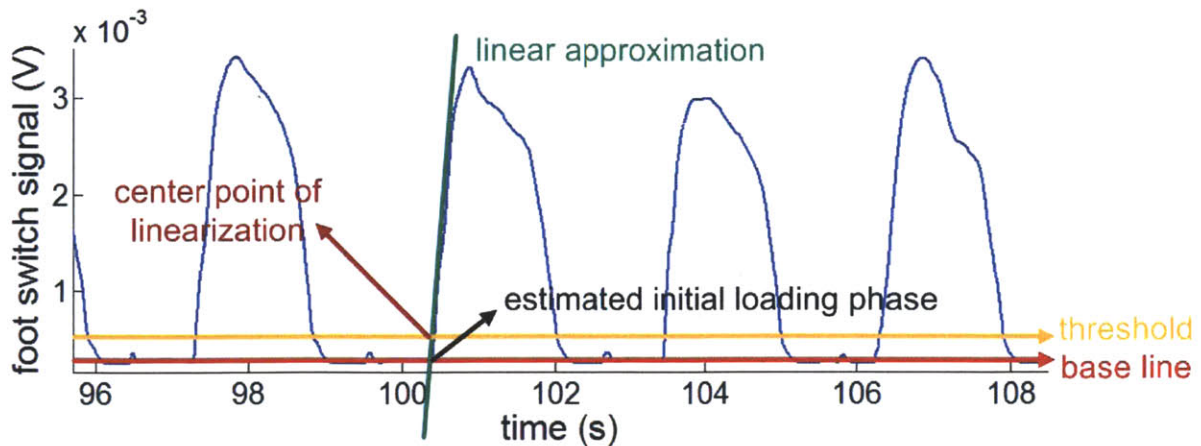
Figure 5-4: Determination of initial loading from the pressure sensor signal
The initial loading phase is estimated as an intersection between the baseline signal of no contact between heel and ground (red) and a linear approximation of the rapid increase (green) which is evaluated based on 5 successive points centered at a point closest to a threshold (orange).

Assessment of Entrainment

Entrainment was assessed in each segment of constant perturbation period (hold1, hold2 etc. in Figure 5-2) and gradual change of perturbation cadence (ramp1, ramp2 etc. in Figure 5-2). Entrainment requires the perturbation phase to be independent of stride number. A linear regression of gait phase (Y) with respect to stride number (x) (i.e., $\mu_{Y|x} = \alpha + \beta x$) was performed on the last 10 strides of each segment with perturbation. Entrainment was assessed by testing whether slope (β) was different from zero. The null hypothesis, H_0: $\beta = 0$ was tested with 95% confidence and if accepted, entrainment was concluded. If H_0 was rejected, $\beta > 0$ was classified as "slow" perturbation; conversely, $\beta < 0$ was classified as "fast" perturbation.

After-Effect

If entrainment occurred, possible after-effects of the perturbation were assessed by comparing the durations of 10 successive strides immediately before the beginning of perturbation

90

with 10 successive strides immediately after the end of perturbation. An after-effect was defined as a statistically significant difference between stride duration before and after perturbation with 95% confidence level.

5.2. Results

One stroke patient (Stroke 1) and one MS patient (MS 1) completed the whole session without significant difficulty. One stroke patient (Stroke 2) exhibited the sign of fatigue and experimenters stopped the session before completion. One stroke patient (Stroke 3) expressed fatigue and requested to stop the procedure before completion.

Table 5-1: Subjects' preferred speeds, walking periods and duration of the session
Abbreviations – SD: standard deviation; CV: coefficient of variation (standard deviation / mean). The comfortable gait speeds of comparably aged unimpaired subjects, ② were obtained from [96].

Subject ID (gender)	Preferred treadmill speed (m/s) ①	Stride period before perturbation (s)			Age	Comfortable mean speed of comparably aged unimpaired subject (m/s) ②	Ratio of ①/② (%)	Range of knee angle (deg)	Session duration (s)	Remarks
		Mean	SD	CV (%)						
Stroke 1 (M)	0.34	2.57	0.055	2.13	57	1.393	24.4	48.4	410	Completed the session
Stroke 2 (F)	0.16	2.30	0.314	13.7	51	1.393	11.5	15.7	490	Experimenters stopped the session
Stroke 3 (M)	0.16	3.48	1.08	30.1	71	1.330	12.0	36.4	300	Requested to stop the session
MS 1 (M)	0.18	3.39	0.298	8.79	48	1.462	12.3	45.9	530	Completed the session

5.2.1. Entrainment

All four subjects showed entrainment in one or more segments of constant perturbation period (hold1, hold2 etc. in Figure 5-2) or gradual change of perturbation cadence (ramp1, ramp2 etc. in Figure 5-2). Figure 5-5 shows the typical results of entrainment during segments of gradual change of perturbation cadence for those who completed the session (Stroke 1 and MS 1).
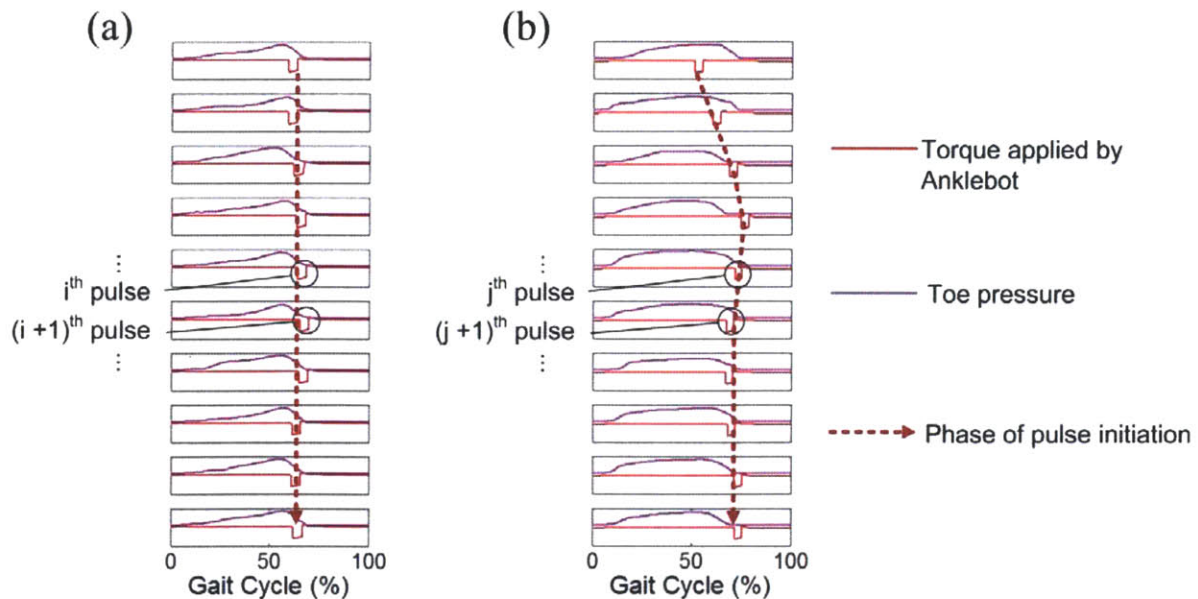
Figure 5-5: Entrained gaits of neurologically impaired subjects

The torque imposed by Anklebot (red) and the pressure at toe (violet) during the last 10 gait cycles are plotted; each row indicates one gait cycle and the cycle number increase from top to bottom. (a) and (b) show the gaits of Stroke 1 and MS 1 respectively. Both subjects completed the session, and the plotted data were obtained during the segments of gradual change of perturbation cadence; the perturbation cadence is faster in the lower gait cycles. The onset of the torque pulse converged to a specific phase of the gait cycle as visualized by the dotted brown arrows. The toe pressure shows that the phase where the robotic pulse locked is close to the toe-off phase (initiation of swing). Phase-locking indicates that the subjects gradually increased stride frequency to synchronize with the gradually increased perturbation frequency.

Before Perturbation

Table 5-1 shows preferred treadmill walking speed, stride duration (mean, standard deviation and coefficient of variation) of 10 successive strides immediately before the beginning of perturbation and session duration for each subject. Variability varies across the subjects.

During Perturbation

Entrainment was observed in all four subjects. Stroke 1 and MS 1 who completed the session showed entrainment for both constant period perturbation and gradually accelerating

92

perturbation. Stroke 2 who did not complete the session showed entrainment in the last segment of constant perturbation period, and Stroke 3 who did not complete the session showed entrainment in the last segment of gradual change of perturbation cadence.

As gaits entrained, the variability of the walking cadence noticeably reduced for all subjects except Stroke 1 who already showed small variability of cadence which was comparable to the variability of normal walking of healthy subjects. The highest walking speed (approximately double of others) and the lowest coefficient of variation (Table 5-1) indicate that Stroke 1 is a much less impaired subject compared to others. Figure 5-6 shows the change of range, interquatile range (IQR) and variance of walking cadence due to entrainment.
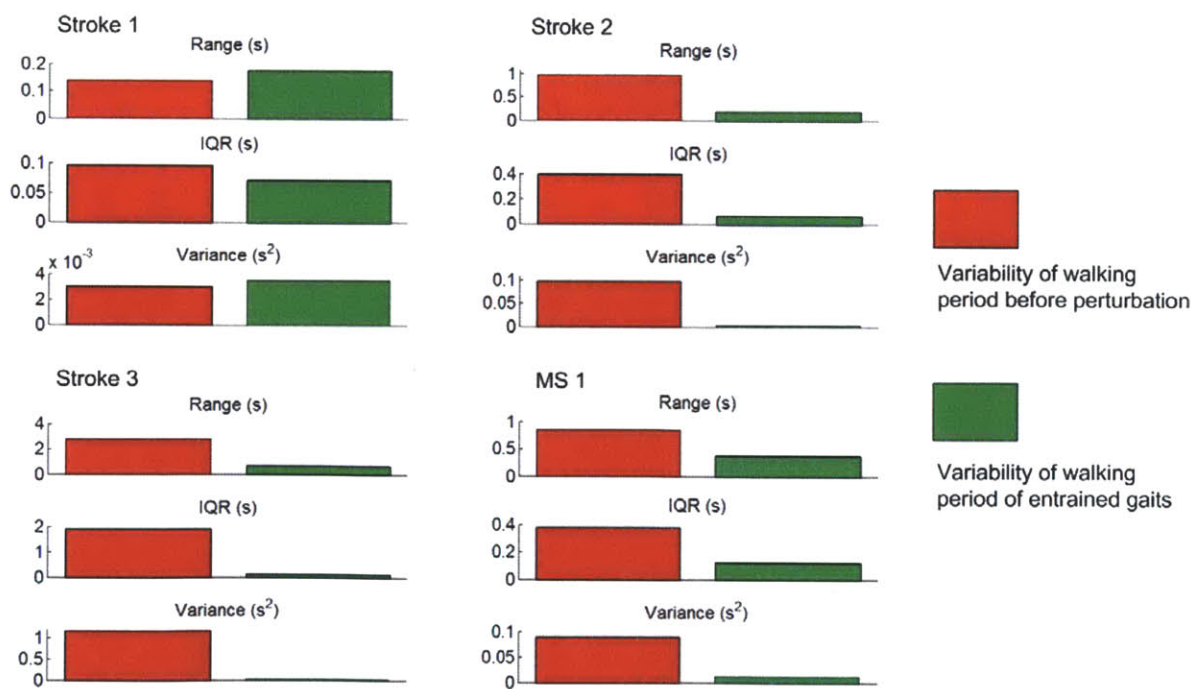
Figure 5-6: Change of variability of walking cadence due to entrainment
Variability of walking cadence was assessed by range, interquatile range (IQR), and variance. Entrainment reduced variability of walking cadence noticeably except for Stroke 1 who showed the sign of the mildest injury among all the four subjects: the highest walking speed and the lowest coefficient of variation among all the subjects.

After Perturbation

An after-effect, which was defined as a statistically significant difference ($p < 0.05$) between stride duration before and after perturbation, was detectable only for Stroke 1 and MS 1 who completed the session. Unfortunately, for Stroke 1, insufficient strides were recorded after the last perturbation, so the after-effect could not be assessed by comparing the stride duration before and after the entire set of perturbations. However, after-effect due to the perturbation was assessed by comparing the stride duration before the perturbation (A in Figure 5-2) and the stride duration after the second segment of constant period perturbation (B in Figure 5-2). For MS 1, more than 10 strides were recorded after the last perturbation, so the after-effect was assessed by comparing the stride duration before and after the entire set of perturbations. For both of the two subjects, walking cadence became significantly faster due to the entrainment with after-effects (Figure 5-7).
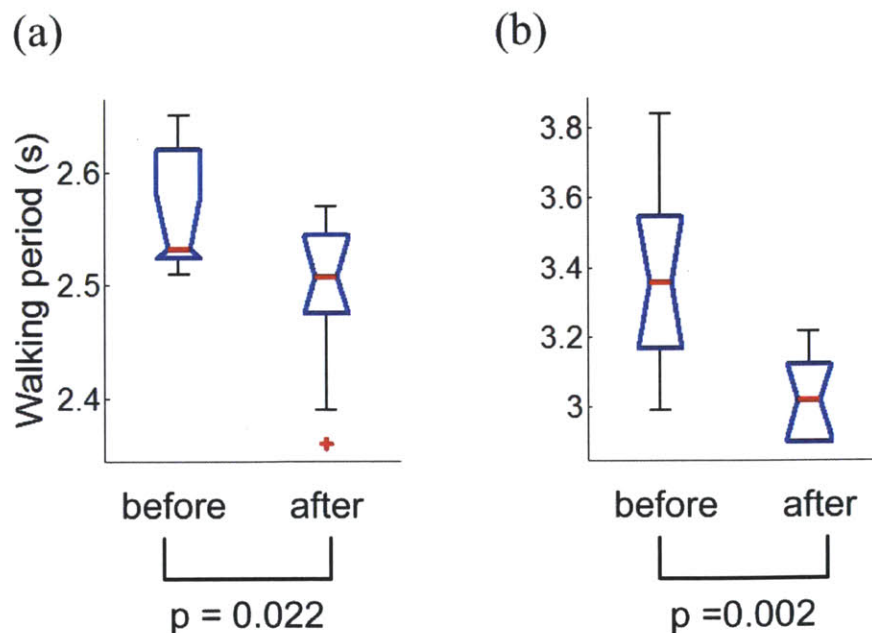
Figure 5-7: After-effect of entrainment of neurologically impaired subjects
(a) and (b) show the durations of 10 successive strides immediately before the beginning of perturbation and 10 successive strides immediately after the end of a set of perturbations for Stroke 1 and MS 1 respectively. Statistical analysis concluded that walking cadence became significantly faster due to the perturbation for both subjects.

Phase-locking

Consistent with the entrainment of unimpaired walking, entrainment always accompanied a specific relation between the gait cycle and the robotic torque pulse; in entrained gaits, the mid-terminal stance phase consistently coincided with the square pulses exerted by Anklebot. This observation of *phase-locking* was reliable; Figure 5-5 clearly shows that the subjects synchronized their cadence to the perturbation to maintain the specific phase relation even under the gradual change of perturbation cadence. The transient behavior of the phase of perturbation pulse shows the robustness of phase-locking more clearly. Figure 5-8 shows the transient behavior of Stroke 2 who did not even complete the session. This kind of transient behavior followed by phase-locking at mid-terminal stance was observed in all four subjects.

The distribution of the gait phases where the perturbation pulses were located in entrained gaits is shown in Figure 5-9. For each subject the distribution is narrow compared to 0 to 100 % gait cycle, which justifies the use of standard statistical tests based on a Gaussian distribution. Due to the large variability across the subjects, comparing the specific phase value where the perturbation pulse locked may not provide useful information. Alternatively, the phase difference between toe-off (initiation of swing) and perturbation pulse was assessed to test whether phase-locking at mid-terminal stance was consistently observed in neurologically impaired subjects (lower left of Figure 5-9). The toe-off phase was assessed using the pressure at toe; the method to detect the toe-off phase was same as the method to detect the heel strike phase using the pressure at the heel (Data Analysis in 5.1.1). Representative data of signal from foot switch at a toe with respect to the gait cycle and how the toe-off phase is estimated are shown in Figure 5-10. The histogram (Figure 5-9) shows that the pulses are clustered at the mid-terminal stance phase.
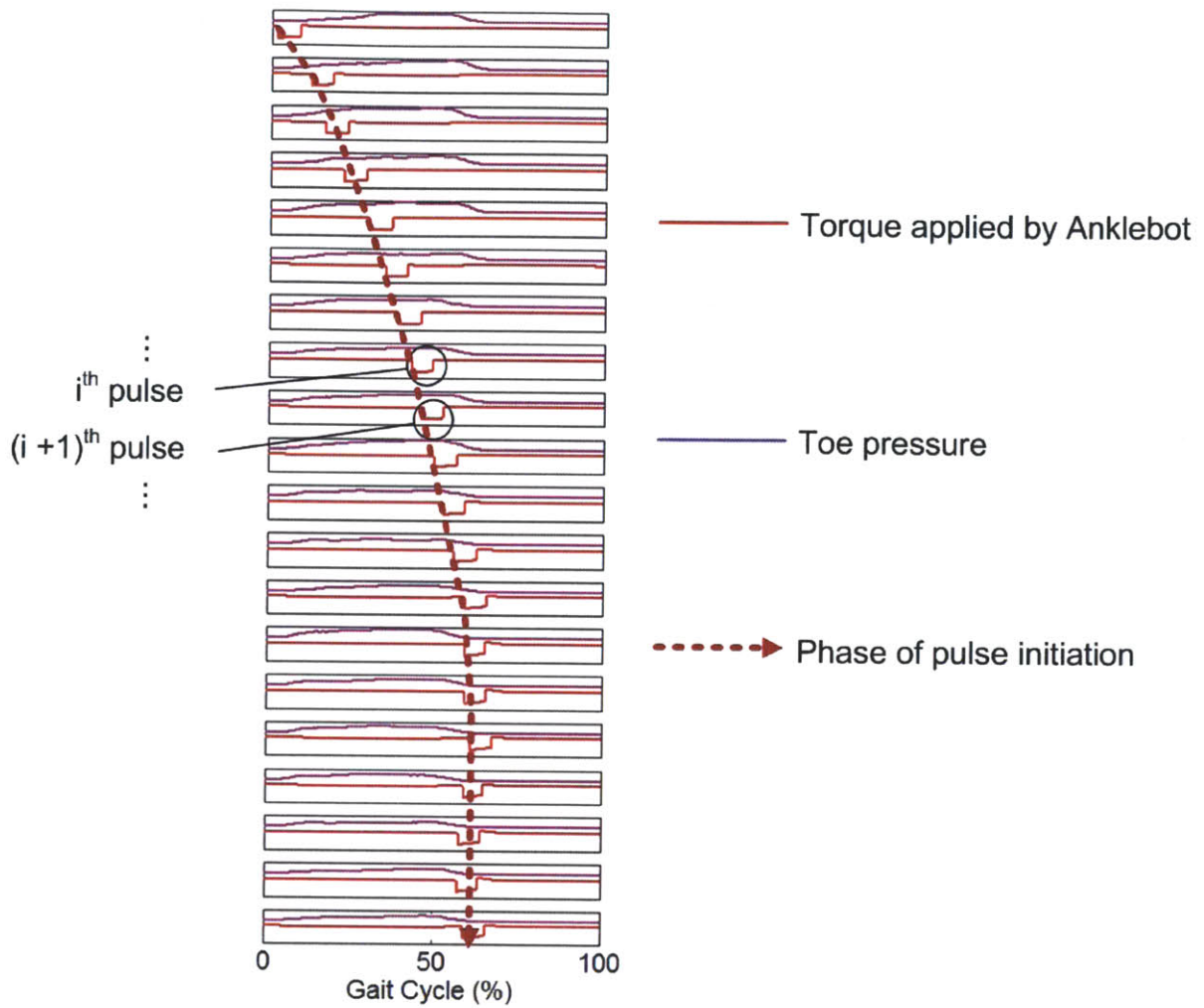
Figure 5-8: Transient behavior of Stroke 2 under perturbation

This figure shows 20 successive strides of Stroke 2 under periodic perturbation. Anklebot torque profile (red) and toe pressure (violet) are plotted. The dotted brown arrow visualizes the trend of the onset of torque pulse. The onset of torque pulse drifted initially, but converged on a specific phase close to toe-off (initiation of swing) phase where the toe pressure dropped to the minimum value, which indicates phase-locking at terminal stance phase.
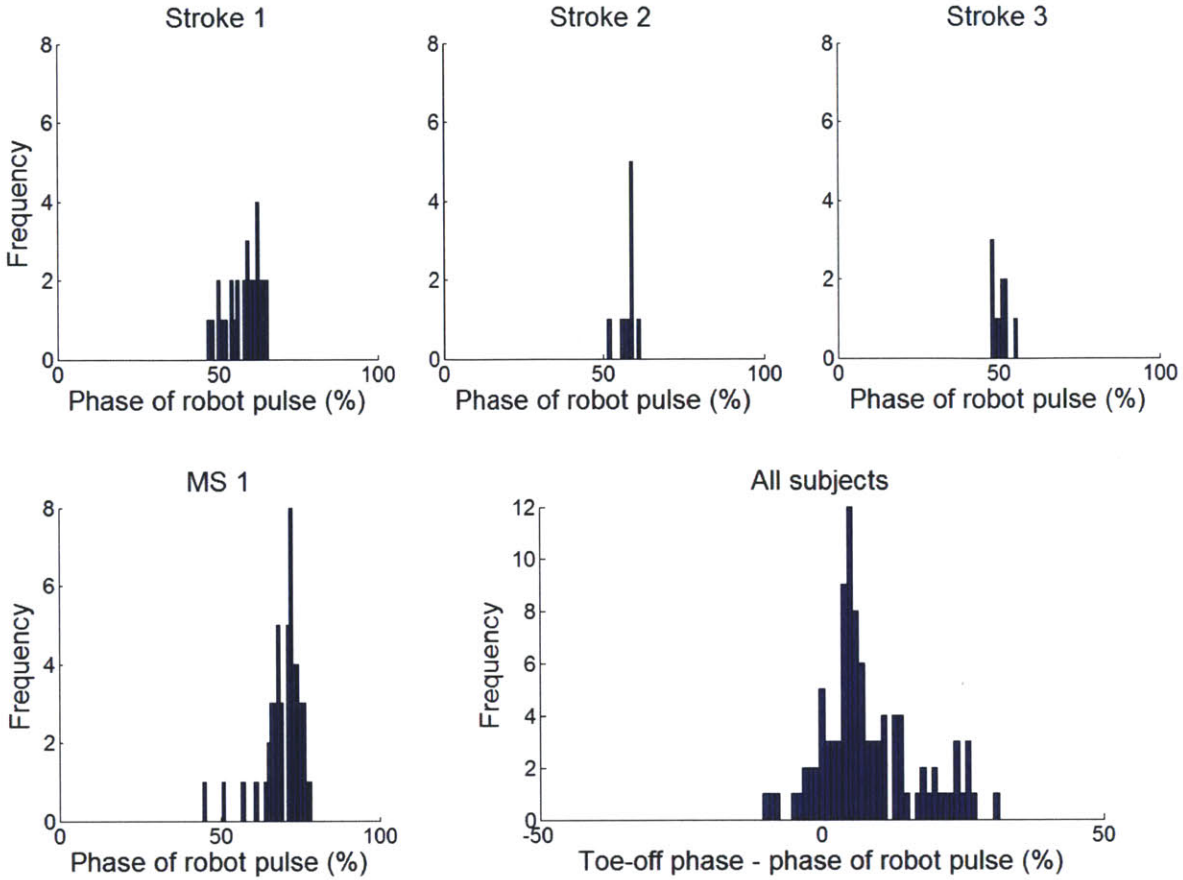
Figure 5-9: Histograms of gait phases where perturbation pulses were located in entrained gaits of each subject and the phase difference between toe-off (initiation of swing) and perturbation pulse in entrained gaits of all subjects

Though the average value of the phase of robot pulse in entrained gaits varies across the subjects, the distribution is narrow for each subject. The distribution of the phase difference between toe-off and perturbation pulse in entrained gaits of all subjects is plotted in the lower left; the highest frequency at around 5% phase difference reflects that most of the perturbation pulses were clustered at the phase slightly prior to toe-off phase, indicating phase-locking at terminal stance.

97
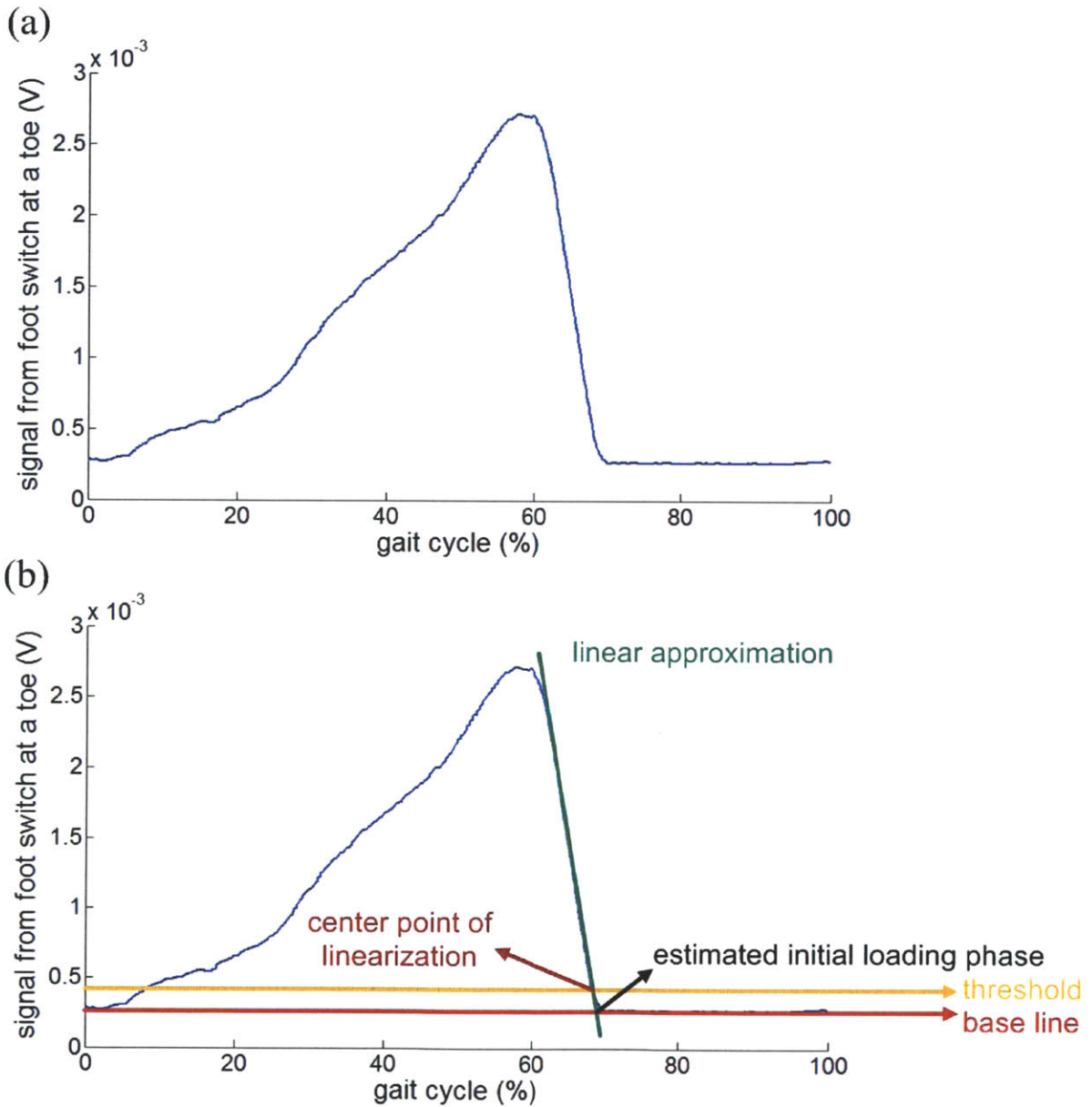
Figure 5-10: Typical data from the pressure sensor at a toe and determination of toe-off (initiation of swing) from the pressure sensor signal

(a) shows a representative data of signal from foot switch at a toe with respect to the gait cycle running from 0 to 100%, and (b) shows how the toe-off phase is estimated as an intersection between the baseline signal of no contact between toe and ground (red) and a linear approximation of the rapid decrease (green) which is evaluated based on 5 successive points centered at a point closest to a threshold (orange).

5.3. Discussion

5.3.1. Evidence of Lower-Level Semi-Autonomous Oscillator in Human Walking

Though the results are based on four subjects, and only two of them completed the session, the preliminary results are consistent with the observations of normal human walking. Entrainment and phase-locking were reliably observed in the neurologically impaired subjects who suffer from two distinct neurological disorders (stroke and MS) as well as unimpaired subjects. Phase-locking occurred at the mid-terminal stance phase for all impaired subjects, which is also consistent with the phase-locking observed in normal walking in response to the same mechanical perturbation. Though the range of the gait phase where the perturbation pulse locked was wider compared with normal walking, the range is still narrow relative to 0 to 100% gait cycle. In addition to the variability of impaired walking and variability across impaired subjects, transient behaviors contributed to the spread of the phases beyond the clustered region of phase-locking. Entrainment was assessed statistically, and some gaits were defined as entrained even with some transient behaviors (e.g., Figure 5-5 (b)). These transient phase dynamics before *steady-state* phase-locking is partly responsible for the spread of phase distribution (lower left of Figure 5-9).

Entrainment to an external periodic perturbation is a distinctive characteristic of nonlinear limit-cycle oscillators. The entrainment to periodic mechanical perturbation I demonstrated indicates that a semi-autonomous oscillator plays a role in the neuro-motor execution of human locomotion. That oscillator may be due to a neural central pattern generator (CPG), the musculo-skeletal periphery, or a combination of both, probably mediated by afferent feedback.

Other possible explanations of entrainment and phase-locking include supra-spinally mediated adaptation. However, the rigorous consistency of the entrainment and phase-locking

across the stroke patient, the MS patient and normal subjects shows that unimpaired supra-spinal control may be nonessential for the observed limit-cycle behavior of human walking. Gait kinematics clearly depends on the type of neurological injury and its severity [68]. However, the subjects with two distinct neurological disorders and normal subjects exhibited the same consistent limit-cycle behaviors despite significant differences in their gait kinematics such as walking speed, walking cadence (Table 5-1) and joint angle trajectory (Figure 5-11). This is consistent with that the essential components responsible for entrainment and phase-locking are embedded in components such as rhythmic pattern generators in the spinal cord or neuro-muscular periphery which may be relatively less affected by stroke or MS.
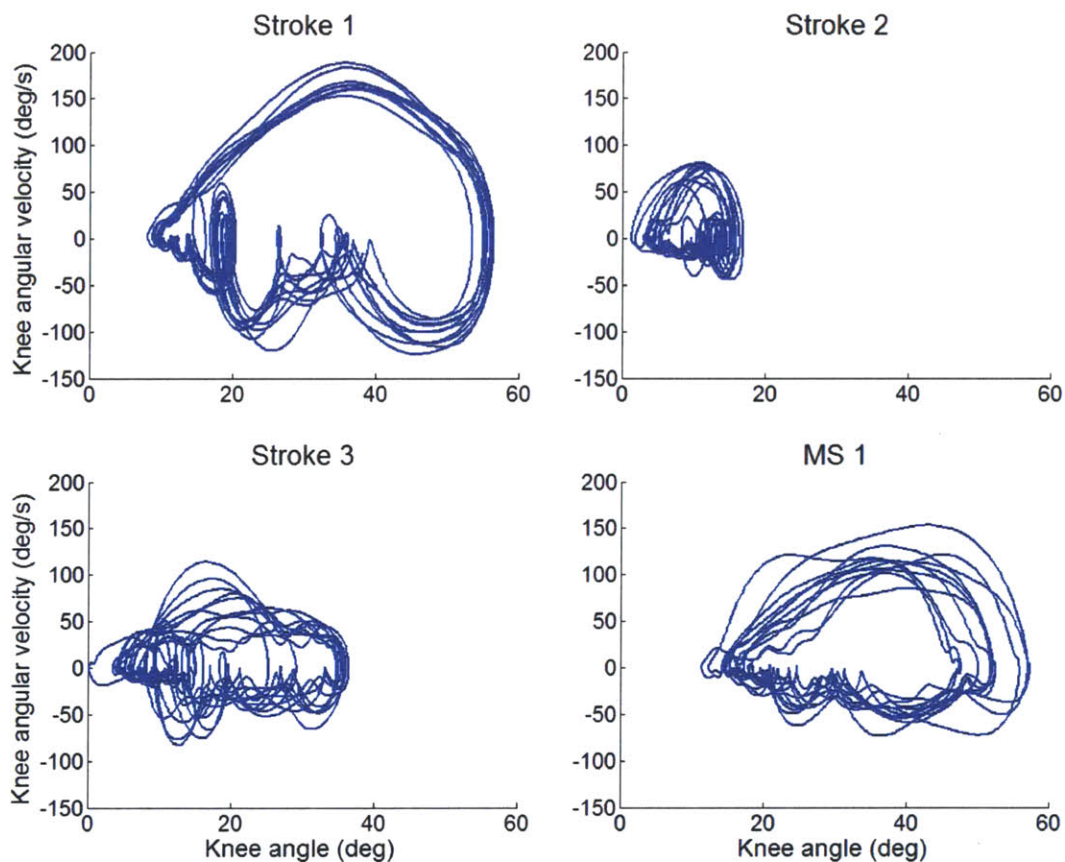
Figure 5-11: Phase plot of knee kinematics of each neurologically impaired subject
Range of knee motion and the qualitative shape of the phase plot vary across the subjects.

As a result of phase-locking and entrainment, the variability of walking cadence reduced noticeably in all the subjects except Stroke 1. However, please note that the variability of the cadence of Stroke 1 before perturbation is already small and even comparable to the variability of normal walking of healthy subjects (Table 4-1 and Table 5-1). It is plausible that the gait of Stroke 1 was already stereotyped enough, and the small variability of neuro-motor execution was due to the inherent noise of neuro-motor system. Sources of such variability have been identified not only in the basal ganglia circuits and premotor cortex [97] but also in the motor units [98]. Indeed, no significant reduction of variability was observed in the entrained gaits of healthy subjects as presented in Appendix D. The reduced variability of entrained gaits of all other impaired subjects is consistent with that the large variability before perturbation is due to the neurological impairment of high-levels of the CNS, and the mechanical perturbation entrains lower-level autonomous oscillator which was less affected by stroke or MS. However, entrainment of supra-spinal structure may not be precluded; further investigation is necessary to interpret the reduced variability as evidence of any form of the control architecture of human locomotion.

5.3.2. Feasibility of a Novel Entrainment Therapy

Entrainment to periodic mechanical perturbations supports a new strategy for locomotor rehabilitation that may have promise: based on a patient's performance, a robot may be programmed to entrain the patient's walking frequency, and gradually "drag" it towards the normal walking frequency as observed in the entrainment to gradually increasing perturbation cadence. If, as the result of this study and numerous studies in neuroscience [28, 30, 33, 99] and robotics [26, 27, 100] suggest, an embedded neural oscillator interacting with peripheral musculo-skeletal mechanics plays a role in normal human locomotion, most current robot-aided walking therapy (which is

focused on controlling limb trajectories) may interfere with the normal execution of locomotor function. Instead, rehabilitation by entraining the embedded oscillator might provide an essential but hitherto neglected element of walking therapy by exploiting the natural oscillating dynamics of walking.

An additional important observation is that entrainment always occurred at a specific phase of the walking cycle. Phase-locking was always achieved such that the torque from Anklebot occurred at ankle push-off, where it assisted in propulsion. Considering this phase-locking, training based on the entrainment to mechanical perturbation is distinct from the training based on the entrainment to auditory input [101]; mechanical interaction may supply the additional power needed to facilitate more normal gait, especially when patients cannot produce enough propulsion. The amplitude of mechanical perturbation as well as its frequency can be adjusted based on a patient's performance, providing assistance only as needed to promote the patient's participation, which is an essential element of neuro-restoration [6-8].

The observed after-effects are also consistent with the feasibility of the entrainment therapy. At least for the robot-aided rehabilitation of upper extremities, it has been reported that beneficial after-effects can be retained to result in rehabilitative significance [102, 103]. Different but possibly related observation is persistence of motor advantages from robotic therapy. For robot-aided therapy for upper limbs, the improved outcome during inpatient rehabilitation was sustained after 3 years post discharge, and the improvement was confined to the muscle groups trained in the robot-aided therapy [104]. Currently, for this study, data are insufficient to conclude how long the after-effects would persist. However, even if the after-effects lasted briefly (e.g., 20 steps), that would not preclude successful therapy. For rehabilitation of upper extremities, a consistent pattern of improvement during and after a therapy session, which was largely erased by the next session, led to a highly significant improvement over many therapy sessions [105]. Considering that lower

variability generally indicates better motor performance [106, 107], the reduced variability due to the phase-locking and entrainment provides other evidence that the proposed rehabilitation strategy may have promise.

Please note that this proposed approach does not preclude an important role of supra-spinal structure in human walking and its rehabilitation. Though the experimental results in this study supported measureable roles of nonlinear oscillators in human walking, that does not mean that we may not affect the execution of the nonlinear oscillators using supra-spinal control. Supra-spinal processes may play a key role in starting, stopping or sustaining locomotion e.g. by descending and ascending communication along the cortico-spinal tract. The effect of supra-spinal control on regulating the "low-level" limit-cycle oscillator is still available; by adjusting the level of assistance, we can promote the voluntary participation, and that voluntary participation can play a role in the process of recovery. Analogy between walking and swing (as discussed in 3.3) may also be helpful here. When we learn to play swing, we use our voluntary participation. We use the interaction between inertia and gravity and the resulting periodic dynamics to execute the motion of swing, but we learn how to use the interaction and how to play swing with our intention. Executing the periodic motion using the periodic interaction does not preclude learning how to exploit that interaction using supra-spinal control or intention-driven participation.

One important limitation of this study is that the subjects were asked to walk on a treadmill at a constant speed. It is not obvious whether the subject can actually improve their walking speed in overground walking through the current preliminary form of the training strategy. However, this study provides clear evidence that propulsive mechanical perturbation to ankle can change the cadence of the neurologically impaired subjects by entraining it to the rhythmic perturbation. One necessary future work is to modify the strategy so that the speed of treadmill is adjusted as the walking cadence of the subjects becomes faster. Whether the effects on treadmill walking can be

translated into the improved motor outcome in overground walking is an additional issue. For healthy subjects, though differences between treadmill and overground walking have been reported [95], they are subtle. For rehabilitation training of neurologically impaired walking, a recent study concluded no different outcome between body weight support treadmill training and conventional overground training [108]. Furthermore, under proper control, speed-dependent treadmill training was reported to show more efficacy than conventional overground training [109], which again encourages the modification of current preliminary form of entrainment therapy in such a way that the speed of treadmill can be properly controlled during the training session.

6. A Minimal Model Encapsulating Limit-Cycle Behaviors of Human Walking

In the previous chapter, experimental work supported the feasibility of the proposed strategy of entrainment to ankle mechanical perturbation. The results of the experiments supports that some form of nonlinear limit-cycle oscillator participates in human locomotion. However, the essential origin of the limit-cycle behavior remains unclear. This chapter demonstrates a minimal model that is competent to reproduce the essence of the observed limit-cycle behaviors of human walking to address minimal components of the neuro-mechanical oscillator.

6.1. Introduction

Understanding the essential mechanism of human locomotor control has remained a primary problem in motor control. Combined with the potential benefits of robotic therapy, the importance of this problem goes beyond scientific interest. Related with the broad goal of this thesis, a more profound understanding of human locomotor control will facilitate refinement and optimization of robotic therapy. Specifically, further understanding of the essential components of the limit-cycle behaviors of human walking may provide critical guidance to refine the proposed rehabilitation strategy of entrainment to ankle mechanical perturbation.

In Chapter 4 and 5, behavioral evidence that some form of nonlinear limit-cycle oscillator plays a measurable role in human walking was presented. Entrainment of human walking to periodic mechanical perturbation, and phase-locking that located the perturbation at the terminal

stance phase were observed. The experiment with healthy subjects suggested that supra-spinal control including auditory feedback or voluntary adaptation may not be a plausible source of these limit-cycle behaviors. The rigorous observation of the limit-cycle behaviors across the subjects with two distinct neurological disorders and normal subjects is also consistent with that the essential components responsible for the limit-cycle behaviors are embedded in the lower levels of the central nervous system or neuro-muscular periphery.

However, the essential origin of the limit-cycle behaviors remain obscure because various mechanisms may contribute to the limit-cycle behaviors of human walking. The success of passive dynamic walkers suggests that the mechanical interaction between the periphery and the environment may be sufficient to demonstrate the stable periodic gaits on a slope, but additional complexity (e.g., active control) is necessary to yield periodic gaits on level ground or up a slope. A rhythmic pattern generator, as an additional controller, may enable stable bipedal walking on level ground [72, 73], but stable periodic gaits on level ground are also achievable by simple state-determined actuation with minimal control as in many bipedal robots including the Cornell biped [100]. Even for the vertebrates which show clear evidence of spinal pattern generators isolated from their peripheries, the role of afferent sensory input is critical in their locomotion [110, 111]. Generating the human locomotor pattern also depends on load-related input, hip afferent input and location-specific information from the skin of the foot [63, 85].

In this chapter, I develop a minimal mathematical model that is competent to quantify the observed limit-cycle behaviors of human locomotion—stable periodic motion, entrainment to periodic mechanical perturbations, and phase-locking. Because the kinematics and dynamics of the human neuro-mechanical system are inordinately complex, the goal was to avoid clutter and its attendant confusion and focus only on essential features that might give rise to observed behavior. In the following I show that a simple model with 1) one degree of freedom, 2) without supra-spinal

control and 3) without a spinal pattern generator can successfully encapsulate the observed behaviors. This suggests that a simple state-dependent controller using afferent feedback may serve as a minimal component model of the limit-cycle behaviors of human walking.

6.2. Model Description

6.2.1. General Depiction

A schematic of the model defining its variables and parameters is shown in Figure 6-1. A point mass moves in a vertical plane under the influence of gravity, restrained by rigid massless legs. The swing leg can instantaneously be moved in front of the mass. Scuffing (contact of the swing leg with the ground) is ignored. Each leg has two joints—a hip and an ankle. Ankle actuation provides propulsion whereas the hip joint is assumed to be a frictionless pivot, which cannot apply any torque. However, I assume that the angle between the legs is always reset as 2α at the beginning of a step. Due to the assumption of massless legs, resetting the angle between the legs does not consume any energy.

Sequential configurations of the model during one step cycle are depicted in Figure 6-2. At the collision of the leading foot, the velocity of the mass changes instantaneously. Immediately after the collision, the model is in double stance and the trailing leg ankle is actuated. During double stance the model behaves as an actuated four-bar linkage. The ankle of the leading leg acts as a hinged joint during double stance and the following single stance phase. I assume that the trailing-leg ankle torque during double stance is determined by a linear torsional spring as

$$T = k(\mu - \psi) \quad (\frac{\pi}{2} - \alpha \leq \psi \leq \mu), \qquad \text{Equation 6-1}$$

where T is torque, k is stiffness, a constant, ψ is ankle angle and μ is maximal plantar flexion. The torque becomes zero when ψ reaches μ. By virtue of the zero mass of the feet, the trailing foot pushes on the ground only as long as the actuation torque is positive; double stance ends at the moment when the ankle torque becomes zero, or equivalently when ψ reaches μ. During the following single stance, there is no actuation torque, and the dynamics of the swing leg is irrelevant because it has no mass; the model acts like an inverted pendulum hinged at the ankle of the stance leg. A step cycle ends when the hip angle θ reaches $-\alpha$, its value at the foot-ground collision.
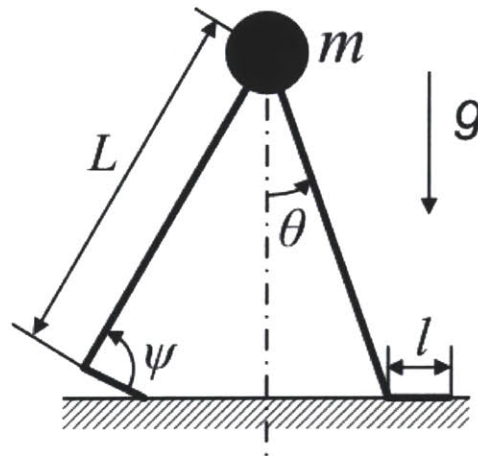
Figure 6-1: A schematic of the walking model
A point mass is restrained by rigid massless legs. The trailing ankle is actuated as a cocked (pre-stretched) spring released at the beginning of double stance. The hip joint and the leading ankle cannot exert any torque.
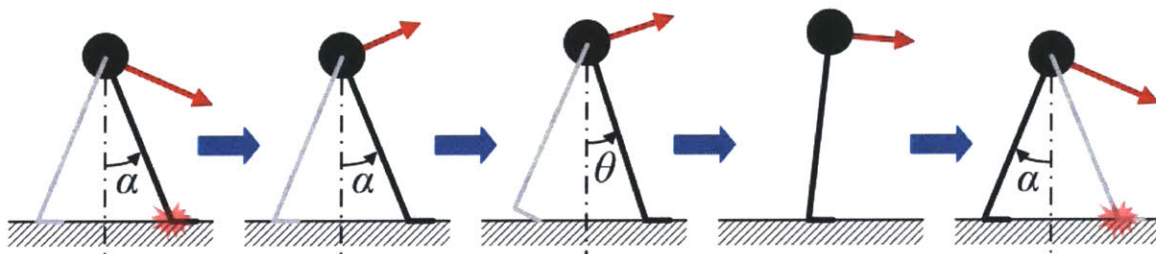
Figure 6-2: One step cycle of the walking model
The end and beginning of a step is the moment when the leading foot collides with ground. During double stance the model moves as four linked bars. During single stance the model moves as an inverted pendulum.

108

6.2.2. Parameter Values

Parameter values of the model are summarized in Table 6-1. Leg length, foot length, maximal plantar extension angle, hip angle at foot-ground contact, and mass, were chosen to approximate morphological data of human adults. The value of ankle actuation stiffness was chosen to match the maximal ankle torque of the model with that of normal human walking. Experimental data shows that peak plantar-extension torque in normal gait is approximately 17% of body weight × leg length [68]. For the model, this value corresponds to 133.4 (N·m) and to match peak ankle torque at the beginning of a double stance with this value, k was determined to be 87.3 (N·m/rad).

This value of k is of the same order of magnitude as the human ankle stiffness with co-contraction of ankle muscles, which is approximately 50 (N·m/rad) [112] though there exists non-negligible discrepancy. One plausible reason for the discrepancy is difference in muscle activation level. The subjects were asked to maintain the muscle activation as 20 % of maximal activation level in terms of electromyography (EMG) amplitude in [112], whereas amplitudes of EMG of ankle plantar extensor muscles are more than 20 % of maximal activation level in normal human walking: 90 % for Soleus, 80 % for Gastrocnemius, 40 % for Posterior Tibialis, 40 % for Flexor Digitorum Longus, 80 % for Flexor Hallicic Longus, 40 % for Peroneus Brevis, and 30 % for Peroneus Longus [68]. The simplicity of the model and the ignored physiological and anatomical realism may be another source of the discrepancy. However, most importantly, comparison between the ankle actuation constant, k and human ankle stiffness during walking may be appropriate only when the human ankle acts as a spring that stores and releases potential energy during stance phase with a *constant equilibrium position*, which might not be a valid assumption.

Table 6-1: Parameter values for the ankle actuated model

Parameter	Meaning	Value
m	mass	80 kg
L	leg length	1 m
l	foot length	0.2 m
g	gravitational acceleration	9.81 m/s^2
α	angle of the leg at heel strike	$\pi/6$ (rad) or 30 (deg)
μ	maximal plantar extension of the ankle	2.6 (rad) or 148 (deg)
k	ankle actuation constant	87.3 N·m/rad

6.3. Analysis Method

I investigated whether the model was able to reproduce key features observed in normal human walking: 1) existence of a period-one gait; 2) stability of this period-one gait; 3) entrainment of this period-one gait to periodic mechanical perturbations with a finite basin of entrainment; and 4) phase-locking so that the perturbation occurred at the end of double stance. Because of the extreme simplicity of the model, many of these questions could be addressed by a straightforward application of calculus and algebra. Additional results were obtained by numerical simulation implemented in MATLAB using the Simulink toolbox (Mathworks Inc.). Numerical integration was performed with a fixed step size of 10^{-4} and absolute and relative error tolerances of 10^{-6}. The validity of the numerical simulation was checked using either available analytical solutions or by repeating simulations with a tenfold smaller tolerance.

6.4. Results

6.4.1. Stride Function

As is common for mathematical analysis of periodic locomotion, I used the concept of a *stride function* [71] whose input and output are state variables at the beginning of one cycle and at the beginning of the next cycle respectively. In the language of dynamical systems, a stride function is a discrete Poincaré map, and a period-one gait is a fixed point of the Poincaré map. As the model has only one degree of freedom (θ), and the dynamics of the model can be fully described with 2nd order ordinary differential equation, evolution of the system can be described in two dimensional state space $(\theta, \dot{\theta})$. If the beginning of one cycle is defined as the moment of a foot-ground collision, or equivalently as the moment when θ reaches $-\alpha$, the stride function is defined as $\mathbf{f} : \dot{\theta}_i\big|_{\theta=\alpha} \to \dot{\theta}_{i+1}\big|_{\theta=\alpha}$. The existence of a period-one gait requires existence of $\dot{\theta}_i\big|_{\theta=\alpha}$ that satisfies $\mathbf{f}(\dot{\theta}_i\big|_{\theta=\alpha}) = \dot{\theta}_i\big|_{\theta=\alpha}$, and the local asymptotic stability of this period-one gait is concluded if the derivative of the stride function evaluated at the period-one gait satisfies $\left|\dfrac{\partial \mathbf{f}(\dot{\theta}_i\big|_{\theta=\alpha})}{\partial \dot{\theta}_i\big|_{\theta=\alpha}}\right| < 1$.

Please note that for this model, the derivative of the stride function is not a matrix but a scalar because the stride function is defined in one dimensional space. Generally, if the stride function is defined in a state space whose dimension is larger than one, the derivative of the stride function becomes a matrix, and stability of the periodic solution may be assessed by investigating the eigenvalues of the matrix, which are *Floquet multipliers.*

6.4.2. Existence of a Period-One Gait

The actuation torque, T is a function of ψ, which is determined by θ and the geometry of the model. Consequently, the work done by the ankle torque can be written as $W = \int_{\theta_0}^{\theta_f} T(\theta)d\theta$, where θ_0 and θ_f indicate the value of θ at the beginning and the end of a double stance respectively. The work done per step is a constant because θ_0 and θ_f in each step are constants. Equivalently, the potential energy initially stored in the ankle spring, which is released during double stance, is determined by the hip angle α, the spring stiffness k, and the maximal plantar flexion μ, all constants. On the other hand, as addressed in the rimless wheel model in 2.1.4, a foot-ground collision reduces the speed of the model by a factor of $\cos2\alpha$, and therefore reduces kinetic energy by $\cos^2 2\alpha$. Taken together, for the model to exhibit a period-one gait, the loss of kinetic energy due to a foot-ground collision must be exactly compensated by the work done by the ankle torque. For this, the speed of the point mass just before a collision, v_C, and the corresponding $\dot{\theta}$, denoted $\dot{\theta}_C$, must satisfy

$$W = \int_{\theta_0}^{\theta_f} T(\theta)d\theta = \frac{1}{2}k(\alpha + \mu - \frac{\pi}{2})^2 = \frac{1}{2}m{v_C}^2(1 - \cos^2 2\alpha) = \frac{1}{2}mL^2\dot{\theta_C}^2(1 - \cos^2 2\alpha).$$

This expression has two solutions differing only in sign. The negative solution corresponds to forward progression; $\dot{\theta_C}$ for a period-one gait is

$$\dot{\theta_C} = -\frac{1}{L}\sqrt{\frac{k(\alpha + \mu - \frac{\pi}{2})^2}{m(1 - \cos^2 2\alpha)}} \qquad \text{Equation 6-2}$$

For a period-one gait to exist, two additional conditions must be satisfied: 1) the point mass must have enough kinetic energy at the beginning of single stance to "vault over" to make the next step, and 2) the ground reaction forces must not be negative, i.e. the model must not "fly off" the ground. These two conditions limit the range of k. Excessively small k cannot supply enough

112

energy to make the model vault over. Conversely, with overly large k, the leading foot is lifted either by an excessive ground reaction force at the trailing foot or by an excessive centrifugal force due to excessive speed.

Using the work-energy principle, the lower limit of k_C can be obtained analytically. Let the marginal stiffness be k_C. The speed of the fixed point comes from the energy balance

$$\frac{1}{2}k_C(\alpha + \mu - \frac{\pi}{2})^2 = \frac{1}{2}mv_C^2(1 - \cos^2 2\alpha)$$

Equation 6-3

In the case in which the model vaults over marginally, the kinetic energy of the model becomes zero at the apex of $\theta = 0$. Therefore,

$$\frac{1}{2}mv_C^2\cos^2 2\alpha + \frac{1}{2}k_C(\alpha + \mu - \frac{\pi}{2})^2 + Lmg\cos\alpha = Lmg + 0$$

Equation 6-4

From Equation 5-3 and 5-4,

$$k_C = \frac{2Lmg(1 - \cos\alpha)(1 - \cos^2 2\alpha)}{(\alpha + \mu - \frac{\pi}{2})^2}.$$

Equation 6-5

With the selected parameter values, k was greater than k_C, which satisfied condition 1).

To check that k was less than its upper limit, I derived the ground reaction forces. Work-energy principle and numerical integration concluded that the ground reaction forces did not go below zero with the parameter values given in Table 6-1, satisfying condition 2). Detailed analysis of the ground reaction forces and resulting range of k are described in Appendix E.

Taken together, the existence and uniqueness of a period-one gait were established. The period of this gait, τ_0, was 0.967 (s) and the average forward speed was 1.03 (m/s), comparable to freely selected low-speed human walking [90].

113

6.4.3. Asymptotic Stability of the Period-One Gait

Asymptotic stability of the period-one gait can be established analytically. Let a collision occur at $t = 0$, and the next collision occur at $t = t_f$. Also, let $t = t_{f+}$, $t = t_{f-}$ and $t = 0_+$ indicate the moments right after $t = t_f$, just before $t = t_f$ and right after $t = 0$, respectively. Using the work-energy principle, $\dot{\theta}(t = t_{f+}) = -\dfrac{\cos 2\alpha}{L}\sqrt{L^2\dot{\theta}_{0+}^2 + \dfrac{k}{m}(\alpha + \mu - \dfrac{\pi}{2})^2} = \mathbf{f}(\dot{\theta}_{0+})$, where $\dot{\theta}_{0+} = \dot{\theta}(t = 0_+)$. The derivative of the stride function f becomes

$$\frac{\partial \mathbf{f}(\dot{\theta}_{0+})}{\partial \dot{\theta}_{0+}} = -\cos 2\alpha \frac{\dot{\theta}_{0+}}{\sqrt{\dot{\theta}_{0+}^2 + \dfrac{k(\alpha + \mu - \dfrac{\pi}{2})^2}{mL^2}}} .$$

Equation 6-6

From Equation 5-2, $\dot{\theta}_{0+}$ at the fixed point (the period-one gait) becomes

$$\dot{\theta}_{0+\text{ fixed}} = -\frac{\cos 2\alpha}{L}\sqrt{\frac{k(\alpha + \mu - \dfrac{\pi}{2})^2}{m(1 - \cos^2 2\alpha)}} .$$

Substituting into Equation 5-6, the derivative of the stride function at the fixed point is $\cos^2 2\alpha$. With the parameter value of $\alpha = \pi/6$ (rad), this becomes 0.25, substantially less than unity, which guarantees local asymptotic stability of the fixed point of the stride function. Numerical evaluation yielded the same value, validating the numerical methods. As mentioned in 2.1.2, the derivative of the stride function, which determines the stability, is same as the reduction ratio of the kinetic energy per step due to foot-ground collision. This is a general property of a model with one dimensional Poincaré section, constant energy supply and constant reduction ratio of kinetic energy. Proof is presented in Appendix B. Simulations demonstrating the asymptotic stability of the period-one gait of this model are shown in Figure 6-3.
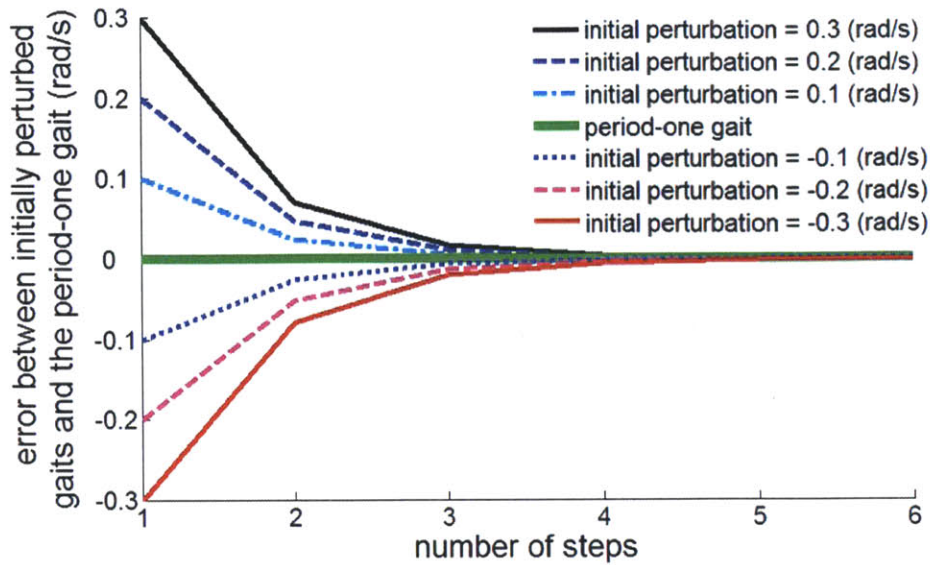
Figure 6-3: Asymptotic stability of period-one gait of the model
Errors in initial conditions of angular velocity converge to zero as the number of steps increases.

6.4.4. Entrainment with a Finite Basin

To investigate the competence of the model to reproduce entrainment to mechanical perturbations, I superimposed periodic plantar-flexion torque pulses to the ankle (in addition to the torque due to the intrinsic ankle actuation). For comparison with the experimental work, the period of the perturbation torque, τ_p was set to be close to the period of the period-one gait of the model, τ_0; the range of τ_p was $\tau_0 \pm 0.1$ sec. The amplitude of the added torque pulse was 10% of the maximal ankle torque of the model, and the pulse width was 0.1 sec as in the experiment. Entrainment to the mechanical perturbations was observed with a narrow basin of entrainment as shown in Figure 6-4; the period of the model entrained to τ_p only if τ_p was close to τ_0. The basin of entrainment was approximately 7.2 % of τ_0, which is remarkably similar to the estimated basin of entrainment observed in the experiment with healthy subjects (6.7 % ± 3.6 % of τ_0).

Perturbations whose period is either shorter than τ_0 - 80 ms or longer than τ_0 could not

115

entrain the model. However, the periodic change of step periods shown in Figure 6-4 (b) suggests that under perturbations whose periods are outside the basin of entrainment, the model may exhibit gaits that recover the state in more than one step cycles. These gaits may be described as period-n gaits (n > 1) opposed to period-one gaits in which the model recovers its state exactly after one step cycle. In period-n gaits (n > 1), with the periodic fluctuation of step period, the average step period over large number of step cycles should change. Particularly, if τ_p is shorter than τ_0, the average step period will stay between τ_p and τ_0. However, the step period cannot converge to τ_p, and this behavior may not be defined as entrainment.
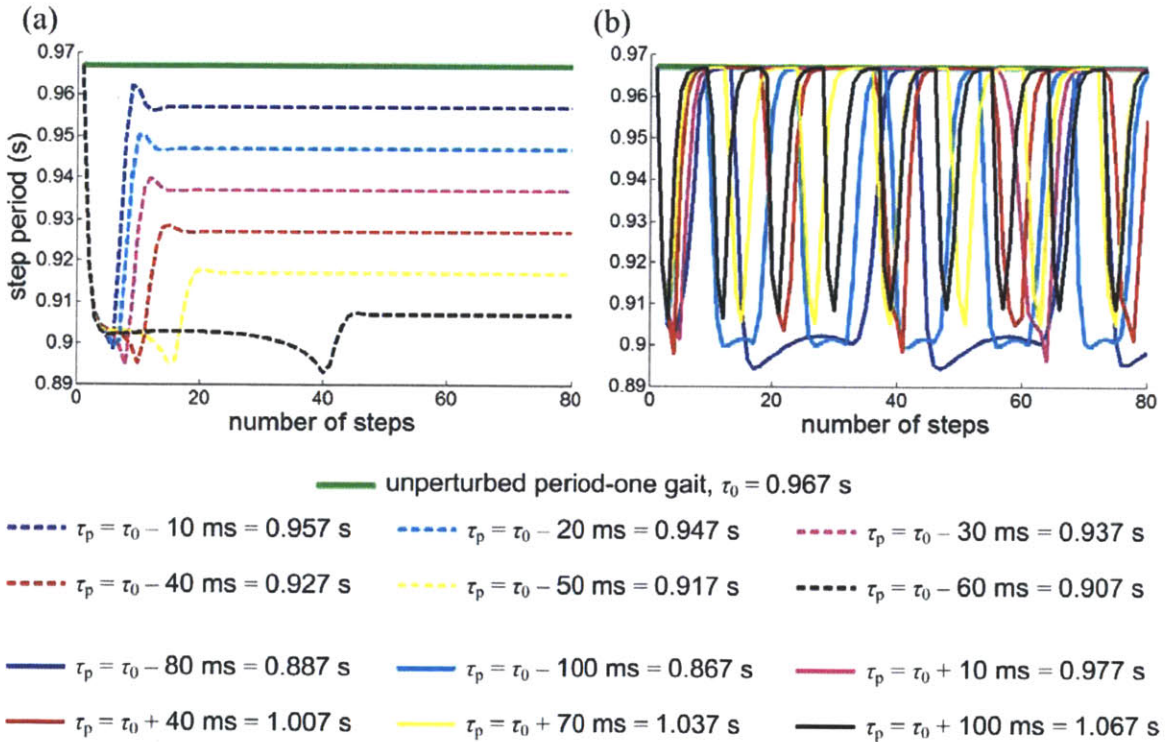
Figure 6-4: Entrainment of the model to mechanical perturbations with a finite basin
Step period is plotted as a function of step number; (a) shows entrained gaits, and (b) shows gaits that failed to entrain. For entrained gaits, the step period converged to the perturbation period, τ_p, whereas step period continued to fluctuate when gait was not entrained. Note that the model shows a narrow basin of entrainment. Any perturbation with $\tau_p > \tau_0$ or $\tau_p \leq \tau_0 - 80$ (ms) did not entrain the model.

116

6.4.5. Phase-Locking at Terminal Stance Phase

In addition to reproducing entrainment, the model also reproduced the phase-locking that was observed in unimpaired human walking. In particular, the perturbation pulse converged to the terminal stance regardless of the gait phase at which the perturbation pulse was initiated as shown in Figure 6-5. Furthermore, the time-course of phase-locking bore a clear qualitative resemblance to the pattern observed in the experiments.
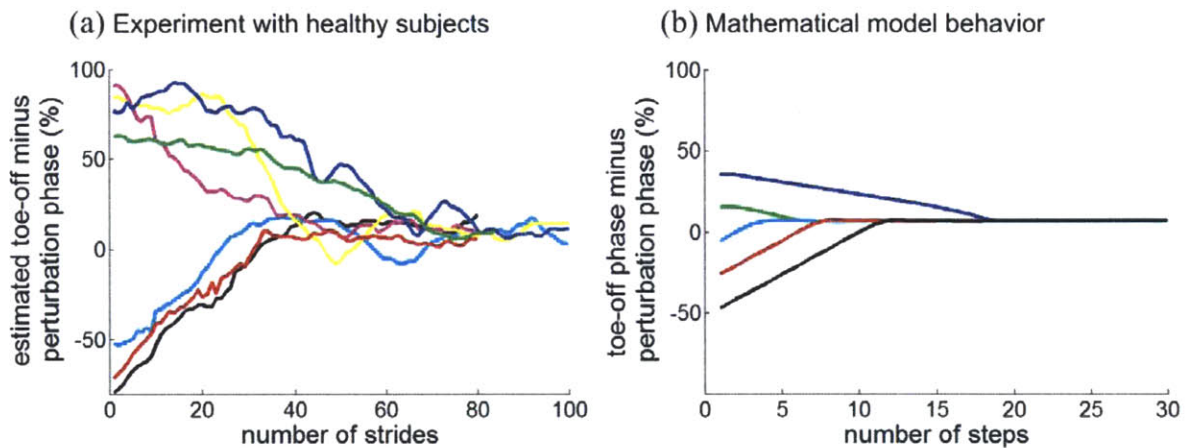
Figure 6-5: Phase-locking at terminal stance of normal human walking and the mathematical model
In (a), the experimental data of normal subjects are shown. The estimated phase difference between toe-off (initiation of swing) and the initiation of the perturbation pulse for all the 7 subjects who participated in the experiment 2 (explained in 4.2.1) is plotted as a function of stride number. In (b), the phase difference between toe-off of the model and the initiation of the perturbation pulse is plotted for entrained gaits with ($\tau_p = \tau_0 - 50$ ms) and various initial phases of the perturbation pulse. In both (a) and (b), regardless of the initial phase, the perturbation pulse converged to a phase close to toe-off; the model successfully reproduced the phase-locking at the end of double stance.

6.5. Discussion

The highly-simplified model presented here reproduced all of the following features observed in human walking: 1) a periodic bipedal walking pattern; 2) local asymptotic stability of

117

that periodic walking pattern; 3) entrainment of that walking pattern to periodic mechanical perturbations with a narrow basin of entrainment; and 4) phase-locking to locate the perturbation at the end of double stance when entrained. The extreme simplicity of the model must be emphasized. All of the complex biomechanics of the human musculo-skeletal system (on the order of 600 muscles activating about 200 degrees of freedom) was distilled into a model with only one degree of freedom. Though those additional complexities no doubt contribute to unimpaired locomotion, the competence of this brutally-simple model suggests that it may capture the essence of sagittal-plane locomotor dynamics.

An important detail of this model is that it involves minimal form of afferent feedback: actuation of the trailing-leg ankle is triggered based on the system state. The required afferent information might be derived from foot contact of the leading leg, reflecting cutaneous input or load-related afferents, e.g. from Golgi tendon organs. Alternatively, it might be derived from stretch receptors, for example those that signal hip extension; or it may arise from a combination of these sources. Regarding the relative importance of each of these afferent sensory inputs, computer simulation of cat locomotion suggested that coordination of stepping of the hind legs depends critically on load-related signal rather than hip extension [113].

However, the model deliberately omitted any self-sustaining intrinsic neural oscillator such as a CPG. It also omitted supra-spinal control specifying limb kinematics. Though either or both of these factors plausibly contribute to human locomotion, the competence of this simple model suggests that they may be nonessential to reproduce observed limit-cycle features of normal human walking—stable periodic oscillation, entrainment and phase-locking—that may instead emerge from the nonlinear dynamics of the neuro-mechanical periphery.

6.5.1. A Finite Basin of Entrainment by Finite Work from Perturbation

The average speed of the model (v) as a function of the initiation phase of a perturbation pulse (φ) is plotted in Figure 6-6; v is bounded when one pulse appears during one double stance. The lower bound of the average speed is the speed of the period-one gait without a perturbation; the model cannot walk slower because the mechanical perturbation, which applies to the trailing ankle, only accelerates the model. It is also clear that the speed of the model has an upper bound because the amount of the acceleration due to the perturbation is limited. The range of the average speed is less than 9 % of the minimum average speed. The limited amount of energy supplied by the mechanical perturbation per step results in the small range of the average speed, and therefore, with a fixed step length, concludes the finite basin of entrainment to the periodic perturbations.

6.5.2. Phase-Locking Occurs at the End of Double Stance

Remarkably, in experiments with humans, for all entrained gaits, phase-locking at a specific phase of the end of a double stance was observed, and this model reproduced it. Here, I interpret this model behavior using the v vs. φ curve (Figure 6-6). If a pulse is assigned to a swing phase, it cannot contribute to acceleration of the model; the average speed of the model is same as the speed of the unperturbed gait, which is lower than the case when the entire pulse is present during a double stance. The speed increases as the perturbation phase approaches 0, the onset of a double stance, because the portion of the pulse inside the double stance increases. Conversely, the speed decreases as a portion of the pulse leaves a double stance and is masked by the following swing phase. Consequently, the v vs. φ curve (Figure 6-6) has a positive slope around the onset of a double stance, and a negative slope around the end of a double stance.
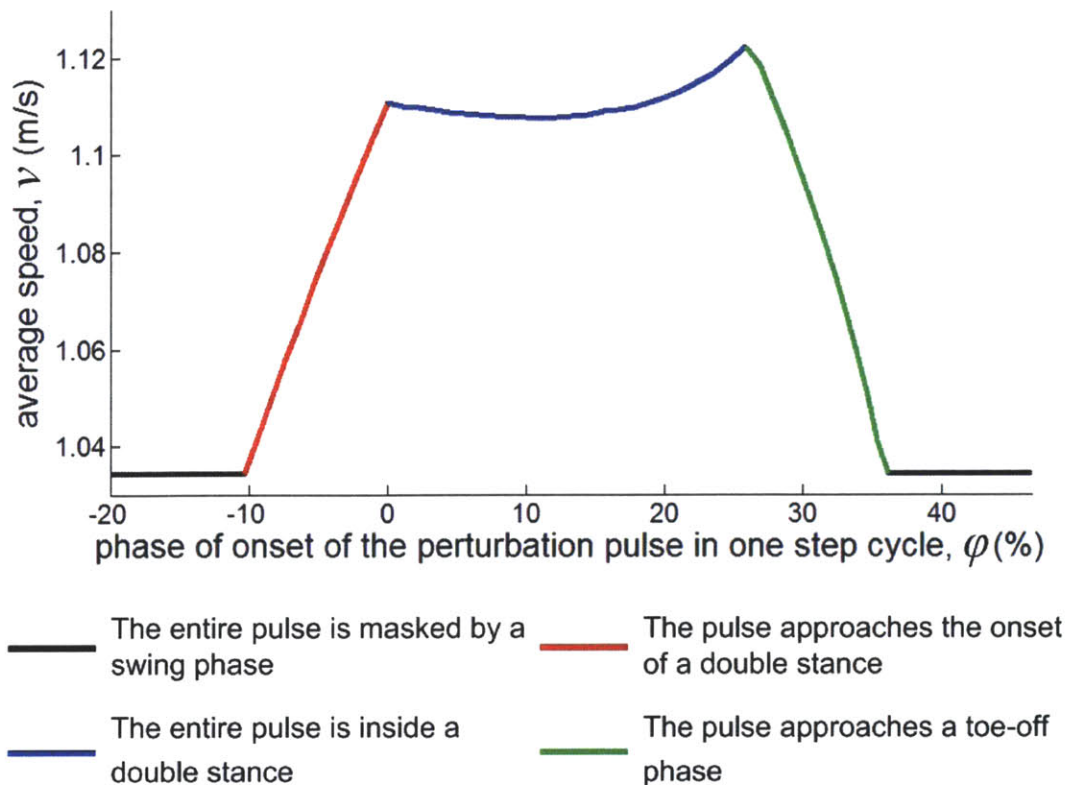
Figure 6-6: The average speed of the model (v) vs. the initiation phase of a perturbation pulse (φ)

With fixed amplitude and duration of the perturbation pulse, period-one gaits are searched for various φ, and v is calculated for each of the period-one gait. When a pulse is located in a swing phase, it cannot accelerate the model, and v is lower than the speed when the entire pulse is inside a double stance. The speed (v) increases as φ approaches 0, the onset of a double stance, and decreases as φ approaches the end of a double stance because a portion of the pulse begins to be masked by the following swing phase.

Suppose the case when the model is entrained to a periodic perturbation; the model's cadence should be same as the perturbation period. Any small additional disturbance accelerating (decelerating) the model makes the perturbation pulse be present at a later (earlier) phase in the following step. In other words, φ increases (decreases) in the next step due to an accelerating (decelerating) disturbance. Around the end of a double stance, if the model is accelerated, increased

φ decreases the speed in the next step because $\frac{dv}{d\varphi} < 0$; the negative slope stabilizes the entrained gait under any accelerating disturbance, and likewise under any decelerating disturbance. Conversely, around the onset of a double stance, the positive $\frac{dv}{d\varphi}$ concludes unstable entrainment.

The v vs. φ curve (Figure 6-6) also has a negative slope in the earlier portion of a double stance. However, the negative slope of this region may be ignored for the following reasons. First, the negative slope in this region is much slighter than the end of a double stance; the strength of the stability is much weaker. Second, this region allows only an extremely narrow basin of entrainment, which is less than 0.25 % of τ_0. Considering the finite but approximately 30 times wider basin observed in the model (Figure 6-4) and the experiment (Table 4-2), this region can possibly account for only an extremely limited fraction of the entrained gaits. Finally, the negative slope inside a double stance heavily depends on the model specification, especially the ankle torque profile (Equation 5-1). With a different ankle actuation profile, the portion of a double stance with a negative slope may move, shrink, or even vanish. In contrast, the presence of the negative slope at the end of a double stance is always evident under the physically reasonable assumption that a torque pulse at an ankle does not provide any propulsion when the leg is in a swing phase.

The mechanism of stability described above also makes the end of a double stance as an *attractor* of phase-locking. When the periodic perturbation is initiated around the end of a double stance, the model is accelerated, but its speed probably does not match the exact initial condition for the entrained periodic gait ($v_{entrained}$). If the speed is lower than $v_{entrained}$, the next perturbation pulse occurs at an earlier phase, and therefore the speed increases toward $v_{entrained}$ due to the negative $\frac{dv}{d\varphi}$.

If the speed is higher than $v_{entrained}$, the next pulse occurs at a later phase, decreasing the speed toward $v_{entrained}$. Though the earlier portion of a double stance also yields a slight negative slope, it

serves as a considerably weak attractor compared to the end of a double stance, and is able to attract an extremely small portion of perturbation periods, as mentioned above. All the other phases with positive $\dfrac{dv}{d\varphi}$ act as repellors. Accordingly, the pulses are phase-locked at the strongest attractor, the end of a double stance in almost all entrained gaits. A very few exceptions may be possible e.g., if (1) the model speed becomes almost same as $v_{entrained}$ in the first step due to proper initial condition, and (2) from the second step, disturbances are small enough not to relocate φ outside the weak attractor. Excluding these few exceptions, the end of a double stance may be regarded as the "global" phase for the phase-locking associated with entrainment.

6.5.3. Limitations of the Model

To maximize simplicity, I neglected various aspects of locomotion. For example, multi-period gaits were not analyzed. Though multi-period asymmetric gaits are also observable in human locomotion, I limited my attention to the existence and the stability of a period-one gait, which represents the most fundamental mode of normal gaits. (Without quantitative analysis, Figure 6-4 (b) suggests that the model may have multi-period gaits under periodic perturbations.) With the simplification of perfect symmetry, I treated one step as an entire period of walking; in human locomotion, one period corresponds to one stride, which consists of two steps. As a result, the periodic mechanical perturbation was applied only to the trailing ankle, accelerating the model; the model was not allowed to be entrained when $\tau_p > \tau_0$ whereas entrainment to $\tau_p > \tau_0$ was observed in the experiment.

Physiological and anatomical realism was ignored by assuming a point mass body and massless legs. The massless legs significantly simplified the evolution rule, and allowed zero torque at hip joints, which relied on the experimental observation that ankle torque is the largest joint

torque in normal human walking [68, 114]. The observation that the model speed (1.03 m/s) is comparable to the speed of freely selected slow human walking [90] may be partly due to that the model has no actuation at hip and knee joints while its ankle actuation parameter (k) is determined based on normal human ankle torque during walking.

6.6. Conclusion

Human walking exhibits many features associated with limit-cycle oscillators. Stable periodic behavior with entrainment and phase-locking requires a non-linear dynamical system, but there are several physiologically-plausible candidates that might be responsible for these limit-cycle behaviors of human walking. Any combination of several peripheral neuro-mechanical factors— self-sustaining oscillatory neural networks (e.g., CPGs in the spinal cord); "chaining" of reflexes based on afferent feedback; gravito-inertial dynamics of the musculo-skeletal system; and discrete, dissipative mechanical interaction with the physical environment—may exhibit limit-cycle behaviors; and they may do so without supra-spinal control. The model presented here does not contain any self-sustaining intrinsic neural oscillator such as a CPG or any related form of explicit control specifying phase dynamics such as a phase-locking loop in a radio device. The remarkable competence of the simple model suggests that a state-determined process based on afferent feedback may be the minimal model component to describe measurable human walking behavior such as asymptotically stable periodic motion and entrainment with phase-locking to a narrow range of periodic perturbations.

The mechanics of periphery accounts for a significant portion of this competence. Particularly, the energy dissipation due to the non-elastic foot-ground interaction is crucial to the asymptotic stability. It was also revealed that simple peripheral mechanics, combined with minimal

123

afferent feedback, can explain the stable mechanism of entrainment and phase-locking of the model. This suggests that such a simple mechanism may play a role in the phase-locking to mechanical perturbations and associated entrainment of human walking, as success of passive walkers suggests plausible importance of gravito-inertia mechanics in human walking.

Related with the application to robot-aided therapy for walking, the competence of this simple model implies that the proposed entrainment therapy may be feasible for wide range of neurological impairment. Though some severe neurological injuries cause *atrophy* as well as impaired functionality of neural control, the essential components for the execution of peripheral mechanics still remain available: foot-ground interaction, gravity and inertia (though may be reduced due to loss of muscle tissues). Therefore, considering the competence of the presented model based on peripheral mechanics mediated by minimal afferent feedback, the proposed entrainment therapy may be applicable to treatment of locomotor deficit due to various neurological impairments including not only stroke or MS but also spinal cord injury (SCI).

7. Conclusions and Future Work

7.1. Summary

Robot-aided therapy is a concept to use robotic devices to rehabilitate human motor function more effectively. For effective robot-aided therapy, correct understanding of human motor control should be accompanied besides implementation of safe human-robot interaction. Robotic therapy for upper-extremities, which discourages the deviation from desired kinematics of reaching movement, has proven its efficacy and is now recommended by the American Heart Association [115]. However, the current form of robotic therapy for lower-extremities, which discourages the deviation from desired walking kinematics is much less effective and is declared "still in its infancy"[115]. One plausible reason of this discrepancy is that human locomotor control may be significantly different from neural control of reaching. From neuroscience studies over decades, the neural control of kinematics has proven to be a key factor in control of reaching movement [21-24]. However, this does not have to be valid for human locomotor control. Fundamentally, locomotion is a hybrid of discrete and continuous dynamics, which is essentially different from reaching movements.

In fact, robotic experiments [26, 27] teach us that much of the detailed coordination required to walk probably emerges from the passive pendular dynamics of the lower limbs rather than control of joint kinematics. In addition, though the evidence is not as strong as in the cases of quadrupeds, there are experimental evidences supporting the existence of rhythmic pattern generator in human spinal cord [33]. Taken together, walking is a periodic process that may partly emerge from some oscillating dynamics from the mechanical interaction of inertia, gravity and

environment, from oscillating neural network or from combination of both. If any of these plays an important role in human locomotor control, the current approach of most therapeutic robots may inadvertently interfere with the natural dynamics of walking by focusing only on the nominal kinematics. To design more effective robotic therapy for walking, we may have to consider and even exploit the naturally oscillating dynamics of human locomotion.

To propose a specific rehabilitation strategy that does not suppress the oscillating dynamics of human locomotion, I first addressed the mechanically essential components of stable periodic walking. To maintain robust stability of locomotion, energy dissipation is necessary; any energy conservative walking cannot be asymptotically stable despite the non-holonomy of legged locomotion. As a related comment, any study that claims an asymptotically stable and robust, but energy-conservative walking model is based on invalid stability analysis which precludes any perturbation that changes the energy level by parameterizing the total energy. Mechanically, the interaction between a foot and the ground is the most important mechanism of energy dissipation [61], which is an essential component for asymptotic stability rather than an accidental or just inevitable outcome. In addition, practically, the foot-ground interaction is the only mechanism for energy dissipation that we can control in the physical therapy through mechanical interaction, and therefore should be considered in rehabilitation of human walking.

To have periodic motion under the energy dissipation which is necessary for robust stability, energy compensation or actuation must be added. In human walking, ankle actuation is the most significant source of propulsion, and therefore should be considered in rehabilitation of human walking. The foot-ground interaction and ankle actuation is also neurologically important; they are closely related with the key components regulating the rhythmic pattern generator that is plausibly embedded in the human spinal cord. Taken together, I defined the design criteria for robot-aided rehabilitation strategy for walking as foot-ground interaction and ankle actuation.

126

To address how to use the robotic aid to exploit the oscillating dynamics of walking, I paid attention to that limit-cycle oscillators may serve as competent models of both rhythmic pattern generator and interaction between periphery and environment, and one of the distinctive features of the limit-cycle oscillators is that they may exhibit *entrainment* and *phase-locking* under proper periodic perturbation. Impaired by the plausible contribution of limit-cycle oscillators to human walking, I proposed entrainment and phase-locking of human locomotion as a method to affect human walking without suppressing its natural oscillating dynamics. Combined with the defined design criteria, *entrainment with ankle mechanical perturbation* was proposed as a novel approach to robot-aided therapy for walking.

The scenario is as follows: the robot initially assists patient at preferred walking cadence, which is usually slower than normal cadence of unimpaired people. Then periodic interaction is applied via ankle to entrain the patient's cadence. With proper control, the robot can progressively increase the perturbation frequency to speed up the patient's cadence. In other words, the robot can drag the patient's gait toward normal cadence.

The feasibility of this approach was assessed by experiments with normal subjects and neurologically impaired subjects. As unimpaired human subjects walked at constant speed, periodic torque pulses to the ankle were applied at periods different from their preferred cadence. The gait period of almost all subjects entrained to this mechanical perturbation, converging to match that of the perturbation. Significantly, entrainment occurred only if the perturbation period was close to subjects' preferred walking cadence: it exhibited a *finite basin of entrainment*. Further, regardless of the phase within the walking cycle at which perturbation was initiated, subjects' gait synchronized or *phase-locked* with the mechanical perturbation at a phase of gait where it assisted propulsion. These results were affected neither by auditory feedback nor by a distractor task. However, the convergence to phase-locking was slow, suggesting a weakly attracting limit-cycle rather than

127

voluntary control or voluntary adaptation.

As observed in normal human walking, neurologically impaired patients adapted their gait periods to synchronize with the perturbation by phase-locking the robotic torque at terminal stance phase. In addition, their gaits maintained entrainment even under gradual increase of the perturbation cadence, and the walking cadence became significantly faster due to the training with clear after-effects when the perturbation ceased. All these results support the feasibility of the proposed strategy for walking therapy that exploits an embedded neural oscillator interacting with peripheral mechanics and the resulting natural dynamics of walking, which are essential but hitherto neglected elements of walking therapy.

A highly simplified one degree of freedom model without any supra-spinal control or any self-sustaining intrinsic neural oscillator reproduced the essence of the observed limit-cycle features of human walking: 1) periodic gait that is 2) asymptotically stable; 3) entrainment to periodic perturbations provided they are close to the model's unperturbed period; and 4) phase-locking to locate the perturbation at the end of double stance. It was revealed that simple peripheral mechanics, combined with minimal afferent feedback, can explain the stable mechanism of entrainment and phase-locking of the model. The competence of this simple model implies that the proposed entrainment therapy may be feasible for wide range of neurological impairment.

7.2. Discussion and Implications

7.2.1. Understanding of Human Locomotion Is Necessary for Better Therapy

One of the key messages in the introduction of this thesis is that robot-aided therapy must

consider essential components of human motor control. The essential components may be filled by knowledge of neuroscience, neurophysiology, bio-mechanics, etc, which means advance in robotics alone cannot be sufficient. Robotics has shown a lot of promise through the high technology. At least for kinematic controllers, we can develop an actuator strong enough to overpower human motion, and we can develop a controller precise enough to impose very smooth motion to our limbs. However, either super strong actuator or super precise and smooth controller may be unnecessary in effective therapy of walking. For neuro-motor-rehabilitation, the actuators must be back-drivable to allow the voluntary motion of patients, and particularly for rehabilitation of walking, rather than super-smooth motion, the "discrete" and "impulsive" contact between foot and ground should be exploited to allow the natural oscillating dynamics of walking.

7.2.2. Energy Consumption Cannot Be the Complete Cost Function of Animal Locomotion

The necessity of energy dissipation for robust stability may be obvious, but it leads to non-trivial arguments. As depicted in the highly simplified models, the Floquet multiplier, which determines the stability of periodic motion, is directly related with the reduction of kinetic energy (Appendix B). This implies a trade-off between energy consumption and stability. Provided the parameter values admit a periodic gait, greater energy dissipation per step yields stronger stability and vice versa.

Many widely-cited (indeed "classical") studies have assumed that animal locomotion evolved to consume the least energy [38-43]. Though the value of minimizing the energy cost of transportation is self-evident, robust stability arguably takes a higher priority. Evolution may be regarded as optimizing the probability of reproduction, supported by optimizing survival (at least

129

until reproduction) [55]. Reliable performance (e.g. robust locomotor stability) therefore may take higher priority than energy efficiency. At a minimum, stability, which requires energy dissipation, should be included in the objective function.

Although collision-free legged locomotion is physically possible, non-elastic interaction between foot and ground, which dissipates kinetic energy, is a common characteristic of legged animal locomotion. Particularly, in human locomotion, muscles do more positive than negative work when walking at constant average speed on level ground which consumes counterbalancing phases of positive and negative work to maintain a constant average energy [57]. This provides evidence of energy dissipation in normal human walking, most of which is due to the non-elastic interaction between a foot and ground [61].

7.2.3. Supervisory Control of Human Locomotion

The results of experiments with healthy and neurologically impaired patients show clear evidence that a neuro-mechanical oscillator participates in human walking, but it is equally clear that much more is required. Like many mammals, humans can control foot placement with precision while walking, even onto irregularly-spaced footholds. A low-level limit-cycle oscillator cannot account for this behavior. Participation from higher levels of the CNS is indicated, especially if the target footholds are visually acquired. Perhaps the neuro-mechanical oscillator is a legacy of more primitive forms of control. The experimental results suggest the hypothesis that motor control of locomotion in humans is hierarchically organized to implement *central supervisory control of a semi-autonomous periphery*. The essence of supervisory control is that the "control operator" (the supra-spinal nervous system) has the *option* to intervene directly in the detailed control of "low-level" system behavior (the spinal neuro-mechanical periphery) but—importantly—need not do so

continuously [92, 93]. Instead, it only intervenes when need arises (e.g. to react to a stumble or place a foot on a target). In this hypothesis, the neuro-mechanical periphery is conceived to be *semi-autonomous*: it is capable of robustly stable rhythmic walking with minimal central intervention. That requires a nonlinear oscillator because robustly sustained autonomous oscillation can only result from a nonlinear dynamical system. In consequence, the neuro-mechanical periphery would exhibit behavior characteristic of limit-cycle oscillations, including a tendency to entrain to periodic perturbations and converge to a constant phase-locked relation with them, as observed.

Supervisory control of a semi-autonomous physical system is proven engineering technology, introduced to minimize the computational burden of control and mitigate detrimental effects of delays due to remote (tele-)operation, especially in space exploration [93, 116]. Applied to human motor control, the key idea is that, because of the limited response speed of muscles and the substantial delays due to neural conduction, in effect *the supra-spinal nervous system tele-operates the neuro-mechanical periphery*. Supervisory control is a plausible compromise that allows the neuro-mechanical periphery to operate semi-autonomously to unburden the supra-spinal nervous system, yet reserves the option of central intervention as needed to offset the limitations of a semi-autonomous periphery. Supervisory control may provide a useful perspective to organize some of the vast literature on mammalian locomotion.

7.3. Future Work

In the experiments with neurologically impaired patients, entrainment to gradually increasing perturbation cadence, phase-locking at mid-terminal stance phase which corresponds to the ankle actuation phase, reduced variability due to entrainment, and clear after-effects were observed. Though all these results support the feasibility of the proposed strategy of entrainment to

ankle mechanical perturbation, there are a lot of aspects to be refined and resolved.

One of the most important limitations of the current preliminary version of the training protocol is that the subjects were asked to walk on a treadmill at a constant speed; it is not obvious whether the subject can actually improve their walking speed in overground walking. One necessary future work is to modify the strategy so that the speed of treadmill is adjusted as the walking cadence of the subjects becomes faster.

Another important limitation of the current preliminary form of the training strategy is that two subjects out of four could not complete the session in a planned way, which suggests that current version of the training is clearly laboring for neurologically impaired patients. This limitation becomes more problematic considering that each session did not take longer than 15 minutes of treadmill walking; the current form of protocol may not be able to provide enough amount of training before the subjects are exhausted. However, there was no body weight support provided in the experiments; though the subjects wore a harness for a body weight support system as in Figure 5-1, it was only for safety in the case of falling down, and no tension was applied in the harness. A very simple update to resolve the fatigue of the patients and limited amount of the training is to provide some body weight support when the patients walk on the treadmill.

Design of the robotic perturbation is another aspect to refine. In the experiment, a train of square pulses whose amplitude and duration are 10 N·m and 0.1 s with a specified cadence was applied. The model based analysis suggests that the role of peripheral mechanics may be important in the observed phase-locking and entrainment. Therefore, it is plausible that the basin of entrainment may be broadened by applying different profile of the perturbation pulse. Quantitative analysis of the effects of design parameters of the robotic pulse on the basin of entrainment and/or on the convergence rate of phase-locking may enable refinement of the training strategy.

Appendix

A. Existence of Derivative Matrices of the Poincaré Maps

In this section, I show that the Poincaré map representing the stride function of each model presented in this thesis is differentiable so that the derivative matrix exists. This argument aims to prove that linearization is valid for the stability analysis of the period-one gaits of the models studied. Before starting the proof, I introduce some relevant terminology and a proven theorem.

Definition   A function has smoothness of C^n ($n \geq 0$) when the nth derivative of the function exists and is continuous. For example, a function $f(x) = \begin{cases} 0 (x \leq 0) \\ x (x > 0) \end{cases}$ is C^0 but not C^1 while a function $f(x) = \begin{cases} 0 (x \leq 0) \\ x^2 (x > 0) \end{cases}$ is C^1 and hence C^0 but not C^2.

Theorem   Assume that a vector $\mathbf{x}$ obeys an evolution rule $\dot{\mathbf{x}} = f(\mathbf{x})$. The solution $\mathbf{x}(t; \mathbf{x_0}, t_0)$ is as smooth in $\mathbf{x_0}$ as f is in $(\mathbf{x}, t)$. For example, if f is C^3 in $(\mathbf{x}, t)$, then $\mathbf{x}(t; \mathbf{x_0}, t_0)$ is C^3 in $(\mathbf{x_0}, t_0)$.

A.1. A Rimless Wheel and an Ankle Actuated Model in a Sagittal Plane

Let a collision occur at $t = 0$ and the next collision occur at T_f. With the definitions of $\mathbf{x} = \begin{pmatrix} x_1 \\ x_2 \end{pmatrix} = \begin{pmatrix} \theta \\ \dot{\theta} \end{pmatrix}$ and $\hat{\mathbf{x}} = (x_2) = (\dot{\theta})$, the Poincaré map, $\mathbf{f}$ is summarized schematically as

$$\mathbf{f} : (\hat{\mathbf{x}}_0, t = 0_+) \xrightarrow{\dot{\mathbf{x}} = f(\mathbf{x})} (\hat{\mathbf{x}}, t = T_{f^-}) \xrightarrow{Collision} (\hat{\mathbf{x}}, t = T_{f^+}),$$

133

where $f(\mathbf{x}) = \begin{pmatrix} x_2 \\ f_2(x_1) \end{pmatrix}$, which is the corresponding evolution rule of each model, and

$$\mathbf{x}\Big|_{t=T_{f+}} = \begin{pmatrix} \theta \\ \dot{\theta} \end{pmatrix}\Big|_{t=T_{f+}} = \begin{pmatrix} -\theta \\ (\cos 2\alpha)\dot{\theta} \end{pmatrix}\Big|_{t=T_{f-}} = \begin{pmatrix} \alpha \\ (\cos 2\alpha)\dot{\theta} \end{pmatrix}\Big|_{t=T_{f-}}.$$

I can obtain an explicit form of $\mathbf{f}$. Using a work-energy principle,

$$\frac{1}{2}mv_0^2 + W = \frac{1}{2}mv_1^2,$$

where $v_0 = v(t = 0_+)$, $v_1 = v(t = T_{f-})$, and W is the work done by an external force. For the

rimless wheel on a slope, $W = 2mgl\sin\alpha\sin\gamma$, and for the ankle actuated walker $W = \frac{1}{2}k(\frac{\pi}{2}+\alpha)^2$.

For both cases, W is a constant, and $v_1 = \sqrt{v_0^2 + \dfrac{2W}{m}}$.

The whole map of $\mathbf{f} : (\hat{\mathbf{x}}_0, t = 0_+) \xrightarrow{\dot{\mathbf{x}}=f(\mathbf{x})} (\hat{\mathbf{x}}, t = T_{f-}) \xrightarrow{\text{Collision}} (\hat{\mathbf{x}}, t = T_{f+})$

becomes

$$\dot{\theta}(t = T_{f+}) = -\frac{\cos 2\alpha}{l}\sqrt{l^2\dot{\theta}_{0+}^2 + \frac{4mgl\sin\alpha\sin\gamma}{m}} = \mathbf{f}(\hat{\mathbf{x}}_0, t = 0_+) = \mathbf{f}(\dot{\theta}_{0+})$$

for the rimless wheel on a slope, and

$$\dot{\theta}(t = T_{f+}) = -\frac{\cos 2\alpha}{L}\sqrt{L^2\dot{\theta}_{0+}^2 + \frac{k}{m}(\frac{\pi}{2}+\alpha)^2} = \mathbf{f}(\hat{\mathbf{x}}_0, t = 0_+) = \mathbf{f}(\dot{\theta}_{0+}),$$

for the ankle actuated model in a sagittal plane, where $\dot{\theta}_{0+} = \dot{\theta}(t = 0_+)$. In each explicit form,

the map $\mathbf{f}$ is differentiable with respect to $\hat{\mathbf{x}}_0$, which means that the derivative matrix of the map of

each model exists.

134

A.2.   A Springy Legged Model

I consider a map representing one step as a combination of two maps. The first part is the map $\mathbf{f}_1$ whose input and output are the reduced state vectors at the beginning and the end of one step respectively. The second part is the map $\mathbf{f}_2$ whose input and output are the reduced state vectors at the end of one step and the beginning of the next step respectively. T_s is the time when a step ends. The combination of $\mathbf{f}_1$ and $\mathbf{f}_2$ makes the whole map corresponding to the Poincaré map whose input and output are the reduced state vectors at $t = 0_+$ and $t = T_{s+}$ respectively, or

$$\mathbf{f} = \mathbf{f}_2 \circ \mathbf{f}_1 : (\hat{\mathbf{x}}_0, t = 0_+) \rightarrow (\hat{\mathbf{x}}, t = T_{s-}) \xrightarrow{\;continuity\;\;of\;\;velocity\;} (\hat{\mathbf{x}}, t = T_{s+}) \ .$$

By the introduced theorem above, I can state that the first map $\mathbf{f}_1$ is smooth enough to be C^1 in $\hat{\mathbf{x}}_0$. Hereafter, I refer to this fact as ⓐ. I will depend on fact ⓐ to complete the proof.

Please see Figure 2-3. Let η be the value of $-\theta$ at $t = T_{s-}$. To be faithful to the Poincaré section I selected, I need the length of the new stance leg l_n to be the unloaded leg length l_0 at $t = T_{s+}$. Then, θ at $t = T_{s+}$ is determined to be η by geometry. Using the geometry and continuity of the velocity vector at $t = T_s$, $x_3 \big|_{t=T_{s+}} = \theta \big|_{t=T_{s+}} = \eta = -\theta \big|_{t=T_{s-}}$, and

$$\begin{pmatrix} x_2 \\ x_4 \end{pmatrix}\bigg|_{t=T_{s+}} = \begin{pmatrix} \dot{l} \\ \dot{\theta} \end{pmatrix}\bigg|_{t=T_{s+}} = \begin{pmatrix} -\sin\eta & -l_0\cos\eta \\ \cos\eta & -l_0\sin\eta \end{pmatrix}^{-1} \begin{pmatrix} \dot{l}(\sin\eta) - l_0\dot{\theta}(\cos\eta) \\ \dot{l}(\cos\eta) + l_0\dot{\theta}(\sin\eta) \end{pmatrix}\bigg|_{t=T_{s-}} .$$

By ⓐ, η is C^1 in $\hat{\mathbf{x}}_0$. Therefore, it is obvious that $x_3 \big|_{t=T_{s+}}$ is at least C^1 in $\hat{\mathbf{x}}_0$. Also, by ⓐ, $\dot{l}$ at $t = T_{s-}$ is at least C^1 in $\hat{\mathbf{x}}_0$. Therefore, $x_2 \big|_{t=T_{s+}}$ and $x_4 \big|_{t=T_{s+}}$ are also at least C^1 in $\hat{\mathbf{x}}_0$. Therefore, the map of $\mathbf{f} = \mathbf{f}_2 \circ \mathbf{f}_1 : (\hat{\mathbf{x}}_0, t = 0_+) \rightarrow (\hat{\mathbf{x}}, t = T_{ss-}) \xrightarrow{\;continuity\;\;of\;\;velocity\;} (\hat{\mathbf{x}}, t = T_{ss+})$ is at least C^1 in $\hat{\mathbf{x}}_0$. This guarantees the existence of the derivative matrix of the Poincaré map.

B.   Floquet Multiplier as Reduction Ratio of Energy

In this section, I show that any model with one dimensional Poincaré section, constant energy supply and constant reduction ratio of kinetic energy shows asymptotic stability, and the Floquet multiplier is same as the constant reduction ratio of the kinetic energy per cycle. The mass, constant amount of energy supply and constant reduction ratio are m, W and ρ respectively. Using work-energy principle, the kinetic energy at the beginning of $(i + 1)^{\text{th}}$ cycle is

$$\frac{1}{2}mv_{i+1}{}^2 = \rho\left(\frac{1}{2}mv_i{}^2 + W\right) \qquad\qquad \text{Equation App-1}$$

where v_i means the speed of the mass at the beginning of ith cycle. For this system with one dimensional Poincaré section, the Poincaré map becomes

$$v_{i+1} = \sqrt{\rho\left(v_i{}^2 + \frac{2W}{m}\right)},$$

and the Floquet multiplier of interest becomes

$$\frac{dv_{i+1}}{dv_i} = \sqrt{\rho}\,\frac{v_i}{\sqrt{v_i{}^2 + \dfrac{2W}{m}}}. \qquad\qquad \text{Equation App-2}$$

From Equation App-1, the fixed point of the Poincaré map satisfies $v_i{}^2 = \rho\left(v_i{}^2 + \dfrac{2W}{m}\right)$ or,

$$v_i{}^2 = \frac{\rho}{(1-\rho)}\left(\frac{2W}{m}\right) \qquad\qquad \text{Equation App-3}$$

Plugging in Equation App-3 to App-2 yields $\left.\dfrac{dv_{i+1}}{dv_i}\right|_{\text{fixed point}} = \rho$, which proves that the Floquet multiplier is same as the constant reduction ratio of the kinetic energy per cycle.

C. Reliability of Measuring Initial Loading by Knee Angle

In this section, I assess the reliability of the method by which I assess initial loading phase using knee angle data. A practical algorithm of estimating initial loading phase from raw foot switch data is described, and the initial loading phases measured by heel pressure profile and knee angle profile are compared for walking of unimpaired subjects. The initial loading phases measured by the two methods are slightly different, and the difference depends on the subject. However, the difference is smaller than the variability of the stride cadence in all subjects, concluding the reliability of defining gait cycle using the knee angel profile.

C.1. Determination of Initial Loading from Foot Switch Data

Experiments

Four young adult subjects (ages 27 to 35) participated in the experiment. They reported no neurological or biomechanical impairment and gave informed consent to participate as approved by MIT's institutional review board. They walked on a treadmill (Sole Fitness F80 with a 0.84 m × 1.90 m deck and 0.1 mph (0.045 m/s) belt speed resolution) at a self-selected comfortable speed while Anklebot was programmed to act like a torsional spring and damper with constant equilibrium position. The parameter values of stiffness, damping and equilibrium position were set as same as in 4.2.1, but there was no mechanical perturbation of square pulses. The knee angle was recorded at a sampling rate of 200 Hz by a potentiometer embedded in the knee brace, and the pressure at heels and toes is measured by foot switches (DS-X02 Myomonitor System, Delsys Inc.).

Data Analysis

The typical data acquired by the foot switch at a heel of a normal gait are shown in Figure App-1. The onset of the rapid increase of the foot switch signal indicates the initial loading phase. To detect these moments systematically, the onset of the increase was estimated as an intersection between the baseline signal and a linear approximation of the rapid increase (Figure App-2). The baseline was measured as a mean value of the signal for a relatively flat region, (1) of Figure App-1. Though the signal from foot switch varies even in those regions, the fluctuation is considerably small compared with the range of the signal. The linear approximation of the rapid increase was evaluated using 11 successive points centered at a point closest to a threshold. The threshold was determined high enough to avoid any improper measure due to the small hills during swing phase ((3) of Figure App-1) but low enough to locate the center point close to the actual onset of the rapid increase (Figure App-2).

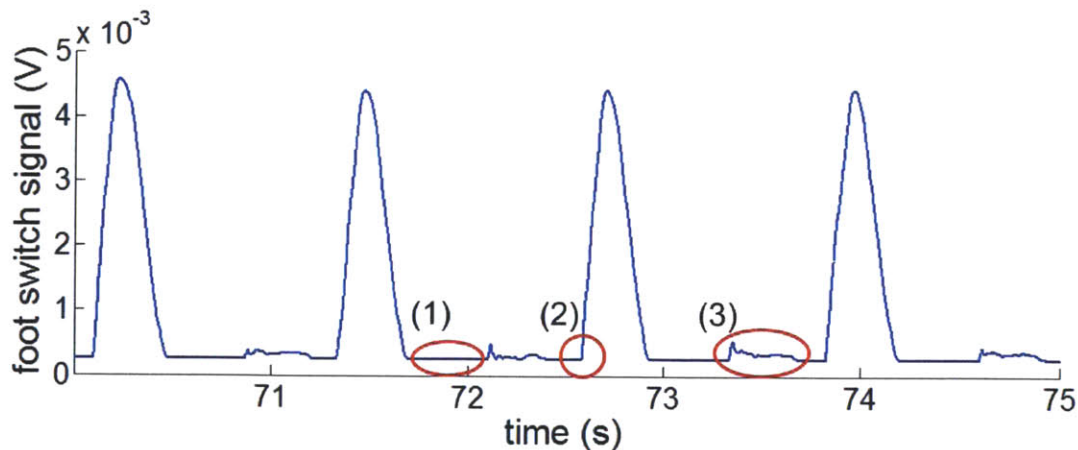Figure App-1: Typical data from the foot switch at a heel
The signal is relatively flat when the heel is detached from the ground and the center of pressure moves to the frontal foot: (1). When the initial loading occurs after swing phase, the pressure increases rapidly: (2). There are some small hills during swing phase: (3), which may be due to the interaction between the shoe and the heel.
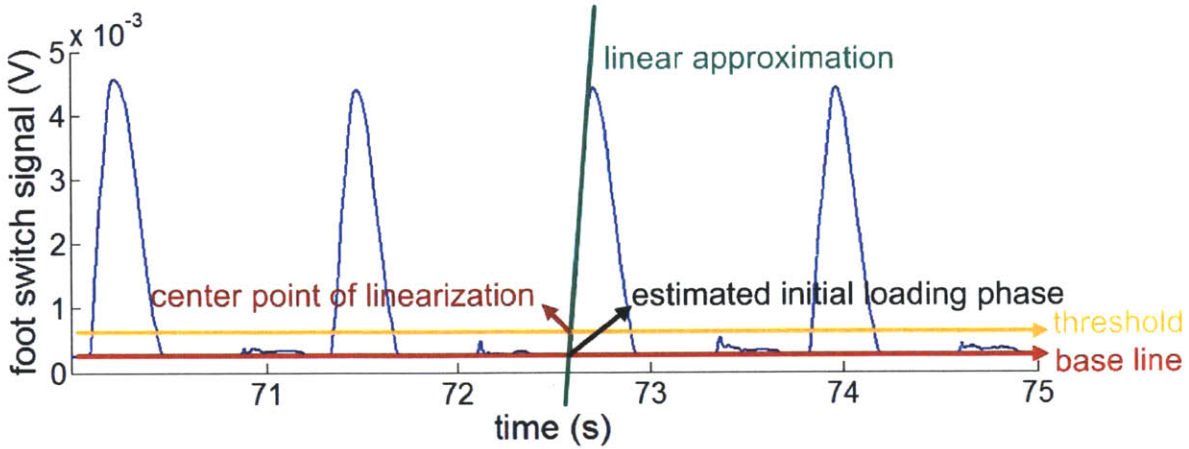
138

Figure App-2: Determination of initial loading from foot switch signal
The initial loading phase is estimated as an intersection between the baseline signal of no contact between heel and ground (red) and a linear approximation of the rapid increase (green). The linear curve is evaluated based on 11 successive points centered at a point closest to a threshold (orange).

It might be argued that the threshold is not uniquely determined and different threshold may cause different estimation of the initial loading phase. Indeed, the value of the threshold directly affects the center point of linearization and therefore may affect the estimation of initial loading phase. However, the effect of threshold on the estimation of the initial loading phase is negligible by virtue of two reasons. First, the rapid change of the foot switch signal around the heel strike is almost linear. Therefore, the intersection point is not sensitive to the location of the center of the linearization. Second, the slope of the rapid increase of the pressure is steep; the difference in the center point of the linearization can change the estimation of a phase only to a negligible extent.

C.2. Statistical Tests to Assess the Reliability

The initial loading phase was also measured by the knee angle profile as described in 4.2.2. By comparing (A) the initial loading phase estimated from knee angle with (B) the initial loading

phase estimated from pressure at the heel, the reliability of measuring initial loading using knee angle profile can be assessed.

Stride Period

To define gait cycle as a normalized time with respect to the stride period, it is critical to assess whether the stride periods measured by (A) and (B) are not statistically different. Figure App-3 shows the distribution of the stride periods of one subject measured by (A) and (B). Two null hypotheses were tested:

  o H_{01}: The stride periods measured by (A) and (B) come from normal distributions with the same variance

  o H_{02}: The stride periods measured by (A) and (B) could have same mean when the standard deviations are assumed equal.

$H_{01}$was tested by F-test. When H_{01} was accepted, H_{02} was tested by T-test. For all four subjects, both hypotheses were accepted with 95 % confidence level, suggesting that both (A) and (B) yielded same measure of stride period. By virtue of this result, it is justifiable to use the mean period of one population as the average period of the gait cycle.
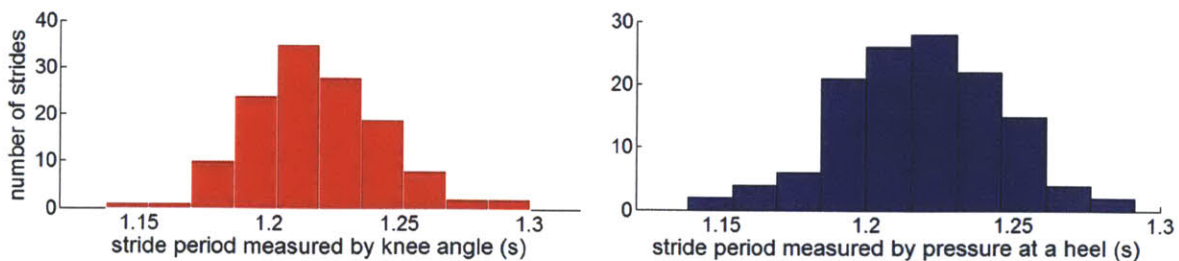

Figure App-3: Distribution of stride periods measured by knee angle and pressure at a heel Statistical tests conclude that the two populations are not significantly different either in the variance or in the mean value.

Initial Loading Phase

To assess the reliability of measuring initial loading by knee angle, I defined an error between (A) and (B) to address the following questions:

o   Is the error significantly different from zero?

o   If so, is the magnitude of the error significant compared to the variability of gaits?

Figure App-4 shows the distribution of the error between (A) and (B) for one subject. The difference in time (s) was normalized as the difference in gait cycle phase (%) using the average stride period. T-test concluded that the error is statistically different from zero. However, the mean of the error was only -1.085 %, whereas the standard deviation of the stride period corresponds to 2.208 % of the mean stride period.

For each of the four subjects, though the mean of the error between (A) and (B) was different from zero and the mean varied across subjects, the mean was always smaller than the standard deviation of the stride periods of each subject. The distribution of the error between (A) and (B) for all subjects has the mean of -0.6896 %. Taken together, measuring initial loading (or 0 % gait cycle) by knee angle profile is reliable for walking of normal subjects.
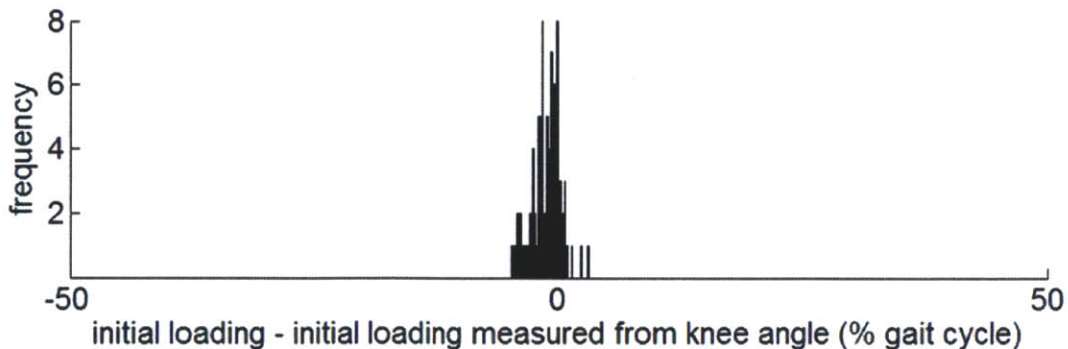

Figure App-4: A histogram of errors between initial loading from knee angle and heel pressure
The mean of the error is different from zero, but the mean is smaller than the standard deviation of the stride period

141

D.   Effects of Entrainment on Variability of Walking Cadence in Unimpaired Walking

In this section, I assess the effects of entrainment on variability of walking cadence of unimpaired subjects. The effect varied across the subjects and did not show clear common tendency. A statistical test on all data of all subjects concluded that the variability of walking cadence of unimpaired subjects did not change significantly due to the entrainment to the periodic perturbation.

D.1.   Assessment Methods

Walking period was measured as the time interval between two successive initial loading phases which were estimated from knee angle profile as in 4.2.2. I selected all the gaits which were defined as *entrained* based on the assessment method in 4.2.2. For each selected gait, walking cadence of the last 15 strides before perturbation, the last 15 strides during perturbation and the first 15 strides after the end of perturbation were chosen as the groups for assessment of variability. The variability of walking cadence of each chosen group was evaluated by three metrics: range, interquatile range (IQR) and variance.

D.2.   Results

Figure App-5 shows that the variability was reduced, unchanged or even increased when the perturbation entrained the gaits depending on subjects. Contrary to the results of neurologically impaired gaits (Figure 5-6), the effects of entrainment on the variability of walking cadence in normal gaits was unclear.
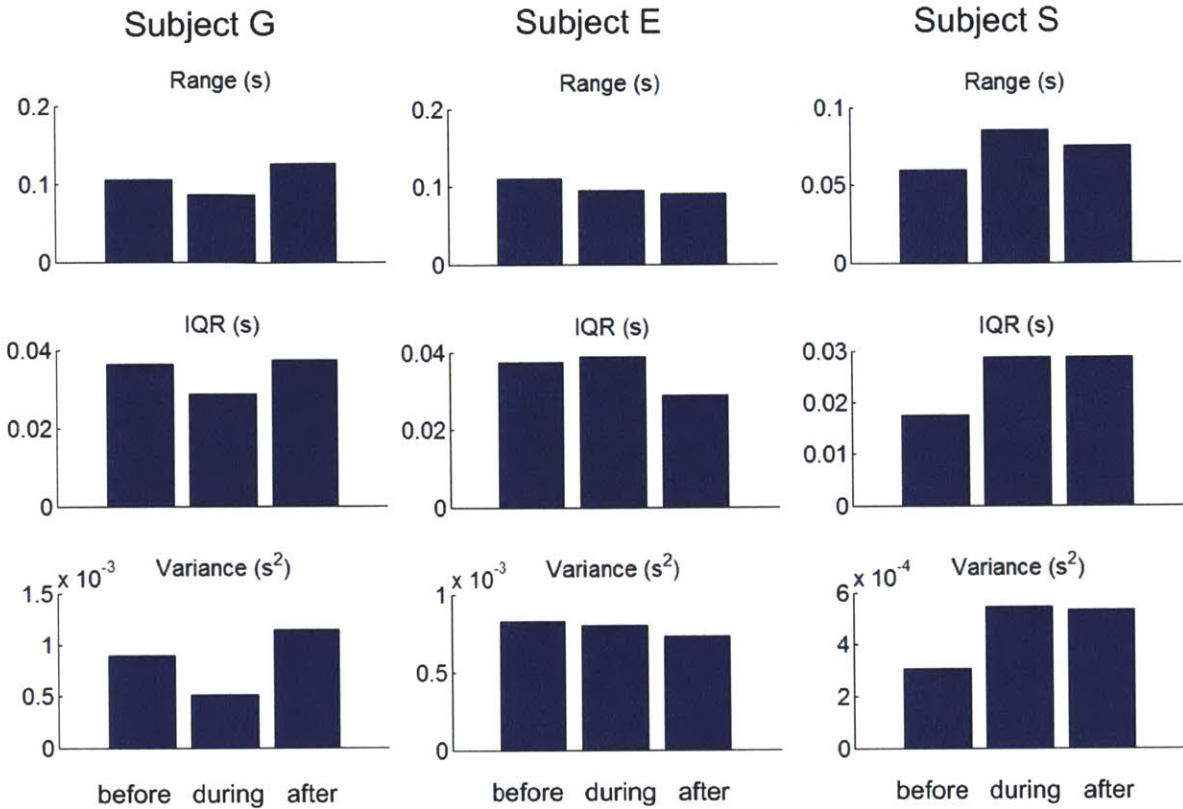
Figure App-5: Change of variability of walking cadence due to entrainment in normal walking

Variability of walking cadence was assessed by range, interquatile range (IQR), and variance of walking period of the last 15 strides before perturbation, the last 15 strides during perturbation and the first 15 strides after the end of perturbation for each subject. Depending on the subject and the metric, entrainment either reduced or increased the measure of variability of walking cadence. Subject G showed reduced variability due to entrainment; Subject E did not show clear trend; and Subject S showed increased variability due to entrainment.

To assess the overall tendency across all the subjects, the distribution of three metrics (range, IQR, and variance) across the subjects were evaluated for each of before, during and after the periodic perturbation which entrained the gaits when applied. Figure App-6 shows the results. None of the three metrics changed significantly due to entrainment to the periodic perturbation.
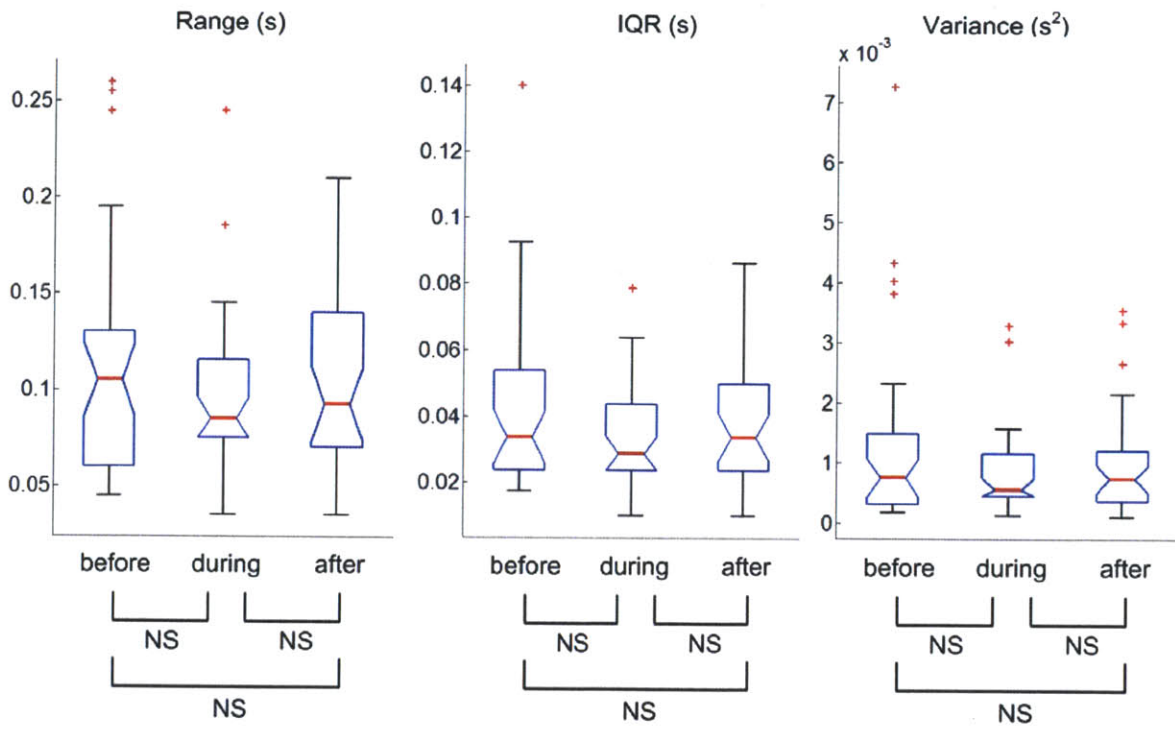
Figure App-6: Three metrics (range, IQR, and variance) across the subjects for each of before, during and after the periodic perturbation
None of the three metrics of variability showed statistically significant change due to entrainment.

E. Ground Reaction Forces of the Ankle Actuated Model

In this section, I assess the ground reaction forces exerting on the ankle actuated model and investigate the proper range of the ankle actuation constant k to keep the forces remain positive during both double stance phase and single stance phase.

E.1. Ground Reaction Forces during Double Stance

Figure App-7 shows the forces exerting on the model during double stance.

Figure App-7: Forces acting on the point mass
F_A and F_B are the ground reaction forces; they are acting on the line of AC and BC respectively.

Ground Reaction Force at A: F_A

F_A is positive as long as the ankle torque is applied the in plantar direction. Therefore, I don't have to worry about F_A.

145

Ground Reaction Force at B: F_B

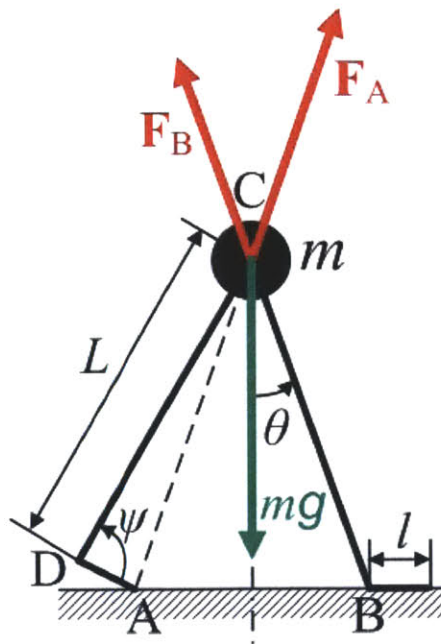F_B can be negative if 1) F_A is so excessive that the mass m is lifted regardless of gravity, or 2) the velocity is so excessive that the mass m is lifted due to centrifugal force. Therefore, I need to investigate the explicit form of F_B. Using a Newtonian approach, the magnitude of the ground reaction force can be directly obtained as

$$F_B = \frac{k(\mu - \psi(\theta))}{l \sin \gamma(\theta)} (\cos \varphi(\theta) \sin \theta - \sin \varphi(\theta) \cos \theta) + mg \cos \theta - mL \dot{\theta}^2 \text{, where}$$

ψ means the ankle angle, $\angle ADC$, γ means $\angle DAC$, and φ means $\angle BAC$, which are obtained as functions of θ as

$$\psi = \cos^{-1} \left(\frac{-4L^2 \sin^2 \alpha + 4Ll \sin \alpha + 2L(2L \sin \alpha - l) \sin(\theta)}{2Ll} \right),$$

$$\gamma = \cos^{-1} \left(\frac{(2L \sin \alpha - l)^2 + l^2 - 2L(2L \sin \alpha - l) \sin(\theta)}{2l \sqrt{L^2 + (2L \sin \alpha - l)^2 - 2L(2L \sin \alpha - l) \sin(\theta)}} \right), \text{ and}$$

$$\varphi = \tan^{-1} \left(\frac{L \cos \theta}{2L \sin \alpha - l - L \sin \theta} \right).$$

The time course of the reaction force F_B is numerically evaluated using MATLAB R2006a (Mathworks Inc.). Absolute error tolerance and relative error tolerance for the numerical integration are 10^{-8}. Figure App-8 shows the results. The moment when F_A becomes zero is the end of double stance phase. With given parameter values the ground reaction force is always kept positive, which means the model yields feasible gaits. F_B is also numerically evaluated under perturbation, and is kept positive with given perturbations.
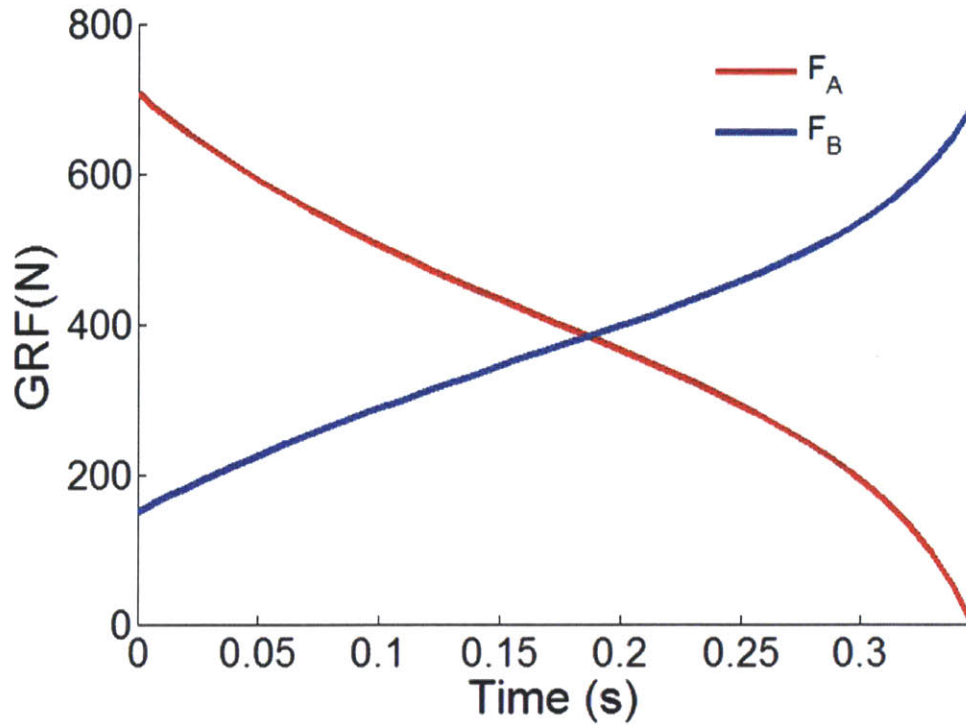
Figure App-8: Ground reaction forces of trailing leg and leading leg during double stance
Large torque at the initial stance results in large F_A and small F_B. F_B is kept positive with the selected parameter values

E.2. Ground Reaction Force during Single Stance

The single stance phase is simply a motion of an inverted pendulum, and the condition that

keeps the model from flying off is to keep $mg \cos \theta - m\dfrac{v^2}{L} = f(\theta)$ above zero. The function $f(\theta)$,

which equals to the magnitude of the ground reaction force, has the minimum at the end of the

single stance phase because $\cos\theta$ has the minimum at $\theta = -\alpha$, and v^2 has the maximum at the same

moment of $\theta = -\alpha$ during the single stance phase. Therefore, the sign of $f(-\alpha)$ concludes whether the

model flies off or not.

Rewriting the condition, we need

$$mg \cos \alpha - m \frac{v_C{}^2}{L} > 0,$$

<div align="right">Equation App-4</div>

where v_C is the speed of the point mass just before a collision. As derived in 6.4.2, the v_C of the periodic motion comes from the energy balance

$$\frac{1}{2}k(\alpha + \mu - \frac{\pi}{2})^2 = \frac{1}{2}mv_C^2(1 - \cos^2 2\alpha).$$

<div align="right">Equation App-5</div>

Plugging Equation App-5 into Equation App-4, the ground reaction force is always kept positive during the entire single stance if and only if

$$k < \frac{mgL \cos \alpha (1 - \cos^2 2\alpha)}{(\alpha + \mu - \frac{\pi}{2})^2}.$$

<div align="right">Equation App-6</div>

Combining Equation App-6 with Equation 5-5, the ankle actuation constant, k must satisfy

$$\frac{2mgL(1 - \cos \alpha)(1 - \cos^2 2\alpha)}{(\alpha + \mu - \frac{\pi}{2})^2} < k < \frac{mgL \cos \alpha (1 - \cos^2 2\alpha)}{(\alpha + \mu - \frac{\pi}{2})^2}$$

as a necessary condition. With the selected parameter values given in Table 6-1, k satisfies this. Please note that this inequality is only a necessary condition. As addressed in E.1, the ground reaction force during the double stance phase must be assessed to investigate whether the model exhibits physically reasonable gaits throughout the entire cycle.

References

[1] D. Hristic and M. Vukobratovic, "New approach to the solution of system for rehabilitation of paralyzed persons," *Automatika*, vol. 12, pp. 12-15, 1971.

[2] N. Hogan, H. I. Krebs, A. Sharon, and J. Charnnarong, "Interactive Robotic Therapist," vol. 5466213. United States, 1995, pp. 27.

[3] G. Kawakkel, B. J. Kollen, and H. I. Krebs, "Effects of robot-assisted therapy on upper limb recovery after stroke: a systematic review," *Neurorehabilitation and Neural Repair*, vol. 22, pp. 111-121, 2008.

[4] J. Hidler, D. Nichols, M. Pelliccio, K. Brady, D. D. Campbell, J. H. Kahn, and G. Hornby, "Multicenter Randomized Clinical Trial Evaluating the Effectiveness of the Lokomat in Subacute Stroke," *Neurorehabilitation and Neural Repair*, vol. 23, pp. 5 - 13, 2009.

[5] G. T. Hornby, D. D. Campbell, J. H. Kahn, T. Demott, J. L. Moore, and H. R. Roth, "Enhanced Gait-Related Improvements After Therapist- Versus Robotic-Assisted Locomotor Training in Subjects With Chronic Stroke," *Stroke*, vol. 39, pp. 1786-1792, 2008.

[6] S. P. Buerger, J. J. Palazzolo, H. I. Krebs, and N. Hogan, "Rehabilitation robotics: Adapting robot behavior to suit patient needs and abilities," Boston, MA, United States, 2004.

[7] H. I. Krebs, J. J. Palazzolo, L. Dipietro, M. Ferraro, J. Krol, K. Rannekleiv, B. T. Volpe, and N. Hogan, "Rehabilitation robotics: Performance-based progressive robot-assisted therapy," *Autonomous Robots*, vol. 15, pp. 7-20, 2003.

[8] L. L. Cai, A. J. Fong, L. Yongqiang, J. Burdick, and V. R. Edgerton, "Assist-as-needed training paradigms for robotic rehabilitation of spinal cord injuries," Piscataway, NJ, USA, 2006.

[9] M. L. Aisen, H. I. Krebs, N. Hogan, F. McDowell, and B. T. Volpe, "The Effect of Robot-Assisted Therapy and Rehabilitative Training on Motor Recovery Following Stroke," *Arch Neurol*, vol. 54, pp. 443-446, 1997.

[10] B. T. Volpe, H. I. Krebs, N. Hogan, L. Edelstein, C. Diels, and M. L. Aisen, "A novel approach to stroke rehabilitation: Robot-aided sensorimotor stimulation " *Neurology*, vol. 54, pp. 1938-1944, 2000.

[11] S. E. Fasoli, H. I. Krebs, J. Stein, W. R. Frontera, and N. Hogan, "Effects of robotic therapy on motor impairment and recovery in chronic stroke," *Archives of Physical Medicine and Rehabilitation*, vol. 84, pp. 477-482, 2003.

[12] P. S. Lum, C. G. Burgar, P. C. Shor, M. Majmundar, and M. Van der Loos, "Robot-Assisted Movement Training Compared With Conventional Therapy Techniques for the Rehabilitation of Upper-Limb Motor Function After Stroke," *Archives of Physical Medicine and Rehabilitation*, vol. 83, pp. 952 - 959, 2002.

[13] J. M. Hidler and A. E. Wall, "Alterations in muscle activation patterns during robotic-assisted walking," *Clinical Biomechanics*, vol. 20, pp. 184-193, 2005.

[14] S. Hesse and D. Uhlenbrock, "A mechanized gait trainer for restoration of gait,"

Journal of Rehabilitation Research and Development, vol. 37, pp. 701-708, 2000.

[15] S. Jezernik, G. Colombo, T. Keller, H. Frueh, and M. Morari, "Robotic Orthosis Lokomat: A Rehabilitation and Research Tool," *Neuromudulation: Technology at the Neural Interface*, vol. 6, pp. 108-115, 2003.

[16] H. Schmidt, C. Werner, R. Bernhardt, S. Hesse, and J. Kruger, "Gait rehabilitation machines based on programmable footplates," *Journal of NeuroEngineering and Rehabilitation*, vol. 4, pp. 2, 2007.

[17] R. N. Wool, D. Siegel, and P. R. Fine, "Task performance in spinal cord injury: effect of helplessness training," *Archives of Physical Medicine and Rehabilitation*, vol. 61, pp. 321-325, 1980.

[18] M. Bernhardt, M. Frey, G. Colombo, and R. Riener, "Hybrid force-position control yields cooperative behaviour of the rehabilitation robot LOKOMAT," Chicago, IL, United States, 2005.

[19] S. K. Banala, K. Seok Hun, S. K. Agrawal, and J. P. Scholz, "Robot Assisted Gait Training With Active Leg Exoskeleton (ALEX)," *Neural Systems and Rehabilitation Engineering, IEEE Transactions on*, vol. 17, pp. 2-8, 2009.

[20] N. Hogan, H. I. Krebs, B. Rohrer, J. J. Palazzolo, L. Dipietro, S. E. Fasoli, J. Stein, R. Hughes, W. R. Frontera, D. Lynch, and B. T. Volpe, "Motions or muscles? Some behavioral factors underlying robotic assistance of motor recovery," *Journal of Rehabilitation Research and Development*, vol. 43, pp. 605-618, 2006.

[21] P. Morasso, "Spatial control of arm movements," *Experimental Brain Research*, vol. 42, pp. 223-227, 1981.

[22] T. Flash and N. Hogan, "The coordination of arm movements: an experimentally confirmed mathematical model," *J. Neurosci.*, vol. 5, pp. 1688-1703, 1985.

[23] J. R. Flanagan and A. K. Rao, "Trajectory adaptation to a nonlinear visuomotor transformation: evidence of motion planning in visually perceived space," *J Neurophysiol*, vol. 74, pp. 2174-2178, 1995.

[24] D. M. Wolpert, Z. Ghahramani, and M. I. Jordan, "Are arm trajectories planned in kinematic or dynamic coordinates? An adaptation study," *Experimental Brain Research*, vol. 103, pp. 460-470, 1995.

[25] Y. P. Ivanenko, R. Grasso, V. Macellari, and F. Lacquaniti, "Control of Foot Trajectory in Human Locomotion: Role of Ground Contact Forces in Simulated Reduced Gravity," *J Neurophysiol*, vol. 87, pp. 3070-3089, 2002.

[26] T. McGeer, "Passive dynamic walking," *International Journal of Robotics Research*, vol. 9, pp. 62-82, 1990.

[27] S. H. Collins, M. Wisse, and A. Ruina, "A Three-Dimensional Passive-Dynamic Walking Robot with Two Legs and Knees," *The International Journal of Robotics Research*, vol. 20, pp. 607 - 615, 2001.

[28] T. G. Brown, "The Intrinsic Factors in the Act of Progression in the Mammal," *Proceedings of the Royal Society of London. Series B, Containing Papers of a Biological Character*, vol. 84, pp. 308-319, 1911.

[29] D. J. Kriellaars, R. M. Brownstone, B. R. Noga, and L. M. Jordan, "Mechanical entrainment of fictive locomotion in the decerebrate cat," *J Neurophysiol*, vol. 71, pp. 2074-2086, 1994.

[30] S. Grillner and P. Wallen, "Central Pattern Generators for Locomotion, with Special Reference to Vertebrates," *Annual Review of Neuroscience*, vol. 8, pp. 233-261, 1985.

[31] P. S. Stein, J. C. Victor, E. C. Field, and S. N. Currie, "Bilateral control of hindlimb scratching in the spinal turtle: contralateral spinal circuitry contributes to the normal ipsilateral motor pattern of fictive rostral scratching," *J. Neurosci.*, vol. 15, pp. 4343-4355, 1995.

[32] J. R. Cazalets, M. Borde, and F. Clarac, "The synaptic drive from the spinal locomotor network to motoneurons in the newborn rat," *J. Neurosci.*, vol. 16, pp. 298-306, 1996.

[33] Y. Gerasimenko, R. Gorodnichev, E. Machueva, E. Pivovarova, D. Semyenov, A. Savochin, R. R. Roy, and V. R. Edgerton, "Novel and Direct Access to the Human Locomotor Spinal Circuitry," *J. Neurosci.*, vol. 30, pp. 3700-3708, 2010.

[34] K. Matsuoka, "Mechanisms of frequency and pattern control in the neural rhythm generators," *Biological Cybernetics*, vol. 56, pp. 345-353, 1987.

[35] J. Collins and S. Richmond, "Hard-wired central pattern generators for quadrupedal locomotion," *Biological Cybernetics*, vol. 71, pp. 375-385, 1994.

[36] I. A. Rybak, N. A. Shevtsova, M. Lafreniere-Roula, and D. A. McCrea, "Modelling spinal circuitry involved in locomotor pattern generation: insights from deletions during fictive locomotion," *The Journal of Physiology*, vol. 577, pp. 617-639, 2006.

[37] B. van der Pol, "LXXXVIII. On Relaxation-Oscillations," *Philosophical Magazine Series 7*, vol. 2, pp. 978 - 992, 1926.

[38] G. A. Borelli, *De Motu Animalium*. Rome, 1680.

[39] D. F. Hoyt and C. R. Taylor, "Gait and the energetics of locomotion in horses," *Nature*, vol. 292, pp. 239-240, 1981.

[40] R. M. Alexander, "Optimization and gaits in the locomotion of vertebrates," *Physiological Reviews*, vol. 69, pp. 1199 - 1227, 1989.

[41] R. M. Alexander, "A Model of Bipedal Locomotion on Compliant Legs," *Philosophical Transactions of the Royal Society of London. Series B: Biological Sciences*, vol. 338, pp. 189-198, 1992.

[42] A. E. Minetti and R. M. Alexander, "A Theory of Metabolic Costs for Bipedal Gaits," *Journal of Theoretical Biology*, vol. 186, pp. 467-476, 1997.

[43] J. Nishii, "Legged insects select the optimal locomotor pattern based on the energetic cost," *Biological Cybernetics*, vol. 83, pp. 435-442, 2000.

[44] J. Schmitt and P. Holmes, "Mechanical models for insect locomotion: dynamics and stability in the horizontal plane I. Theory," *Biological Cybernetics*, vol. 83, pp. 501-515, 2000.

[45] R. M. Ghigliazza, R. Altendorfer, P. Holmes, and D. Koditschek, "A Simply Stabilized Running Model," *SIAM Review*, vol. 47, pp. 519 - 549, 2005.

[46] H. Geyer, "Simple Models of Legged Locomotion based on Compliant Limb Behavior," vol. Ph.D.: Friedrich-Schiller-Universit¨at Jena, 2005.

[47] G. T. Walker, "On a Dynamical Top," *Quart. J. Pure Appl. Math*, vol. 28, pp. 175-184, 1896.

[48] A. M. Bloch, P. S. Krishnaprasad, J. E. Marsden, and R. M. Murray,

"Nonholonomic Mechanical Systems with Symmetry," *Arch. Rational Mech. Anal.*, vol. 136, pp. 21-99, 1996.

[49]   D. V. Zenkov, A. M. Bloch, and J. E. Marsden, "The Energy-Momentum Method for the Stability of Nonholonomic Systems," California Institute of Technology CIT-CDS 97-010, 1997.

[50]   A. M. Bloch, J. E. Marsden, and D. V. Zenkov, "Nonholonomic Dynamics," *Notices of the American Mathematical Society*, vol. 52, pp. 320-329, 2005.

[51]   A. Ruina, "Nonholonomic stability aspects of piecewise holonomic systems," Calgary, Alta., Canada, 1998.

[52]   M. Coleman and P. Holmes, "Motions and Stability of a Piecewise Holonomic System: The Discrete Chaplygin Sleigh," *Regular and Chaotic Dynamics*, vol. 4, pp. 55-77, 1999.

[53]   M. J. Coleman, A. Chatterjee, and A. Ruina, "Motions of a rimless spoked wheel: A simple three-dimensional system with impacts," *Dynamics and Stability of Systems*, vol. 12, pp. 139-159, 1997.

[54]   M. J. Coleman, "A Stability Study of a Three-Dimensional Passive-Dynamic Model of Human Gait," in *Theoretical and Applied Mechanics* vol. Doctor of Philosophy: Cornell University, 1998.

[55]   R. Dawkins, *The Extended Phenotype*. Oxford, UK: Freeman, 1982.

[56]   M. Garcia, A. Chatterjee, A. Ruina, and M. Coleman, "Simplest walking model: Stability, complexity, and scaling," *Journal of Biomechanical Engineering, Transactions of the ASME*, vol. 120, pp. 281-288, 1998.

[57]   P. DeVita, J. Helseth, and T. Hortobagyi, "Muscles do more positive than negative work in human locomotion," *J Exp Biol*, vol. 210, pp. 3361-3373, 2007.

[58]   C. H. Barnett and A. F. Cobbold, "LUBRICATION WITHIN LIVING JOINTS," *J Bone Joint Surg Br*, vol. 44-B, pp. 662-674, 1962.

[59]   A. L. Hof, "Muscle mechanics and neuromuscular control," *Journal of Biomechanics*, vol. 36, pp. 1031-1038, 2003.

[60]   G. Venture, K. Yamane, and Y. Nakamura, "In-vivo estimation of the human elbow joint dynamics during passive movements based on the musculo-skeletal kinematics computation," presented at Robotics and Automation, 2006. ICRA 2006. Proceedings 2006 IEEE International Conference on, 2006.

[61]   A. D. Kuo, J. M. Donelan, and A. Ruina, "Energetic Consequences of Walking Like an Inverted Pendulum: Step-to-Step Transitions," *Exercise and Sport Sciences Reviews*, vol. 33, pp. 88-97, 2005.

[62]   V. Dietz, A. Gollhofer, M. Kleiber, and M. Trippel, "Regulation of bipedal stance: dependency on "load" receptors," *Experimental Brain Research*, vol. 89, pp. 229-231, 1992.

[63]   V. Dietz and S. J. Harkema, "Locomotor activity in spinal cord-injured persons," *Journal of Applied Physiology*, vol. 96, pp. 1954 - 1960, 2004.

[64]   J. Duysens and K. G. Pearson, "Inhibition of flexor burst generation by loading ankle extensor muscles in walking cats," *Brain Research*, vol. 187, pp. 321-332, 1980.

[65]   L. Shen and R. E. Poppele, "Kinematic analysis of cat hindlimb stepping," *Journal*

of Neurophysiology, vol. 74, pp. 2266-2280, 1995.

[66] E. P. Zehr, T. Komiyama, and R. B. Stein, "Cutaneous Reflexes During Human Gait: Electromyographic and Kinematic Responses to Electrical Stimulation," *Journal of Neurophysiology*, vol. 77, pp. 3311-3325, 1997.

[67] C. Bastiaanse, J. Duysens, and V. Dietz, "Modulation of cutaneous reflexes by load receptor input during human walking," *Experimental Brain Research*, vol. 135, pp. 189-198, 2000.

[68] J. Perry, *Gait Analysis*: SLAK Incorporated, 1992.

[69] T. F. Novacheck, "The biomechanics of running," *Gait & Posture*, vol. 7, pp. 77-95, 1998.

[70] N. Hogan, "Impedance Control: An Approach to Manipulation: Part I - Theory," *Journal of Dynamic Systems, Measurement, and Control*, vol. 107, 1985.

[71] T. McGeer, "Dynamics and Control of Bipedal Locomotion," *Journal of Theor. Biol.*, vol. 163, pp. 277 - 314, 1993.

[72] S. Miyakoshi, G. Taga, Y. Kuniyoshi, and A. Nagakubo, "Three dimensional bipedal stepping motion using neural oscillators-towards humanoid motion in the real world," presented at Intelligent Robots and Systems, 1998. Proceedings., 1998 IEEE/RSJ International Conference on, 1998.

[73] S. Aoi and K. Tsuchiya, "Self-stability of a simple walking model driven by a rhythmic signal," *Nonlinear Dynamics*, vol. 48, pp. 1-16, 2007.

[74] M. Bennett, M. F. Schatz, H. Rockwood, and K. Wiesenfeld, "Huygens's Clocks," *Proceedings: Mathematical, Physical and Engineering Sciences*, vol. 458, pp. 563-579, 2002.

[75] S. Grillner, A. McClellan, and C. Perret, "Entrainment of the spinal pattern generators for swimming by mechano-sensitive elements in the lamprey spinal cord in vitro," *Brain Research*, vol. 217, pp. 380-386, 1981.

[76] K. G. Pearson, J. M. Ramirez, and W. Jiang, "Entrainment of the locomotor rhythm by group Ib afferents from ankle extensor muscles in spinal cats," *Experimental Brain Research*, vol. 90, pp. 557-566, 1992.

[77] A. D. McClellan and W. Jang, "Mechanosensory inputs to the central pattern generators for locomotion in the lamprey spinal cord: resetting, entrainment, and computer modeling," *J Neurophysiol*, vol. 70, pp. 2442-2454, 1993.

[78] A. Roy, H. I. Krebs, D. J. Williams, C. T. Bever, L. W. Forrester, R. M. Macko, and N. Hogan, "Robot-Aided Neurorehabilitation: A Novel Robot for Ankle Rehabilitation," *IEEE Transactions on Robotics*, vol. 25, pp. 569 - 582, 2009.

[79] I. Khanna, A. Roy, M. Rodgers, H. Krebs, R. Macko, and L. Forrester, "Effects of unilateral robotic limb loading on gait characteristics in subjects with chronic stroke," *Journal of NeuroEngineering and Rehabilitation*, vol. 7, pp. 23, 2010.

[80] J. F. Yang and M. Gorassini, "Spinal and Brain Control of Human Walking: Implications for Retraining of Walking," *The Neuroscientist*, vol. 12, pp. 379-389, 2006.

[81] Y. P. Ivanenko, N. Dominici, G. Cappellini, and F. Lacquaniti, "Kinematics in Newly Walking Toddlers Does Not Depend Upon Postural Stability," *J Neurophysiol*, vol. 94, pp. 754-763, 2005.

[82] R. Grasso, Y. P. Ivanenko, M. Zago, M. Molinari, G. Scivoletto, V. Castellano, V. Macellari, and F. Lacquaniti, "Distributed plasticity of locomotor pattern generators in spinal cord injured patients," *Brain*, vol. 127, pp. 1019-1034, 2004.

[83] E. Todorov and M. I. Jordan, "Optimal feedback control as a theory of motor coordination," *Nat Neurosci*, vol. 5, pp. 1226-1235, 2002.

[84] V. S. Gurfinkel, Y. S. Levik, O. V. Kazennikov, and V. A. Selionov, "Locomotor-like movements evoked by leg muscle vibration in humans," *European Journal of Neuroscience*, vol. 10, pp. 1608-1612, 1998.

[85] B. M. H. Van Wezel, F. A. M. Ottenhoff, and J. Duysens, "Dynamic Control of Location-Specific Information in Tactile Cutaneous Reflexes from the Foot during Human Walking," *J. Neurosci.*, vol. 17, pp. 3804-3814, 1997.

[86] NASA, "Anthropometry and Biomechanics," NASA, 2008.

[87] A. H. Hansen, D. S. Childress, S. C. Miff, S. A. Gard, and K. P. Mesplay, "The human ankle during walking: Implications for design of biomimetic ankle prostheses," *Journal of Biomechanics*, vol. 37, pp. 1467-1474, 2004.

[88] M. P. Murray, A. B. Drought, and R. C. Kory, "Walking Patterns of Normal Men," *J Bone Joint Surg Am*, vol. 46, pp. 335-360, 1964.

[89] M. P. Kadaba, H. K. Ramakrishnan, M. E. Wootten, J. Gainey, G. Gorton, and G. V. B. Cochran, "Repeatability of kinematic, kinetic, and electromyographic data in normal adult gait," *Journal of Orthopaedic Research*, vol. 7, pp. 849-860, 1989.

[90] P. Terrier and Y. Schutz, "Variability of gait patterns during unconstrained walking assessed by satellite positioning (GPS)," *European Journal of Applied Physiology*, vol. 90, pp. 554-561, 2003.

[91] E. v. Holst, "Entwurf eines Systems der lokomotorischen Periodenbildungen bei Fischen. Ein kritischer Beitrag zum Gestaltproblem," *Journal of Comparative Physiology A: Neuroethology, Sensory, Neural, and Behavioral Physiology*, vol. 26, pp. 481-528, 1939.

[92] W. R. Ferrell and T. B. Sheridan, "Supervisory control of remote manipulation," *Spectrum, IEEE*, vol. 4, pp. 81-88, 1967.

[93] T. B. Sheridan, *Telerobotics, automation, and human supervisory control.* Cambridge, MA: MIT Press, 1992.

[94] L. Sim, M. L. Cummings, and C. A. Smith, "Past, present and future implications of human supervisory control in space missions," *Acta Astronautica*, vol. 62, pp. 648-655, 2008.

[95] S. J. Lee and J. Hidler, "Biomechanics of overground vs. treadmill walking in healthy individuals," *Journal of Applied Physiology*, vol. 104, pp. 747-755, 2008.

[96] R. W. Bohannon, "Comfortable and maximum walking speed of adults aged 20 - 79 years: reference values and determinants," *Age and Ageing*, vol. 26, pp. 15-19, 1997.

[97] M. M. Churchland, A. Afshar, and K. V. Shenoy, "A Central Source of Movement Variability," *Neuron*, vol. 52, pp. 1085-1096, 2006.

[98] K. E. Jones, A. F. d. C. Hamilton, and D. M. Wolpert, "Sources of Signal-Dependent Noise During Isometric Force Production," *Journal of Neurophysiology*, vol. 88, pp. 1533-1544, 2002.

[99] M. R. Dimitrijevic, Y. Gerasimenko, and M. M. Pinter, "Evidence for a Spinal

Central Pattern Generator in Humans," *Annals of the New York Academy of Sciences*, pp. 360-376, 1998.

[100] S. Collins, A. Ruina, R. Tedrake, and M. Wisse, "Efficient bipedal robots based on passive-dynamic walkers," *Science*, vol. 307, pp. 1082-1085, 2005.

[101] M. H. Thaut, G. C. McIntosh, R. R. Rice, R. A. Miller, J. Rathbun, and J. M. Brault, "Rhythmic auditory stimulation in gait training for Parkinson's disease patients," *Movement Disorders*, vol. 11, pp. 193-200, 1996.

[102] J. Patton, M. Stoykov, M. Kovic, and F. Mussa-Ivaldi, "Evaluation of robotic training forces that either enhance or reduce error in chronic hemiparetic stroke survivors," *Experimental Brain Research*, vol. 168, pp. 368-383, 2006.

[103] B. Brewer, S. McDowell, and L. Worthen-Chaudhari, "Poststroke Upper Extremity Rehabilitation: A Review of Robotic Systems and Clinical Results," *Topics in Stroke Rehabilitation*, vol. 14, pp. 22-44, 2007.

[104] H. I. Krebs, B. T. Volpe, M. L. Aisen, and N. Hogan, "Increasing productivity and quality of care : Robot-aided neuro-rehabilitation," *Journal of Rehabilitation Research and Development*, vol. 37, pp. 639-652, 2000.

[105] J. J. Palazzolo, "Robotic Technology to Aid and Assess Recovery and Learning in Stroke Patient," in *Mechanical Engineering*, vol. Doctor of Philosophy. Cambridge: Massachusetts Institute of Technology, 2005, pp. 343.

[106] R. Cohen and D. Sternad, "Variability in motor learning: relocating, channeling and reducing noise," *Experimental Brain Research*, vol. 193, pp. 69-83, 2009.

[107] H. Müller and D. Sternad, "Motor Learning: Changes in the Structure of Variability in a Redundant Task," in *Progress in Motor Control*, vol. 629, *Advances in Experimental Medicine and Biology*, N. Back, I. R. Cohen, D. Kritchevsky, A. Lajtha, and R. Paoletti, Eds.: Springer US, 2009, pp. 439-456.

[108] B. Dobkin, D. Apple, H. Barbeau, M. Basso, A. Behrman, D. Deforge, J. Ditunno, G. Dudley, R. Elashoff, L. Fugate, S. Harkema, M. Saulino, M. Scott, and G. the Spinal Cord Injury Locomotor Trial, "Weight-supported treadmill vs over-ground training for walking after acute incomplete SCI," *Neurology*, vol. 66, pp. 484-493, 2006.

[109] M. Pohl, J. Mehrholz, C. Ritschel, and S. Ruckriem, "Speed-Dependent Treadmill Training in Ambulatory Hemiparetic Stroke Patients: A Randomized Controlled Trial," *Stroke*, vol. 33, pp. 553-558, 2002.

[110] S. Grillner, Ö. Ekeberg, A. El Manira, A. Lansner, D. Parker, J. Tegnér, and P. Wallén, "Intrinsic function of a neuronal network -- a vertebrate central pattern generator," *Brain Research Reviews*, vol. 26, pp. 184-197, 1998.

[111] K. G. Pearson, S. Mori, D. G. Stuart, and M. Wiesendanger, "Generating the walking gait: role of sensory feedback," in *Progress in Brain Research*, vol. Volume 143: Elsevier, 2004, pp. 123-129.

[112] H. Lee, P. Ho, M. Rastgaar, H. I. Krebs, and N. Hogan, "Quantitative Characterization of Steady-State Ankle Impedance with Muscle Activation," presented at ASME 3rd Dynamic Systems and Control Conference, Boston, USA, 2010.

[113] Ã. r. Ekeberg and K. Pearson, "Computer Simulation of Stepping in the Hind Legs of the Cat: An Examination of Mechanisms Regulating the Stance-to-Swing

Transition," *Journal of Neurophysiology*, vol. 94, pp. 4256-4268, 2005.

[114] S. T. McCaw and P. DeVita, "Errors in alignment of center of pressure and foot coordinates affect predicted lower extremity torques," *Journal of Biomechanics*, vol. 28, pp. 985-988, 1995.

[115] E. L. Miller, L. Murray, L. Richards, R. D. Zorowitz, T. Bakas, P. Clark, S. A. Billinger, and C. on behalf of the American Heart Association Council on Cardiovascular Nursing and the Stroke, "Comprehensive Overview of Nursing and Interdisciplinary Rehabilitation Care of the Stroke Patient: A Scientific Statement From the American Heart Association," *Stroke*, vol. 41, pp. 2402-2448.

[116] L. Sim, M. L. Cummings, and C. A. Smith, "Past, present and future implications of human supervisory control in space missions," *Acta Astronautica*, vol. 62, pp. 648-655.